

Institute of Molecular and Cellular Anatomy

Head of institute: Prof. Dr. Stefan Britsch



**The transcription factor Bcl11b regulates the function of adult
hippocampal mossy fiber synapses through a C1ql2/Nrxn3
pathway**

Dissertation

Submitted in partial fulfillment of the requirements for the degree of “Doctor of
Philosophy” (PhD) of the Medical Faculty of Ulm University

Efstathia Artemis Koumoundourou

Born in Kalamata, Greece

2023

Current dean of the Medical Faculty:

Prof. Dr. Thomas Wirth

Current dean of the International Graduate School in Molecular Medicine Ulm:

Prof. Dr. Bernd Knöll

Thesis Advisory Committee:

- First supervisor: Prof. Dr. Stefan Britsch
- Second supervisor: Prof. Dr. Dennis Kätzel
- Third supervisor: Prof. Dr. Bernd Heimrich

External reviewers:

PD Dr. Andrea Wizenmann

Day doctorate awarded:

19.12.2023

Adherence to copyright laws in dissertations

Students name: Koumoundourou Efstathia Artemis

Herewith I indicate that parts of the text data, figures, pictures and graphs shown in my dissertation were already published in the following journals (please cite the article completely):

- Koumoundourou, A., Rannap M., De Bruyckere, E., Nestel, S., Reißner, C., Egorov, A. V., Liu, P., Missler, M., Heimrich, B., Draguhn, A., Britsch, S. (2023). Regulation of hippocampal mossy fiber-CA3 synapse function by a Bcl11b/C1ql2/Nrxn3(25b+) pathway. *eLife*, 12:RP89854. <https://doi.org/10.7554/eLife.89854.1>

Open access article distributed under the terms and conditions of the Creative Commons Attribution 4.0 International (CC BY 4.0) License, <https://creativecommons.org/licenses/by/4.0/>)

I confirm that I own the right to use all text, figures, pictures and graphs in my dissertation.

Text and figures taken from other publications are correctly cited.

Date: Ulm, 22.11.23

Acknowledgements

First, I would like to thank Jacqueline Andratschke and Luisa Schmid, not only for their excellent technical support, but mainly for the moral support and their friendship (and the early breakfast sessions). I would also like to thank Matthias Toberer for saving my laptop that one time and mostly for geeking out with me. This long journey wouldn't have been the same without them. I want to offer a big apology to them as well for my nonstop complaining in the last stretch of the PhD.

I would also like to thank Prof. Britsch, as well as past and present members of the Institute of Molecular and Cellular Anatomy for the nice times we had together and for their support throughout the years, in whatever shape and form it came.

In addition, I would like to express my gratitude to Bernd Heimrich, who supported me above and beyond what is expected of a TAC member and a collaborator. His expertise and feedback, as well as his belief in me were crucial to the success of my studies. I would also like to thank Sigrun Nestel for her nonstop support with the Electron Microscopy imaging. Moreover, I would like to thank Dennis Kätzel for his feedback and his advice on technical matters in the initial phase of my PhD. Many thanks to Carsten Reißner and Markus Missler for their support with the Neurexin part, their hospitality when I visited their lab and their great feedback during our collaboration. I would also like to thank Julien Guy for teaching me how to do stereotaxic surgeries in the very beginning of my PhD.

Last but not least, I would like to thank all of my friends and family who patiently listened to me rant about things they did not necessarily understand and had always had my back.

Table of Contents

Abbreviations	7
1 Introduction	12
1.1 Synapses.....	12
1.1.1 Synaptic diversity and function	12
1.2 Transcriptional regulation of synaptic function.....	15
1.2.1 The transcription factor Bcl11b.....	16
1.3 Synaptic organizers	17
1.3.1 The synaptic organizer C1ql2	19
1.4 The hippocampus.....	21
1.5 The mossy fiber synapses.....	23
1.6 Aim of the study	27
2 Materials and Methods	28
2.1 Animals.....	28
2.2 Genotyping	28
2.3 Stereotaxic Injections.....	30
2.4 RNA isolation and quantitative real-time PCR	31
2.5 Production of digoxigenin-labeled riboprobes.....	32
2.6 mRNA in situ Hybridization	33
2.7 Western blots	35
2.8 Immunohistochemistry	36
2.9 Transmission electron microscopy.....	38
2.10 DNA constructs	39
2.11 Structural protein modelling	39
2.12 C1ql2 mutagenesis.....	39
2.13 Primary Hippocampal Cultures.....	40
2.14 HEK293 Cell Culture	41
2.15 Neuronal and HEK293 co-culture and immunostaining.....	41
2.16 Image acquisition and analysis.....	41
2.17 Quantification and statistical analysis	42

3	Results	43
3.1	Rescue of C1ql2 expression in dentate granule cells of <i>Bcl11b</i> mutants	43
3.1.1	AAV-mediated reintroduction of C1ql2 restores expression level in dentate granule cells	43
3.1.2	Reintroduction of C1ql2 in dentate granule cells of <i>Bcl11b</i> mutants rescues synaptic vesicle recruitment at the mossy fiber synapse.....	45
3.1.3	Reintroduction of C1ql2 in dentate granule cells of <i>Bcl11b</i> mutants rescues mossy fiber long-term potentiation	51
3.1.4	Reintroduction of C1ql2 in dentate granule cells of <i>Bcl11b</i> mutants does not rescue loss of mossy fiber synapses and of mossy fiber bouton ultrastructural complexity	53
3.2	Reintroduction of C1ql2 in dentate granule cells of <i>Bcl11b</i> mutants increases the number of postsynaptic spines containing a spine apparatus	53
3.3	Overexpression of C1ql2 in dentate granule cells has no effect on mossy fiber synapse.....	56
3.4	Knock-down of C1ql2 in wild-type dentate granule cells perturbs mossy fiber synapse organization and function	58
3.5	C1ql2-Nrxn3(25b+) is required for synaptic vesicle recruitment at the mossy fiber synapse	62
3.5.1	C1ql2-Nrxn3(25b+) is required for synaptic vesicle recruitment <i>in vitro</i>	62
3.5.2	Introduction of C1ql2.K262E in dentate granule cells of <i>Bcl11b</i> mutants does not rescue synaptic vesicle recruitment at the mossy fiber synapse.....	67
3.5.3	Suppression of Nrxn3 expression in dentate granule cells perturbs synaptic vesicle recruitment at the mossy fiber synapse	72
4	Discussion	76
4.1	<i>Bcl11b</i> regulates mossy fiber synapse integrity through both C1ql2-dependent and -independent mechanisms	76
4.2	A novel function for C1ql2 at the mossy fiber synapse.....	77
4.3	C1ql2-Nrxn3(25b+) interaction drives synaptic vesicle recruitment and C1ql2 targeting to the mossy fiber synapse	79
4.4	<i>Bcl11b</i> /C1ql2/Nrxn3(25b+) in the understanding of neurodevelopmental and neuropsychiatric disorders	82
4.5	<i>Bcl11b</i> - a regulator of synaptic specification and function	83
5	Summary.....	85
6	References	87

Abbreviations

AAV	Adeno-associated virus
AD	Alzheimer's disease
AMPA	α -amino-3-hydroxy-5-methyl-4-isoxazolepropionic
ANOVA	Analysis of variance
AP	Alkaline phosphatase
AZ	Active zone
ASD	Autism Spectrum Disorders
Bai3	Brain-specific angiogenesis inhibitor 3
Bcl11b	B cell leukemia 11b
BCL11BRD	BCL11B Related Disorder
Bp	Base pairs
BSA	Bovine serum albumin
C1qI2	Complement C1q like 2
C1qI3	Complement C1q like 3
C1qTNF10	C1q And Tumor Necrosis Factor-Related Protein 10
CA	Cornu ammonis
CA10	Carbonic Anhydrase 10
CA11	Carbonic Anhydrase 11
CaMKIIa	Calcium/calmodulin-dependent protein kinase type II alpha chain
Cat #	Catalogue number
Cbln	Cerebelin
cDNA	Complementary deoxyribonucleic acid
cKO	Conditional knock-out
CNS	Central nervous system
C_T	Threshold cycle
Ctip2	Chicken ovalbumin upstream promoter transcription factor interacting protein 2
DAPI	4',6-Diamidino-2-phenylindole
DCC	Deleted in colorectal cancer Netrin 1 Receptor

DEPC	Diethyl pyrocarbonate
DG	Dentate gyrus
DGC	Dentate granule cell
DIG	Digoxigenin
DIV	Days <i>in vitro</i>
DNA	Deoxyribonucleic acid
DRD1	D1 Dopamine receptor
E	Embryonic day
EDTA	Ethylenediaminetetraacetic acid
EGFP	Enhanced green fluorescent protein
EM	Electron microscopy
ER^{T2}	Estrogen receptor with high affinity for tamoxifen
et al.	<i>et alii</i> ; and others
FBS	Fetal bovine serum
FLRT	Fibronectin leucine rich transmembrane protein
g.c.l.	Granule cell layer
GABA	γ -Aminobutyric acid
GFP	Green fluorescent protein
GluA	Glutamate Ionotropic Receptor AMPA Type
GluD	Glutamate Dehydrogenase
GluK	Glutamate Ionotropic Receptor Kainate Type
GS	Goat serum
GWAS	Genome-wide association studies
HEK293	Human Embryonic Kidney 293 cells
HFS	High frequency stimulation
Homer1	Homer Scaffold Protein 1
HS	Horse serum
ICC	Immunocytochemistry
IHC	Immunohistochemistry
IL-1RAP	Interleukin 1 receptor accessory protein
ISH	In situ hybridization

KAR	Kainate receptors
KD	Knock-down
Lhx	LIM-homeodomain
LRRTM	Leucine-rich repeat transmembrane protein
LTP	Long-term potentiation
m.l.	Molecular layer
m.p.i.	Months post induction
MDGA	MAM Domain Containing Glycosylphosphatidylinositol Anchor
MEF2	Myocyte Enhancer Factor 2
MF	Mossy fiber
MF-LTP	Mossy fiber long-term potentiation
MFB	Mossy fiber bouton
MFS	Mossy fiber synapse
mGluR	Metabotropic glutamate receptors
mRNA	Messenger RNA
MSN	Medium spiny neurons
nCLP2	Neural C1q-like protein 2
NDD	Neurodevelopmental disorder
NMDA	<i>N</i> -methyl-d-aspartate
Nrxn	Neurexin
Nrxn3	Neurexin 3
Nrxn3(25b+)	Neurexin 3 containing SS5 ^{25b} sequence
NS	Non-sense
ns	Not significant
o/n	Overnight
OCT	Optimal cutting temperature
P	Postnatal day
PBS	Phosphate buffer saline
PCR	Polymerase chain reaction
PFA	Paraformaldehyde
PHC	Post-hoc comparison

P_r	Release probability
PSD	Postsynaptic density
PTPR	Protein Tyrosine Phosphatase Receptor Type
qPCR	Quantitative polymerase chain reaction
RNA	Ribonucleic acid
RT	Room temperature
Rtip1	Radiation-induced tumor suppressor gene 1
s.l.	Stratum lucidum
s.l.m.	Stratum lacunosum-moleculare
s.o.	Stratum oriens
s.p.	Stratum pyramidale
s.r.	Stratum radiatum
SA	Spine apparatus
SALM	Synaptic adhesion-like molecule
SDS	Sodium dodecyl sulfate
SEM	Standard error of the mean
Sema5b	Semaphorin 5b
shRNA	Short-hairpin RNA
SL	Stratum lucidum
SliTrk	SLIT And NTRK Like Family Member
SNP	Single-nucleotide polymorphism
SSC	Saline-sodium citrate
Sub.	Subiculum
SV	Synaptic vesicles
SynCam	Synaptic cell adhesion molecule
Synpo	Synaptopodin
TAM	Tamoxifen
TBS	Tris-buffered saline
TEM	Transmission electron microscopy
TF	Transcription factor
T_m	Melting temperature

TrkC	Tropomyosin receptor kinase C
Unc5	Unc-5 Netrin Receptor
vGlut1	Vesicular glutamate transporter 1
WB	Western blot
WT	Wild type

1 Introduction

1.1 Synapses

The synapses are vital structures within the nervous system, serving as the fundamental communication nodes for neural transmission. As the junctions between neurons, they enable the transmission of information. Moreover, the complexity and plasticity of the synapses, as well as the range of timescales over which they operate, highlights their ability to function as computational units within the brain, allowing for learning, memory formation, and active information processing (Foster & Sherrington, 1897; Maass & Zador, 1999; Zador, 2000). Early investigations of synaptic transmission resulted in the classification of synapses into electrical, in which ions can flow directly from one neuron into the next (Bennett & Zukin, 2004), and chemical, in which transmission is mediated by a neurotransmitter. The chemical synapses are the most common synapses in the brain. All chemical synapses exhibit the same overall structure. They consist of a presynaptic terminal aligned to a postsynaptic specialization, separated by a uniform 15-20 nm synaptic cleft. Upon stimulation, synaptic vesicles in the presynapse fuse with the plasma membrane and release neurotransmitters to the synaptic cleft. The neurotransmitters then bind to receptors on the postsynaptic membrane, leading to excitation or inhibition of the postsynaptic neurons, determined by the types of neurotransmitters and receptors (Sheng et al., 2012).

1.1.1 Synaptic diversity and function

Despite the main shared rule of synaptic function, the synapses are not uniform structures. They exhibit a remarkable diversity in their molecular composition, morphology, and functional characteristics (Atwood & Karunanithi, 2002; O'Rourke et al., 2012; Reimann et al., 2017). Synaptic heterogeneity is a hallmark of complex nervous systems, with different synapse types responding differently to patterns of neural activity and thereby shaping the circuit activity and enabling higher-order cognitive functions (Orvis et al., 2022; Perez-

Nieves et al., 2021). Furthermore, the synapses are not static structures. They are inherently dynamic and highly plastic and possess the ability to undergo constant changes. Synapses can strengthen or weaken their connections in response to neural activity and experience. This enables synapses to encode new information, consolidate memory and adapt to evolving environments (Choquet & Triller, 2013; De Roo et al., 2008; Wolff & Missler, 1992). The morphological and functional diversity of the synapses emerges from the unique combination of the synaptic proteins and their spatial organization on a nanoscale level (Medeiros et al., 2023; Newman et al., 2022; Nusser, 2018; Zhu et al., 2018). On the other hand, synaptic plasticity, and thus the emergence of learning, relies on the reorganization of this molecular machinery and the subsequent protein interactions (Bocchiaro & Feldman, 2004; Hazan & Ziv, 2020; Kirchner et al., 2023; Lautz et al., 2021). The synapses contain a number of diverse proteins that underlie establishment, maintenance and modulation of synaptic connections, as well as transmitter release, activation, and modulation of transmitter receptors and signal transduction cascades. The synaptic proteins are organized in intricate networks and form large complexes. Neuronal computations are conducted by these network of interacting proteins that mediate intracellular signal transduction and synaptic modifications. (Bayes et al., 2011; Frank & Grant, 2017; Sorokina et al., 2021). Synapses are very sensitive to changes in synaptic proteins, with even subtle alterations in the composition, localization or function of these proteins causing large effects on synaptic function. Moreover, similar synaptic molecular complexes can emerge from distinct relative protein abundances, while quite different protein complexes can be formed from almost identical initial protein abundances (Kiss-Toth et al., 2019; Miski et al., 2022; Yang et al., 2014). Therefore, formation of synapses that are precise, reliable and plastic requires constant and tight regulation of the molecular machineries. This regulation involves multiple mechanisms acting with spatiotemporal precision on various levels such as transcription, translation, protein complex formation and interactions, protein trafficking and subcellular organization (Figure 1; Chen et al., 2017a; Frerking & Wondolowski, 2008; Richter & Klann, 2009; Shao et al., 2022).

Perturbations in these regulatory mechanisms can lead to the destabilization of the synapse and in alterations in synaptic function. Synaptic dysfunction is increasingly recognized as a significant contributing factor in various neurological and neuropsychiatric conditions.

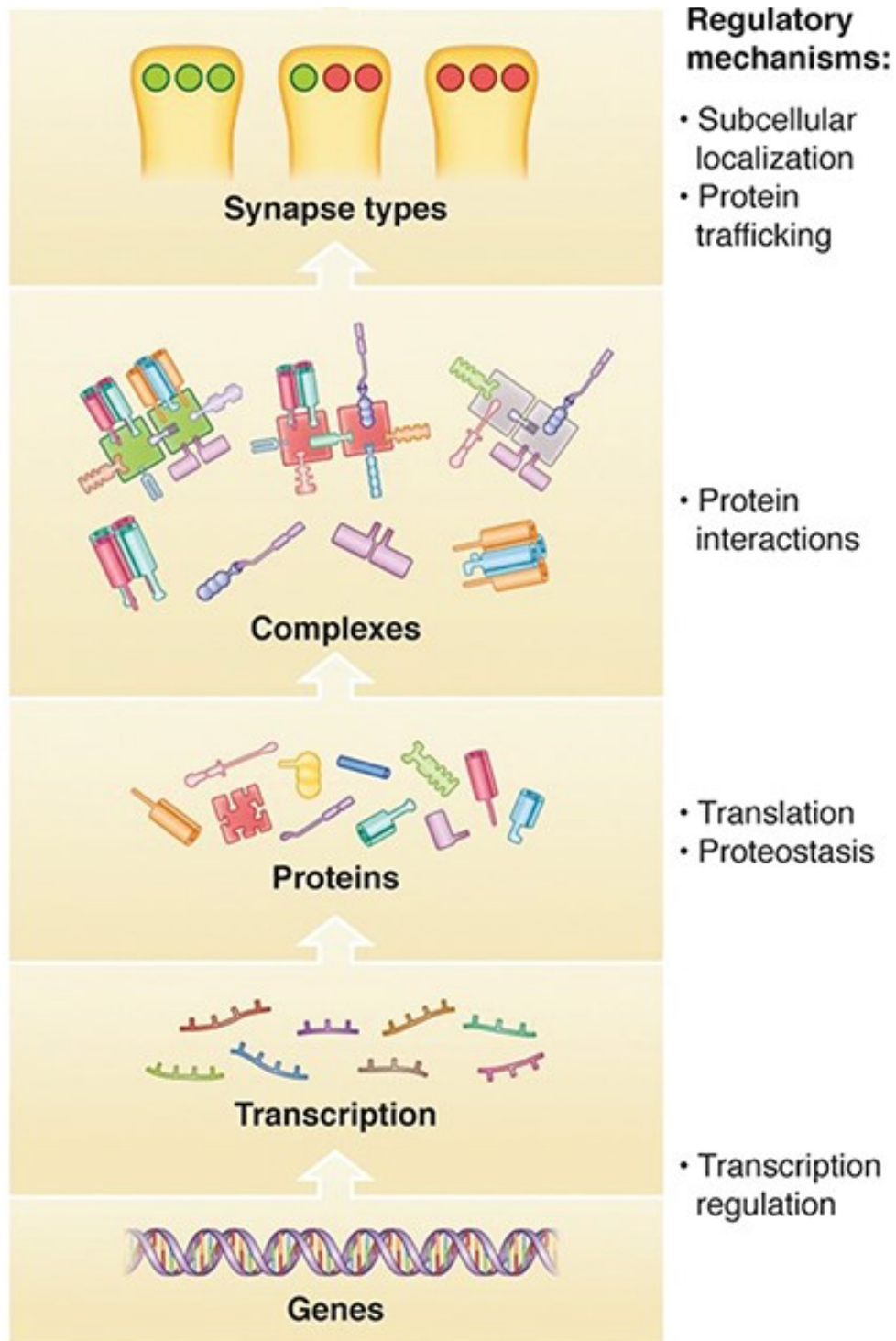


Figure 1. Regulatory mechanisms for synapse specification and function. The diversity of synapses arises from regulatory mechanism controlling gene and protein expression, assembly of proteins into complexes and supercomplexes and distribution of these supramolecular assemblies into synapses (Adapted from Grant, 2019; Published under CC BY 4.0, <https://creativecommons.org/licenses/by/4.0/>).

Alterations in the synaptic elements including the pre- and postsynaptic terminals, the synaptic cleft, and all the surrounding components, such as glial cells and extracellular matrix can lead to the manifestation of several such disorders, such as autism spectrum disorder (ASD), Epilepsy, Alzheimer's Disease (AD) and schizophrenia (Brose et al., 2010; Grant, 2012; Guang et al., 2018; Hayashi-Takagi, 2017; Lepeta et al., 2016; Meftah & Gan, 2023; Spoto et al., 2022). Mutations in genes encoding for synaptic proteins that result in altered protein levels and/or function have been recently associated to a number of neurological, neurodevelopmental disorders (NDDs) and neuropsychiatric disorders (Bayes et al., 2011; Sudhof 2021; Torres et al., 2017; Wang et al., 2018).

1.2 Transcriptional regulation of synaptic function

Transcription factors (TFs) have a central role in shaping the molecular composition and functional properties of synapses by controlling the expression of genes encoding for synaptic proteins crucial for synapse formation, function, and plasticity. Gene expression of synaptic proteins can be divided in three types: synaptic genes expressed in specific cell types or cell classes, genes showing a gradient of expression in specific cell classes and genes with a similar gradient of expression in all cell types. The unique combinatorial expression of these genes defines synaptic function (Hannou et al., 2020; Meng et al., 2020; Paul et al., 2017; Roig Adam et al., 2023; Valor et al., 2007). Moreover, TFs can act in response to neuronal activity. Calcium influx and signaling pathways induced during synaptic activity can activate specific transcriptional programs, altering gene expression and promoting synaptic remodeling and plasticity (Chen et al., 2017; Yap & Greenberg, 2018). Several TFs crucial for synapse specification and function have been already identified. For example, TFs from the LIM-homeodomain (Lhx) family, such as Lhx2, are involved in specifying glutamatergic synapses. Lhx2 regulates the expression of various genes involved in synapse formation, including cell adhesion molecules, synaptic scaffolding proteins, and neurotransmitter receptors (Chou & Tole, 2019). Myocyte Enhancer Factor 2 (MEF2) TFs have been shown to control expression of a network of synaptic genes that regulate a variety of different aspects of synaptic function including excitatory synapse weakening, excitatory synapse maturation, inhibitory synapse development and presynaptic vesicle

release (Flavell et al., 2008). TFs represent a point of convergence for different disease associated risk factors and are thus of high interest for multifactorial disorders such as NDDs and neuropsychiatric conditions. Genetic studies have associated genetic alterations of several TFs to such disorders (Santos-Terra et al., 2021). Their mechanisms of action, however, remain highly elusive.

1.2.1 The transcription factor Bcl11b

B cell leukemia 11b (Bcl11b), also named Radiation induced tumor suppressor gene 1 (Rit1) or Coup-TF interacting protein 2 (Ctip2), is a Krüppel-like TF that possesses six C₂H₂ zinc finger binding domains (Avram et al., 2000; Satterwhite et al., 2001). Bcl11b acts both by directly binding to promoter regions and by forming complexes with other proteins that are bound on promoter regions and can either repress or activate gene expression (Avram et al., 2000; Avram et al., 2002; Cismasiu et al., 2005; Cismasiu et al., 2006). Bcl11b is expressed and has been demonstrated to be essential for the development and function of various tissues and organs, such as T-cells, the skin, teeth and the CNS (Arlotta et al., 2005; Arlotta et al., 2008; Cai et al., 2017; Enomoto et al., 2011; Golonzhka et al., 2009; Kyrylkova et al., 2012; Nikouei et al., 2016; Simon et al., 2012; Wakabayashi et al., 2003). Bcl11b is of clinical relevance, as a growing number of individuals with mutations in the *BCL11B* gene present with severe deficits inside and outside the nervous system, such as immunodeficiency, T-cell-abnormalities, dermatitis, mental retardation, autistic features, speech impairment and motoric deficits (Che et al., 2022; Eto et al., 2022; Lessel et al., 2018; Punwani et al., 2016; Yang et al., 2020; Yu et al., 2023). Moreover, genome-wide association studies (GWAS) and animal studies have linked Bcl11b with NDDs, neuropsychiatric and neurodegenerative disorders characterized by synaptic dysfunction, including schizophrenia, Huntington's disease, AD and amyotrophic lateral sclerosis (Ahmed et al., 2015; Despalts et al., 2008; Kunkle et al., 2016; Lennon et al., 2016; Song et al., 2022; Whitton et al., 2016).

Bcl11b is highly expressed in the hippocampus in both the developing and the mature brain. In the murine hippocampus Bcl11b expression starts in post-mitotic cells of the putative

Cornu ammonis 1 (CA1) and 2 (CA2) areas at embryonic day 15 (E15) and extends into the dentate gyrus (DG) at E18. Expression in CA1, CA2 and DG continues postnatally and throughout adulthood (Figure 2; Leid et al., 2004; Simon et al., 2012). In the DG, *Bcl11b* is essential for postnatal development and function. Forebrain specific ablation of *Bcl11b* leads to reduction in the proliferation of the neuronal progenitor cells, cell loss and impairments in neuronal differentiation (Simon et al., 2012). The DG of the hippocampus is one of the two known brain areas with an adult neurogenic stem cell niche. Adult-specific ablation of *Bcl11b* in the DG of mice impairs the survival, differentiation and functional integration of adult born granule cells (Simon et al., 2016). Loss of *Bcl11b* in both the developing and the mature DG reduced the number of thorny excrescences and negatively affects the learning and memory capacities of the animals (Simon et al., 2012; Simon et al., 2016). Furthermore, the structural and functional integrity of the mature mossy fiber synapses is perturbed, with *Bcl11b* mutants presenting with a reduced number of mossy fiber synapses, loss of ultrastructural complexity of the mossy fiber boutons, misorganization of the synaptic vesicles and a dramatic decline in the long-term potentiation (De Bruyckere et al., 2018). While the role of *Bcl11b* in the DG has been well characterized both in development and in adulthood, the downstream mechanisms through which *Bcl11b* exerts its complex functions remain unclear. Transcriptome analysis has revealed the deregulation of several genes associated with synaptic transmission in the DG of adult *Bcl11b* mutant mice, among which the synaptic organizer molecule *C1ql2* (De Bruyckere et al., 2018). However, the role of *C1ql2* as an effector of *Bcl11b* was not further investigated.

1.3 Synaptic organizers

Among the synaptic proteins controlling synaptic specification and function is a group of proteins referred to as synaptic organizers. Synaptic organizers are molecules that play a pivotal role in guiding the formation, maturation, and maintenance of synapses within the nervous system. The synaptic organizers are responsible for the assembly of the active zone and the machinery responsible for the trafficking, the endo- and exocytosis of the synaptic

vesicles on the presynaptic side, as well as the organization of the neurotransmitter receptors and their anchoring proteins on the postsynaptic side (Shen & Scheiffele, 2010). In the last decades many such molecules have been identified (Figure 3; Fox & Umemori, 2006; Missler et al., 2012). The synaptic organizers are further classified into two categories: cell-adhesion molecules and secreted factors. The cell adhesion molecules are transmembrane proteins on both the pre- and the postsynaptic side that directly associate with their counter partners through extracellular domains (Arikkath & Reichardt, 2008; Hruska & Dalva, 2012; Sudhof, 2008; Takahashi & Craig, 2013; Um & Ko, 2013), while the secreted synaptic organizers serve as a scaffold between the two sides at the synaptic cleft (Christopherson et al., 2005; Fukata et al., 2006; Schlimgen et al., 1995; Sudhof, 2017; Yuzaki, 2008). Recent genetic studies have implicated several of these molecules in NDDs and neuropsychiatric disorders (Sudhof 2021; Torres et al., 2017; Wang et al., 2018).

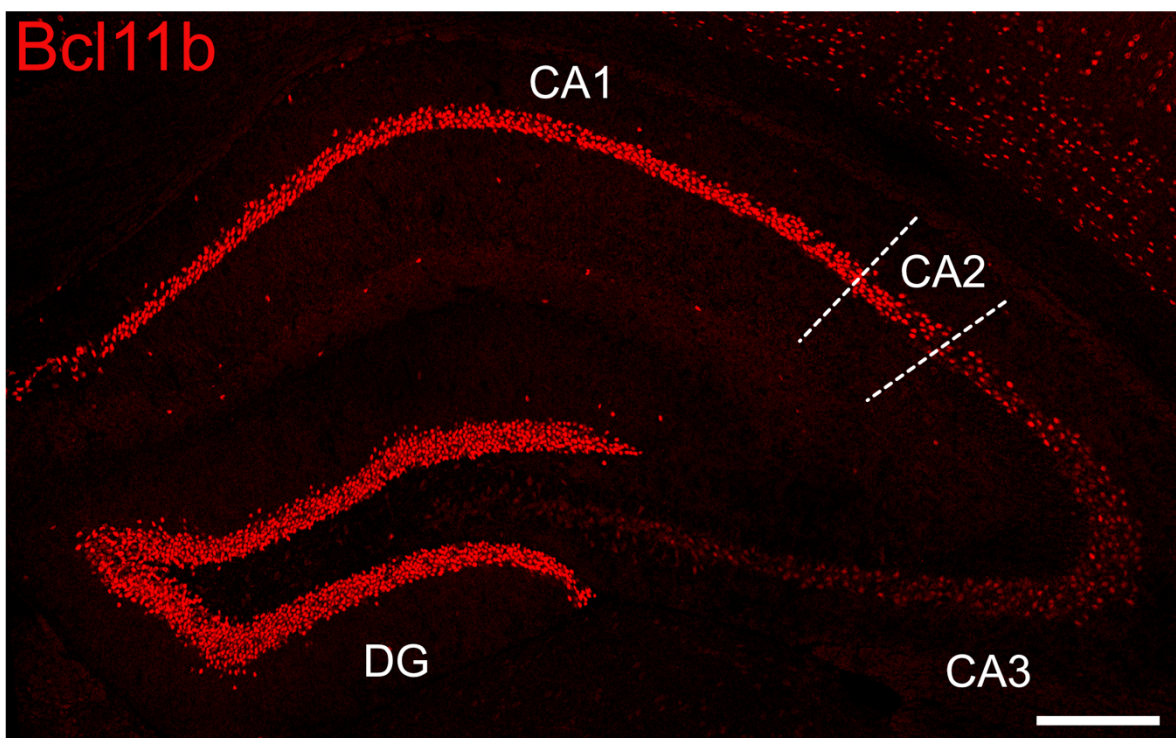


Figure 2. Expression of Bcl11b in the adult hippocampus. Bcl11b (red) is expressed by granule cells of the dentate gyrus and pyramidal neurons of CA1 and CA2 areas but not by pyramidal neurons of the CA3 area. Scale bar: 200 μ m. DG: dentate gyrus; CA: Cornu ammonis. (Adapted from Koumoundourou et al., 2023; Published under CC BY 4.0, <https://creativecommons.org/licenses/by/4.0/>).

1.3.1 The synaptic organizer C1ql2

C1ql2 (Complement C1q like 2), also known as C1q And Tumor Necrosis Factor-Related Protein 10 (C1qTNF10) and neural C1q-like protein 2 (nCLP2), a member of the C1ql subfamily, belongs to the secreted synaptic organizers (Figure 3). The C1ql subfamily consists of four proteins, C1ql1-4 that are highly expressed in the CNS, but with differential expression patterns. C1ql2 is expressed predominantly in the dentate granule cells and localizes at the synaptic cleft between the DG mossy fiber boutons and the thorny excrescence of the CA3 pyramidal cells (Iijima et al., 2010; Matsuda et al., 2016; Shimono et al., 2010; Yuzaki, 2008; 2017). C1ql2 is comprised by a N-terminal collagen-stalk domain and, like all members of the C1q superfamily, by a C-terminal globular C1q domain that contains Ca²⁺-binding sites and is able to form higher order oligomers (Ressler et al., 2015; Shimono et al., 2010).

Biochemical studies have shown that C1ql2 interacts with Bai3, a brain-specific, cell-adhesion–type G protein-coupled receptor that is involved in synapse development and plasticity (Bolliger et al., 2011; Duman et al., 2016). At the mossy fiber synapse, C1ql2 forms functional heteromers with C1ql3, another member of the C1ql subfamily that is co-expressed in dentate granule cells, and together they cluster postsynaptic kainate receptors. Selective deletion of either C1ql2 or C1ql3 in mice results in no overt phenotype in the hippocampus, while ablation of both leads to perturbation of synaptic transmission, suggesting functional compensation of the two proteins (Matsuda et al., 2016). Moreover, *in vitro* experiments suggested that at the mossy fiber synapse, C1ql2 interacts with a particular splice variant of neurexin 3 (Nrxn3) containing the SS5^{25b} sequence (Nrxn3(25b+)) (Matsuda et al., 2016). Nrxns are one of the best studied groups of cell adhesion molecules that act as synaptic organizers and regulate several synaptic properties (Reissner et al., 2013; Sudhof, 2017).

Recent animal and GWAS studies have associated C1ql2 with NDDs and neuropsychiatric conditions, such as schizophrenia, addiction, ASD and psychological distress, highlighting the importance of this protein (Huggett & Stallings, 2020a; 2020b; Kim et al., 2019; Kisaretova et al., 2023; Marballi et al., 2022; Unroe et al., 2021).

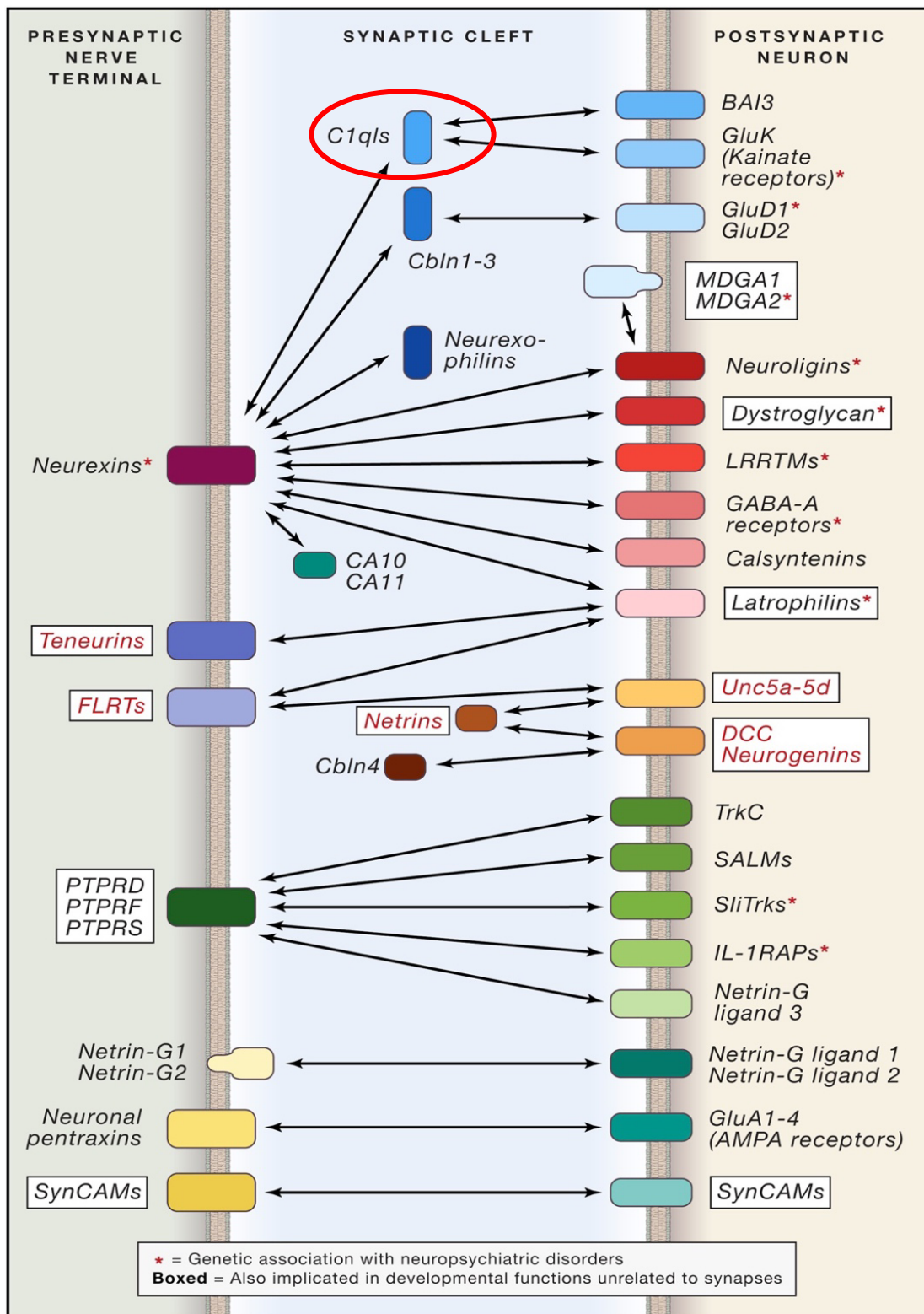


Figure 3. Overview of synaptic organizer proteins. Arrows show proteins that physically bind to each other. Red typeface highlights proteins with uncertain pre- versus postsynaptic localization. Red circle highlights the C1ql family of secreted synaptic organizers (Adapted from Sudhof, 2017; Permission to use and adjust from Elsevier).

1.4 The hippocampus

The hippocampal formation is a compound structure of the brain, located in the medial temporal lobe. It is part of the limbic system with a distinct role in memory processing, learning, spatial navigation, and emotions. The well-established role of the hippocampus in such higher cognitive functions largely relies on its unique anatomical features. It consists of three, spatially distinct areas, the dentate gyrus (DG), the cornu ammonis (CA) and the subiculum (Sub). The CA can be further divided in the CA1, CA2 and CA3 subfields. Moreover, the hippocampal formation is characterized by a highly organized laminar morphology and relatively simple organization of its principal cell layer and differs from other cortical regions due to its unidirectional information processing (Amaral and Witter, 1989; Andersen et al., 2006).

The DG is comprised of three distinct layers: the outer molecular layer (m.l.), the middle granule cell layer (g.cl.), and the inner polymorphic layer or hilus. The granule cell layer contains the cell bodies of the principal cells of the structure, the dentate granule cells, while the molecular layer is occupied by the dendrites of the dentate granule cells and the polymorphic layer, by the mossy fibers, the axonal projections of the dentate granule cells (Amaral et al., 2007; Andersen et al., 2006). On the other hand, the CA is composed of four main layers. The stratum pyramidale (s.p.) that contains densely packed pyramidal cells, the principal cells of the structure. The basal dendrites of the pyramidal cells extend to the outer or infrapyramidal region of CA, the stratum oriens (s.o.), while the apical dendrites extend towards the inner or the suprapyramidal region of CA, the stratum radiatum (s.r.) and terminate in the stratum lacunosum-moleculare (s.l.m.). Additionally, in CA3, but not in CA1 or CA2, an extra layer, the stratum lucidum (s.l.), intersects the pyramidal cell layer and stratum radiatum. In this layer incoming mossy fibers originating from the dentate granule cells make synaptic contacts with CA3 pyramidal cells. The subiculum is an anatomical prolongation of CA1, characterized by a widening of the cell layer (Figure 4; Andersen et al., 2006).

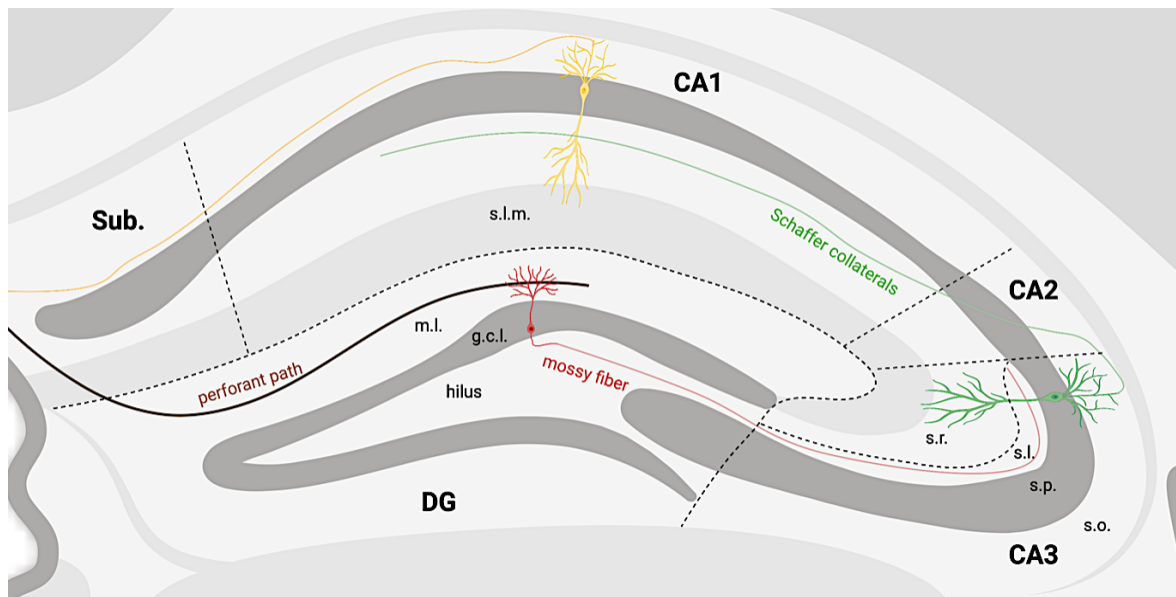


Figure 4. Anatomy and circuitry of the hippocampus. The hippocampus is a multilayered structure that consists of three distinct areas the dentate gyrus, the cornu ammonis that can be further subdivided in three regions and the subiculum. Dentate granule cells (red) that receive synaptic input from the entorhinal cortex through the perforant path (brown), extend their axons, the mossy fibers, to the CA3 area where they form synapses with CA3 pyramidal neurons (green). CA3 pyramidal neurons connect through the Schaffer collaterals with CA1 pyramidal neurons (yellow), that complete the circuit by projecting back to the EC. DG: Dentate gyrus; CA: Cornu ammonis; EC: Entorhinal Cortex; Sub.: Subiculum; m.l.: molecular layer; g.c.l.: granule cell layer; s.o: stratum oriens; s.p.: stratum pyramidale; s.l.: stratum lucidum; s.r.: stratum radiatum; s.l.m.: stratum lacunosum-moleculare. Created with BioRender.

The main relay of synaptic transmission within the hippocampus, also known as the trisynaptic circuit (Figure 4), is comprised of three consecutive, excitatory (glutamatergic), unidirectional synapses (Amaral and Witter, 1989; Andersen, 1975). Projections from predominantly layer II neurons of the entorhinal cortex transferring sensory information enter the hippocampal formation through the perforant path and form connections with the dendrites of dentate granule cells, making the circuit's first synapse (Tamamaki and Nojyo, 1993; Witter, 2007). The dentate granule cells give rise to unmyelinated mossy fibers, that innervate the stratum lucidum of CA3 and form synapses with CA3 pyramidal cells, named mossy fiber synapses. The mossy fiber synapses comprise the second synapse of the trisynaptic circuit (Amaral and Witter, 1989; Amaral et al., 2007). From there, the CA3

pyramidal cells extend their axons, the Schaffer collaterals, contacting CA1 pyramidal cells, thereby completing the hippocampal trisynaptic circuit (Szirmai et al., 2012). The CA1 pyramidal cells project back to the entorhinal cortex either directly or through the subiculum (Naber et al., 2001; Witter et al., 2000). Within the trisynaptic circuit, associational loops, interneuronal feedforward and feedback inhibitory circuits, as well as back-projections of the principal cells are present (Andersen et al., 2006, Bartos et al., 2007; Elgueta & Bartos, 2019; van Strien et al., 2009). Moreover, the entorhinal cortex also projects directly to CA1, 2 and 3 as well as the subiculum (Lopez-Rojas et al., 2022; Witter et al., 2000). Additionally, the hippocampal areas involved in the trisynaptic circuit receive direct input from several other regions such as the hypothalamus, the medial septum and the brain stem (Amaral et al., 2007; Colom et al., 2005; Pasquier & Reinoso-Suarez, 1978; Wyss et al., 1979).

1.5 The mossy fiber synapses

In my thesis I focused on the mossy fiber synapses, the connections between the dentate granule cells and the CA3 pyramidal cells. Each dentate granule cell extends a single unmyelinated axon, the mossy fiber, through the hilus towards the CA3 (Claiborne et al., 1986). In the hilus the mossy fibers give rise to a number of fine collaterals providing input to polymorphic neurons of the area (Buckmaster et al., 1992), while the main axons travel through the stratum lucidum forming the suprapyramidal bundle that corresponds to the proximal 100 μm of the apical dendrites of CA3 pyramidal cells. In the proximal CA3, mossy fibers also run through the stratum oriens forming the infrapyramidal bundle but eventually cross through the pyramidal cell layer and enter the stratum lucidum (Blackstad et al., 1970). In CA3, the mossy fibers establish synapses with both CA3 pyramidal neurons through large boutons (4-10 μm) and with GABAergic interneurons through filopodia arising from mossy fiber boutons (0.2-2 μm) and small “en passant” terminals (0.5-2 μm) (Acsády et al., 1998; Rollenhagen et al., 2007; Yu and Brown, 1994).

Each mossy fiber contacts on average 15 CA3 pyramidal cells, while each pyramidal cell is in contact with an average of 50 dentate granule cells (Amaral et al., 1990; Patton & McNaughton, 1995). The mossy fiber synapses are characterized by unique structural

features (Figure 5). Each of the large presynaptic mossy fiber boutons engulfs a large multi-headed postsynaptic spine, called a thorny excrescence, forming a complex three-dimensional structure that includes multiple synaptic interfaces, called mossy fiber synapses (Amaral & Dent, 1981; Chicurel & Harris, 1992). The giant presynaptic boutons exhibit distinct ultrastructural organization, with a large number of release sites and an enormous pool of releasable synaptic vesicles (Chicurel & Harris, 1992; Rollenhagen et al., 2007). The active zones, the sites of transmitter release, are generally characterized by asymmetric pre- and postsynaptic densities and the widening of the synaptic cleft. At mossy fiber boutons, active zones with frequently interrupted pre- and postsynaptic densities, as well as with one-side perforations or no perforations at all are present. The shape and the size of active zones, as well as the average distance between neighboring active zones vary substantially (Rollenhagen et al., 2007). The active zones are further characterized by the accumulation of synaptic vesicles in the proximity of the presynaptic density. In mature mossy fiber boutons, an enormous pool of synaptic vesicles is distributed throughout the entire terminal, with the synaptic vesicles forming clusters of various sizes at the proximity of individual active zones or a number of neighboring active zones. The synaptic vesicles also vary in shape and size, with three types being present at the mossy fiber boutons including small clear synaptic vesicles with a mean diameter of approximately 31 nm, a small number of large clear vesicles with a mean diameter of approximately 70 nm as well as a small number of large dense core vesicles (Henze et al., 2002; Rollenhagen et al., 2007). Moreover, mossy fiber synapses function through a distinct set of transmitters and their associated receptors. As in most excitatory synapses in the CNS, neurotransmission in the mossy fiber synapses is mediated by glutamate (Crawford & Connor, 1973; Sandler & Smith, 1991). However, other neurotransmitters such as γ -Aminobutyric acid (GABA) are present at the mossy fiber synapses (Sandler & Smith, 1991; Sloviter et al., 1996), as well as neuropeptide transmitters such as dynorphin, enkephalin, cholecystokinin, neuropeptide Y and neurokinin-B (Chafez et al., 1995; Chandy et al., 1995; Commons & Miller, 1995; Gall et al., 1990; McGuity et al., 1983; Schwarzer & Sperk, 1995). Additionally, the mossy fiber terminals contain high levels of zinc, that is co-released with glutamate (Budde et al., 1997; Wenzel et al., 1997). Postsynaptically, three types of ionotropic glutamate receptors are available, α -amino-3-hydroxy-5-methyl-4-isoxazolepropionic acid (AMPA) sensitive

receptors, kainate receptors (KARs) and *N*-methyl-d-aspartate (NMDA) sensitive receptors. NMDA receptors at the mossy fiber synapses are in smaller quantities in comparison to other synapses of the CNS (Baude et al., 1995; Castillo et al., 1997; Jonas et al., 1993; Siegel et al., 1994). Interestingly, KARs are also found at the presynaptic side (Represa et al., 1987; Schmitz et al., 2001). In addition, metabotropic glutamate receptors (mGluR) are also present in both the pre- and the postsynaptic side (Blümcke et al., 1996; Kamiya & Ozawa, 1999).

The mossy fiber synapses also exhibit unique transmission and plasticity properties, possibly related to the structural and molecular determinants of the synapses. Mossy fiber synapses are one of the most efficient and temporally precise excitatory synapses in the brain, able to undergo substantial changes in synaptic strength and exhibit paired pulse and frequency facilitation, post tetanic potentiation and reliable short-term and long-term potentiation (LTP) (Salin et al., 1996; Nicoll & Schmitz, 2005). The mossy fiber LTP differs from that found in other excitatory synapses, as it has been shown to not depend on NMDA receptor activation (Harris & Cotman, 1986). However, the mechanisms underlying the induction of mossy fiber LTP remain to a large extent unclear. The involvement of postsynaptic mechanisms in the induction of mossy fiber LTP has become a topic of controversy, with studies supporting a NMDA-independent rise of postsynaptic Ca^{2+} to have a role in the LTP (Bashir et al., 1993; Conquet et al., 1994; Ito & Sugiyama, 1991; Jaffe & Johnston, 1990; Urban & Barrionuevo, 1996; Yeckel et al., 1999), while others failed to find a link suggesting a strictly presynaptic form of LTP (Hsia et al., 1995; Kakegawa et al., 2002; Manzoni et al., 1994; Mellor & Nicoll, 2001; Tong et al., 1996; Zalutsky & Nicoll, 1990). KARs have been shown to have a role in mossy fiber LTP with conflicting results concerning the specific subunits involved (Bortolotto et al., 1999; Breustedt & Schmitz, 2004; Contractor et al., 2001). In contrast to the controversies concerning the induction of mossy fiber LTP, it is broadly accepted that for the expression of mossy fiber LTP, an increase in the neurotransmitter release that involves presynaptic Ca^{2+} influx and activation of the adenylyl cyclase pathway is essential (Breustedt et al., 2003; Dietrich et al., 2003; Huang et al., 1994; López-García et al., 1996; Tong et al., 1996; Xiang et al., 1994).

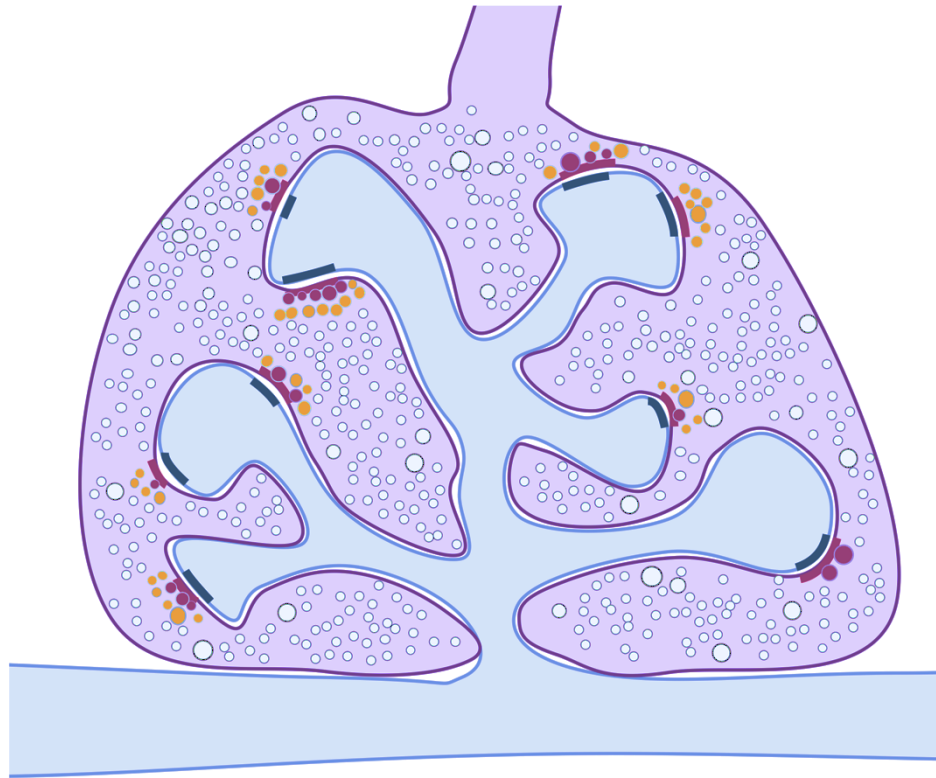


Figure 5. Structure of adult mossy fiber bouton. A large mossy fiber bouton (purple) engulfs a multi-headed postsynaptic spine (blue). Multiple mossy fiber synapses (magenta line: presynapse; grey line: postsynapse) can be formed between the two structures. The mossy fiber bouton includes a large number of synaptic vesicles (white circles) of various sizes, distributed throughout the whole bouton. Synaptic vesicles accumulate (yellow circles) and attach themselves (magenta circles) at the presynaptic active zone (magenta line). Created with BioRender.

In addition to its unique structural and functional properties and its physiological role in learning and memory, the mossy fiber synapse has been of scientific interest due to its frequent implication in NDDs, neurodegenerative and neuropsychiatric disorders. Studies have shown that morphofunctional alterations in the mossy fiber circuit occur in animal models of neurodevelopmental disorders such as Fragile X Syndrome, ASD and Intellectual disability (Lanore et al., 2012; Martin et al., 2015; Scharkowski et al., 2018; Sgritta et al., 2023). Moreover, mouse models of AD presented even on early stages with disruption of the mossy fiber synapses specifically (Viana de Silva et al., 2019; Wilke et al., 2014). Reorganization and alterations of the mossy fiber synapses have also been identified in both animal models, and human patients of temporal lobe epilepsy (Babb et al., 1991; Mello et al., 1993; Sutula et al., 1989; Zhang et al., 2014) and schizophrenia (Abulaiti et al., 2022;

Kolomeets et al., 2005; Kolomeets et al., 2007). However, the pathomechanisms driving the impairments of mossy fiber synapses in such disorders and their phenotypic readout is not yet fully understood.

1.6 Aim of the study

Synaptic function is directly linked to the molecular composition of the individual synapses and requires strict and constant transcriptional regulation. Changes in synaptic protein expression lead to synaptic dysfunction and have been linked to several neurological and neuropsychiatric disorders. Understanding the molecular basis of synapses and its transcriptional regulation could, thus, aid in the development of synapse-targeted therapies for such disorders. Bcl11b, a transcription factor associated with several disorders characterized by synaptic dysfunction, has been previously shown to play a crucial role in the structural and functional stability of the mature mossy fiber synapses. The downstream regulatory pathways, however, remained unclear. Aim of my work was to identify the molecular mechanisms through which Bcl11b regulates the structure and function of the mature mossy fiber synapses and offer new entry points for the mechanistic understanding of disorders associated with Bcl11b. I first tried to identify transcriptional targets of Bcl11b that act directly at the mossy fiber synapse. I focused on the synaptic organizer C1ql2, previously shown to be a direct transcriptional target of Bcl11b at the dentate granule cells that is downregulated upon *Bcl11b* deletion. I reintroduced C1ql2 in the dentate gyrus of mice with an adult-induced *Bcl11b* deletion and analyzed whether it was able to rescue the *Bcl11b*-mutant phenotype at the mossy fiber synapses. To further study and to ensure the specificity of the C1ql2-dependent functions, I knocked-down *C1ql2* in the dentate gyrus of wild-type mice. To understand how C1ql2 exerts its functions on the mossy fiber synapses, I investigated its interaction with other synaptic proteins. I focused on a particular Neurexin 3 isoform, Nrnx3(25b+), a previously hypothesized interaction partner of C1ql2 at the mossy fiber synapses. To understand the importance of their interaction both *in vitro* and *in vivo*, I interrupted the C1ql2-Nrnx3(25b+) interaction by expressing a C1ql2 variant that does not bind to Nrnx3(25b+) or by deleting *Nrxn3* in the dentate gyrus granule cells and examined the mossy fiber synapse.

2 Materials and Methods

2.1 Animals

To study the functions of transcriptional targets of *Bcl11b* in the adult DG, mice with inducible *Bcl11b* ablation were used. *Bcl11b^{flox}* mice (Li et al., 2010) were crossbred with *CaMKII α -CreER^{T2}* (Erdmann et al., 2007). In this model, Cre recombinase that is under the control of the forebrain-specific *Calcium–calmodulin (CaM)-dependent protein kinase II α chain (CaMKII α)* promoter, is fused to a modified mouse estrogen receptor (ER^{T2}). CreER^{T2} is maintained in the cytoplasm, and only upon binding of tamoxifen to the estrogen receptor can Cre translocate to the nucleus, where it can recombine loxP-flanked DNA sequences (Feil et al., 2009). *Bcl11b^{flox/flox}*; *CaMKII α -CreER^{T2}* (*Bcl11b* cKO) and *Bcl11b^{+/+}*; *CaMKII α -CreER^{T2}* (controls) were used for the analysis. *Bcl11b* mutation was induced at the age of 60 days by intraperitoneal injection of 2 mg tamoxifen (Sigma Aldrich, Cat #5648; 10 mg/mL, in 1:9 ethanol/peanut oil, Sigma Aldrich. Cat #P2144) for five consecutive days (Madisen et al., 2010). Wild-type C57BL/6JRj mice were obtained from Janvier-Labs (Cat #2670020). For pan-*neurexin* knock-out, *Nrxn123^{flox}* mice (Chen et al., 2017b) were used. Animals were kept in a 12:12-h light–dark cycle and at a constant temperature (22 ± 1 °C) in individually ventilated cages. All experiments were performed in accordance with the European law and were approved by the government office in Tübingen, Germany (Licenses 1224.TschB:O, 1517.TschB and o.161-5.TschB:O).

2.2 Genotyping

Tissue was collected from ears at postnatal day 21 (P21) or tails post-mortem and digested for 2 h at 55 °C with lysis-buffer (100mM Tris pH8.0, 5mM EDTA, 0.2% SDS, 200mM NaCl, 250 μ g Proteinase K). Proteinase K was inactivated at 97 °C for 10 min and the resulting DNA solution was diluted with 200 μ L H₂O before being used for genotyping by polymerase chain reaction (PCR) with the appropriate primers (Table 1; Eurofins), according to the

protocol (Table 2; FastGene Taq DNA Polymerase: Nippon, Cat #LS21) and thermocycler program below (Table 3).

Table 1. List of primers used for genotyping by PCR.

Gene	Primer sequences	Allele	Size
<i>Bcl11b</i>	5'-TGAGTCAATAAACCTGGGCGAC-3'	WT	243 bp
	5'-GGAATCCTTGGAGTCACTTGTGC-3'	floxed	345 bp
<i>CamKIIa-CreER^{T2}</i>	5'-TCTCCAACCTGCTGACTGTG-3'	WT	-
	5'-CCAGCATCCACATTCTCCTT-3'	Positive band	382 bp
<i>Neurexin 1</i>	5'-GTAGCCTGT TTA CTG CAG TT CATT CC-3'	WT	200 bp
	5'-CAAGCACAGGATGTAATG GCCTTTC-3'	floxed	350 bp
<i>Neurexin 2</i>	5'-CAGGGTAGGGTGTGGAATGAGGTC-3'	WT	200 bp
	5'-GTTGAGCCTCACATCCATTTGTCT-3'	floxed	350 bp
<i>Neurexin 3</i>	5'-AATAGCAGAGGGGTGTGACAC-3'	WT	300 bp
	5'-CGTGGGGTATTTACGGATGAG-3'	floxed	350 bp

Table 2. PCR protocol for genotyping.

PCR protocol	
FastGene	12.5 µL
Primer 1 (10 µM)	1.25 µL
Primer 2 (10 µM)	1.25 µL
DNA	1.0 µL
H ₂ O	9.0 µL

Table 3. Thermocycler programs for genotyping by PCR.

<i>Bcl11b</i>	<i>CamKIIa-CreER^{T2}</i>	<i>Neurexin 1</i>	<i>Neurexin 2</i>	<i>Neurexin 3</i>
94°C 2 min	95°C 2 min	94°C 2 min	94°C 2 min	94°C 2 min
94°C 15 sec	95°C 30 sec	94°C 15 sec	94°C 15 sec	94°C 15 sec
63°C 30 sec	60°C 60 sec	55°C 30 sec	55°C 30 sec	55°C 30 sec
72°C 60 sec	72°C 90 sec	72°C 60 sec	72°C 60 sec	72°C 60 sec
x39 repeats	x35 repeats	x30 repeats	x30 repeats	x30 repeats
from step 2	from step 2	from step 2	from step 2	from step 2
72°C 7 min	72°C 10 min	72°C 7 min	72°C 7 min	72°C 7 min

2.3 Stereotaxic Injections

For the expression of *C1ql2* and *C1ql3*, adeno-associated virus (AAV) vectors expressing EGFP-2A-*C1ql2* or EGFP-2A-*C1ql3* were injected in the DG of 80 days old *Bcl11b* cKO mice, respectively. To exclude that any putative observed effects were due to the procedure or the AAV itself, *Bcl11b* cKO and control mice were injected with an AAV vector with the same backbone, expressing EGFP only. To knock-down *C1ql2* in the adult DG, AAV expressing 4 short-hairpin RNAs (shRNA) against *C1ql2* (4xsh*C1ql2*-EGFP) or control AAV expressing 4 non-sense (NS) shRNAs (4xshNS-EGFP) was injected in the DG of 60 days old C57BL/6JRj mice. For pan-*neurexin* knock-out in the adult DG, AAV expressing EGFP-Cre or control AAV expressing EGFP-CreY324F, an inactive Cre (Klatt et al., 2021; Wang et al., 2016), was injected in the DG of 60 days old *Nrxn123^{flox/flox}* mice. All AAVs used in this study (Table 4) were produced by the Viral Vector Facility of the Neuroscience Center Zurich on request. The four selected non-sense shRNAs and the four sh*C1ql2* sequences were checked for and presented with no off-target bindings on the murine exome with up to two mismatches by siRNA-Check (<http://projects.insilico.us/SpliceCenter/siRNACheck>). The mice were anesthetized with 5% isoflurane and were placed in a mouse stereotaxic apparatus. During the entire procedure, anesthesia was maintained by constant administration of 2.2% isoflurane. Eye ointment was applied to prevent eyes from drying. Butorphanol and Meloxicam (5 µg/g) was administered subcutaneously, as well as local anesthetic Bupivacaine (5 µg/g) subcutaneously at the incision site. After 10 min the head of the mouse was shaved and disinfected and an incision was made in the skin. The injection sites were identified based on preestablished coordinates and a small craniotomy was performed for each site. The injector was placed at the individual sites and the viral solution was injected at 100 nL/min, with a 5-10 min recovery before removing the injector. After injection at all sites, the incision was sutured and the animal was placed in a heated chamber for recovery from anesthesia, after which it was returned to its home cage. AAVs were injected at three sites per hemisphere with the following coordinates: AP -2 mm; ML ±1 mm; DV -2 mm. AP -2.5 mm; ML ±1.5 mm; DV -1.8 mm. AP -3.1 mm; ML ±2, DV -2.2 mm with Bregma being the starting point (AP 0; ML: 0; DV:0). 200 nL of AAV (1e12 vg/mL) were injected in each location.

Table 4. List of AAV vectors.

AAV vector	Cat #
AAV-DJ_8/2-mCaMKII α -EGFP-WPRE-hGHp(A)	v113-DJ/8
AAV-DJ_8/-2-mCaMKII α -EGFP_2A_C1QL2-WPRE-hGHp(A)	n/a
AAV-DJ_8/-2-mCaMKII α -EGFP_2A_C1QL3-WPRE-hGHp(A)	n/a
AAV-DJ_8/-2-mCaMKII α -EGFP_2A_C1QL2.K262E-WPRE-hGHp(A)	n/a
AAV-8/2-hSyn1-chI[4x(m/rshNS)]-EGFP-WPRE-bGHp(A)	v668-DJ/8
AAV-8/2-hSyn1-chI[4xsh(mC1ql2)]-EGFP-WPRE-bGHp(A)	n/a
AAV-DJ_8/2-hSyn1-chI-EGFP_iCre-WPRE-bGHp(A)	v750-DJ/8
AAV-DJ_8/2-hSyn1-chI-EGFP_Cre(Y324F)-WPRE-bGHp(A)	n/a

2.4 RNA isolation and quantitative real-time PCR

All procedures were performed in an RNase-free environment. Animals were sacrificed under deep CO₂-induced anesthesia, brains were quickly dissected in ice-cold 1x phosphate buffer saline (PBS), cryopreserved in 20% sucrose overnight (o/n) at 4 °C, embedded in optimal cutting temperature (OCT) compound (Polysciences Inc., Cat. Nr. 19636) and stored at -80 °C. 20 μ m thick coronal sections were prepared with a cryostat and collected on UV-treated, and 0.05% poly-L-lysine (Sigma Aldrich, Cat #P8920)-coated membrane-covered PEN slides (Zeiss, Cat. Nr. 415190-9041-000). The sections were fixed for 1 min in ice-cold 70% EtOH, incubated for 45 sec in 1% cresyl violet acetate solution (Waldeck) and washed for 1 min each in 70% EtOH and 100% EtOH. The sections were then briefly dried on a 37 °C warming plate and immediately processed. The granule cell layer of the DG was isolated by laser capture microdissection (Zeiss, Axio Observer Z 2.1 with PALM Microbeam and RoboMover, and PALM RoboSoftware 4.6.) and collected in adhesive cap tubes (Zeiss, Cat #415190-9211-000). RNA was isolated from the collected tissue using the RNeasy Micro Kit (Qiagen, Cat #74004) and reverse transcribed using the SensiFAST cDNA Synthesis Kit (Bioline, Cat #BIO-65053) according to the supplier's protocol. Quantitative real-time PCR (qPCR) was performed using the LightCycler DNA Master SYBR Green I Kit (Roche Molecular

Systems Inc., Cat #04707516001) according to the supplier's protocol, with 1 μ L cDNA and 1 μ L of each primer (10 μ M; Table 5) in a LightCycler 480 System (Roche Molecular Systems Inc., Cat #05015278001) with an adapted program (Table 6). The relative copy number of Gapdh RNA was used for normalization. Data were analyzed using the comparative C_T method (Schmittgen & Livak, 2008).

Table 5. List of primers for qPCR.

Gene	Sequence	T_m (°C)
C1qI2	5'-TTGGCAATCACTACGACCCC-3'	58
	5'-CCCGAGAACGTGCTGTACTT-3'	
C1qI3	5'-AGTTCACCTGCTCCATACCG-3'	58
	5'-CTAGCACGCACCTGGTTG-3'	
Neurexin 3	5'-TGCCACCTGAAATGTCTACC-3'	54
	5'-ATCTGACGTGGGCTGAATG-3'	
Gapdh	5'-GAGTTGCTGTTGAAGTCGCA-3'	54-58
	5'-TGGAGAAACCTGCCAAGTATG-3'	

2.5 Production of digoxigenin-labeled riboprobes

The plasmids containing the target sequences (previously constructed by colleagues) were linearized with corresponding restriction enzymes (New England Biolabs) at the 5' end of the sequence. The linearized DNA was purified with the Nucleospin Gel and PCR Clean-up Kit (Macherey-Nagel, Cat #740609) according to the supplier's protocol. 1 μ g of the linearized plasmid was used as a template for in vitro transcription with a suitable RNA polymerase (T7/Sp6; Roche, Cat #10881767001 & #10810274001 respectively) and digoxigenin (DIG) RNA labeling Mix (Roche, Cat #11277073910) according to the supplier's protocol. The produced RNA was immediately purified after the end of the reaction with the RNeasy MinElute Cleanup-Kit (Qiagen, Cat #74204) according to the supplier's protocol.

The DIG-labeled RNA products were eluted in equal parts of RNase free H₂O and formamide (Merck, Cat # 1096841000) and stored at -80°C.

Table 6. LightCycler program for qPCR.

Program Name		pre-incubation					
Cycles		1	Analysis Mode None				
Target (°C)	Acquisition Mode	Hold (hh:mm:ss)	Ramp Rate (°C/s)	Acquisitions (per °C)	Sec Target (°C)	Step size (°C)	Step Delay (cycles)
95	None	00:10:00	4.40		0	0	0
Program Name		amplification					
Cycles		45	Analysis Mode Amplification				
Target (°C)	Acquisition Mode	Hold (hh:mm:ss)	Ramp Rate (°C/s)	Acquisitions (per °C)	Sec Target (°C)	Step size (°C)	Step Delay (cycles)
95	None	00:00:10	4.40		0	0	0
T _m	None	00:00:10	2.20		0	0	0
72	Single	00:00:10	4.40		0	0	0
Program Name		pre-incubation					
Cycles		1	Analysis Mode Quantification				
Target (°C)	Acquisition Mode	Hold (hh:mm:ss)	Ramp Rate (°C/s)	Acquisitions (per °C)	Sec Target (°C)	Step size (°C)	Step Delay (cycles)
95	None	00:00:05	4.40		0	0	0
65	None	00:01:00	2.20		0	0	0
97	Continuous		0.11	5	0	0	0
Program Name		cooling					
Cycles		1	Analysis Mode None				
Target (°C)	Acquisition Mode	Hold (hh:mm:ss)	Ramp Rate (°C/s)	Acquisitions (per °C)	Sec Target (°C)	Step size (°C)	Step Delay (cycles)
40	None	00:00:30	2.20		0	0	0

2.6 mRNA *in situ* Hybridization

Animals were sacrificed under deep CO₂-induced anesthesia, brains were dissected quickly, collected in ice-cold 1x PBS, fixed for 4 h in 4% paraformaldehyde (PFA; AppliChem GmbH,

Cat #A3813) in 1x PBS at 4 °C and cryopreserved in 20% sucrose in 1x PBS o/n at 4 °C. The next day the brains were embedded in OCT compound and stored at -80 °C. Coronal sections were prepared at 14 µm with a cryostat, collected on Superfrost™ Plus glass slides (ThermoFisher Scientific, Cat #J1800AMNT) and stored at -80 °C. Before staining, the sections were thawed at room temperature (RT) for 30 min, fixed in 4% PFA in Diethyl pyrocarbonate (DEPC)-treated (1:1000; BioChemica, Cat #A0881) 1x PBS (PBS_{DEPC}) for 5 min at RT and then washed 3x 5 min in 1x PBS_{DEPC}, followed by a 5 min wash with H₂O_{DEPC} for 5 min at RT. The slides were placed in acetylation buffer (1.5% v/v triethanolamine, 0.15% v/v HCl 37%, 0.25% v/v acetic anhydride in H₂O_{DEPC}) for 10 min at RT, washed in H₂O_{DEPC} for 5 min at RT and then placed in 6x Saline-sodium citrate buffer (SSC)/formamide (1:1; 20x SSC: 3M NaCl, 0.3M triNaCitrat-Dihydrate pH 7.0) for 2h at RT. Shortly before use, hybridization solution was prepared by adding 3 µL of DIG-labeled antisense riboprobe, respectively, in 150 µL Hybridization mix per slide, heated for 5 min at 80 °C and placed for 2 min on ice. Once hybridization solution was applied to the sections, they were covered with cleaned (100% ETOH) glass coverslips (Marienfeld-Superior, Cat #0107222). The slides were transferred in a hybridization chamber containing 6x SSC/formamide (1:1) and incubated o/n at 65 °C. The next day the slides were submerged in prewarmed 5x SSC and placed in a water bath at 65 °C for 10 min to remove the coverslips and were then placed in 4x SSC/formamide (1:1) for 45 min at 65 °C. Afterwards the slides were transferred in NTE buffer (10mM Tris HCl pH 7.6, 1mM EDTA, 500mM NaCl) for 1 h at 37 °C, and then in 1x SSC/formamide (1:1) for 45 min at 65 °C. The sections were washed for 5 min at RT with 0,5x SSC, followed by 3x 5 min with TBS (0.1M Tris HCl pH 7.6, 150mM NaCl). The sections were blocked with 10% goat serum (GS; Thermo Fisher Scientific Inc, Cat #16010-072) in TBS for 60 min at RT and were then incubated o/n at 4 °C with anti-DIG-AP Antibody (1:2000; Roche Molecular Systems Inc., Cat #11093274910) in TBS containing 10% GS. The next day, sections were washed 3x 10 min with TBS at RT and then placed in alkaline phosphatase (AP) Buffer (100mM Tris HCl pH 9.5, 50mM MgCl₂, 100mM NaCl) for 10 min at RT. Finally, the sections were submerged in the filtrated AP solution containing 0.45% v/v 4-Nitro blue tetrazolium chloride (Roche Molecular Systems Inc., Cat #11383213001) and 0.35% v/v 5-Brom-4-chlor-3-indolyl-phosphate (Roche Molecular Systems Inc., Cat #11383221002) and kept in dark at RT until signal development. The sections were washed

with H₂O for 5 min, fixed with 4% PFA in 1x PBS and washed again with H₂O multiple times. Slides were mounted with Shandon Immu-Mount (ThermoFisher Scientific, Cat #9990402) and covered with glass coverslips.

2.7 Western blots

Animals were sacrificed under deep CO₂-induced anesthesia, brains were dissected quickly and collected in ice-cold 1x PBS. Hippocampi from freshly removed brains were dissected in ice-cold 1x PBS, collected in Lysis Buffer (50mM Tris pH 7.5, 150mM NaCl, 0.5% sodium deoxycholate, 1% triton-X100, 0.1% SDS) and manually homogenated. Samples were centrifuged for 25 min at 13200 rpm at 4 °C and the supernatant was collected. Protein concentration was calculated with Bradford assay. Briefly, 30 µL of 6 different dilutions (0 mg/mL, 0.05 mg/mL, 0.1 mg/mL, 0.2 mg/mL, 0.25 mg/mL and 0.3 mg/mL) of BSA Standard (Interchin, Cat #UP36859D) were prepared along with 30 µL of protein suspension diluted 1:50 in H₂O and were mixed with 750 µL Bradford Reagent (Sigma Aldrich, Cat #B6916) each. After 5 min incubation each sample was loaded in triplets of 250 µL on a 96-well plate. Spectroscopic analysis was done with SpectraMax i3x Multi-Mode Microplate Reader (Molecular Devices) and protein concentration of the individual samples was calculated based on the BSA Standards. Once protein concentration was determined, protein suspension containing 40 µg of protein was mixed 1:1 with 2x Sodium dodecyl sulfate (SDS) loading dye (62.5mM Tris, 10% Glycerol, 5% β-mercaptoethanol, 80mM SDS, 1.5mM bromophenol blue), boiled at 95 °C for 5 min, separated by SDS-PAGE and electrophoretically transferred onto PVDF membranes (Merck, Cat #IPVH00010). Membranes were blocked with 5% skim milk (Sigma Aldrich, Cat #70166) in TBS (50mM Tris HCl pH 7.6, 150mM NaCl) containing 0.1% Tween-20 (TBS-T; Sigma Aldrich, Cat #P7949) and were incubated o/n at 4 °C with primary antibodies (Table 7) diluted accordingly in TBS-T containing 2.5% milk. The following day membranes were washed 3x 5 min with TBS-T and were then incubated with Peroxidase-conjugated secondary antibodies (Table 8). Membranes were washed 6x 5min with TBS-T and incubated for 1 min with Pierce ECL Western Blotting Substrate (ThermoScientific, Cat #32209). Signal was detected with

ChemiDoc Imaging System (BioRad, Cat #12003153) and analyzed with Image Lab Software (BioRad, Cat #110000076953). Protein signal was normalized with the signal of β -actin.

2.8 Immunohistochemistry

For immunohistochemistry on fixed tissue, animals were sacrificed under deep CO₂-induced anesthesia, brains were dissected quickly, collected in ice-cold 1x PBS, fixed for 4 h in 4% PFA in 1x PBS at 4 °C and cryopreserved in 20% sucrose in 1x PBS o/n at 4 °C. The next day the brains were embedded in OCT and stored at -80 °C. Coronal sections were prepared at 14 μ m with a cryostat, collected on Superfrost Plus glass slides and stored at -80 °C. Before staining the sections were thawed at RT for 30 min and rehydrated 3x 5min with 1x PBS. Sections were covered with 10mM citrate buffer (pH 6.0) and heat-induced antigen retrieval was performed for 2 min in a steamer. After a 2 min cool-down period, sections were washed with 1x PBS for 5 min and permeabilized 2x 5 min with 1x PBS containing 0.1% Triton[®]-X100 (0,1% PBT-X; AppliChem, Cat #A4975). Sections were blocked for 1h with 10% horse serum (HS; Thermofisher Scientific, Cat #26050088) in 0,1% PBT-X at RT and then incubated o/n at 4 °C with primary antibodies (Table 7) in 0,1% PBT-X containing 5% HS. The following day the sections were washed 3x 10 min with 0,1% PBT-X and then incubated for 90 min at RT with fluorophore-conjugated secondary antibodies (Table 8) and 4',6-Diamidino-2-phenylindole (DAPI; 1:5000; Invitrogen, Cat #D1306) in 0,1% PBT-X containing 5% HS. Finally, the sections were washed 3x 5 min with 0,1% PBT-X and rinsed in milliQ-H₂O. Slides were mounted with Shandon Immu-Mount and covered with glass coverslips.

For immunohistochemistry on unfixed tissue, animals were sacrificed under deep CO₂-induced anesthesia, brains were dissected quickly, collected in ice-cold 1x PBS and cryopreserved in 20% sucrose in 1x PBS o/n at 4 °C. The next day the brains were embedded in OCT compound and stored at -80 °C. Coronal sections were prepared at 14 μ m with a cryostat, collected on Superfrost Plus glass slides and stored at -80°C. Before staining, the sections were thawed at RT for 30 min, fixed with 4% PFA in 1x PBS for 20 min, washed 3x 10 min with 1x PBS, permeabilized with 0.2% PBT-X for 2 h at RT and blocked with 10% fetal bovine serum (FBS; Sigma Aldrich, Cat #12133C) in 0.1% PBT-X for 1 h at RT. Sections were then incubated o/n at 4 °C with primary antibodies (Table 7) in 0,1% PBT-X containing 5%

FBS. The following day the sections were washed 3x 10 min with 0,1% PBT-X and then incubated for 90 min at RT with fluorophore-conjugated secondary antibodies (Table 8) and DAPI (1:5000) in 0,1% PBT-X containing 5% FBS. Finally, the sections were washed 3x 5 min with 0,1% PBT-X and rinsed in milliQ-H₂O. Slides were mounted with Shandon Immu-Mount and covered with glass coverslips.

Table 7. List of Primary antibodies.

Targeted molecule	Host	Application	Dilution	Company	Cat #
β-actin	Mouse	WB	1:5000	Sigma	A5441
Bcl11b	Guinea pig	IHC (fixed)	1:1000	Charles Rivers	Custom; Simon et al., 2012
C1ql2	Rabbit	IHC (fixed&unfixed)	1:1000	Invitrogen	PA5-63504
		WB	1:500		
C1ql2	Rabbit	IHC (fixed&unfixed)	1:500	Sigma	HPA057934
		WB	1:500		
C1ql3	Rabbit	IHC (fixed)	1:500	Biozol	bs-9793R
GFP	Chicken	IHC (fixed)	1:2000	Sigma	Ab13970
		ICC	1:2000		
Homer1	Guinea pig	IHC (unfixed)	1:250	Synaptic Systems	160004
Myc-tag	Rabbit	ICC	1:1000	Abcam	ab9106
Synaptopodin	Rabbit	IHC (unfixed)	1:250	Synaptic Systems	163002
vGlut1	Guinea pig	ICC	1:250	Synaptic Systems	35311
vGlut1	Mouse	IHC (unfixed)	1:100	Synaptic Systems	135304
ZnT3	Rabbit	IHC (unfixed)	1:250	Synaptic Systems	197003

2.9 Transmission electron microscopy

Animals were sacrificed by CO₂-inhalation and quickly perfused transcardially with 0.9% NaCl for 1 min followed by a fixative solution containing 1.5% glutaraldehyde (Carl Roth GmbH, Cat #K028.2) and 4% PFA in 0.1M PB pH 7.2 for 13 minutes. Brains were dissected and placed in fixative solution for 4 h at 4 °C, washed 6x 10 min with 0.1M PB pH 7.2 and immersed in 0.1M PB containing 0.05% NaN₃. The brains were then sent to Prof. Dr. Bernd Heimrich and Sigrun Nestel at the Institute of Anatomy and Cell Biology, Albert-Ludwigs-University, Freiburg (Germany), where ultrathin sections of 60 nm were prepared, stained with lead citrate and imaged using the transmission electron microscope LEO 906 (Zeiss) with the sharp-eye 2k CCD camera. Images were processed with ImageSP (Tröndle, Germany). Measurements for the perimeter, area, number of contacting postsynaptic spines, number and length of synaptic profiles, number and number of folds of postsynaptic SA were taken. Synapse score (De Bruyckere et al., 2018) was calculated according to the following criteria: 0-5 vesicles above the active zone = 0; 5-20 vesicles = 1; small group of vesicles ($\leq 200000 \text{ nm}^2$) with distance between density and closest vesicle $> 100 \text{ nm}$ = 2; small group of vesicles ($\leq 200000 \text{ nm}^2$) with distance between density and closest vesicle $\leq 100 \text{ nm}$ = 3; big group of vesicles ($> 200000 \text{ nm}^2$) with distance between density and closest vesicle ($> 100 \text{ nm}$) = 4; big group of vesicles ($> 200000 \text{ nm}^2$) with distance between density and closest vesicle $\leq 100 \text{ nm}$ = 5. Vesicles with a distance $\leq 5 \text{ nm}$ from the plasma membrane were considered docked (Vandael et al., 2020; Kusick et al., 2022).

Table 8. List of Secondary antibodies

Description	Dilution	Company	Cat #
Alexa Fluor® 488-AffiniPure Donkey Anti-Chicken IgY (IgG)	1:500	Dianova	703-545-155
Cy™3-conjugated AffiniPure Donkey Anti-Guinea Pig IgG	1:500	Dianova	706-165-148
Cy™3-conjugated AffiniPure Donkey Anti-Mouse IgG	1:500	Dianova	715-165-151
Cy™3-conjugated AffiniPure Donkey Anti-Rabbit IgG	1:500	Dianova	711-165-52
Cy™5-conjugated AffiniPure Donkey Anti-Guinea Pig IgG	1:500	Dianova	706-175-148
Peroxidase-AffiniPure Donkey Anti-Mouse IgG	1:500	Dianova	715-035-150
Peroxidase-AffiniPure Donkey Anti-Rabbit IgG	1:500	Dianova	711-035-152

2.10 DNA constructs

C1ql2 was cloned from mouse cDNA and ligated in pGEM-Teasy (Promega, Cat. #A1360) by Jaqueline Andratschke. For expression of C1ql2, C1ql2-pGEM-Teasy was used as template. *C1ql2* was cloned, a 6xHis-myc tag was added to the N-terminus, a stop codon was introduced directly after *C1ql2* and the construct was ligated into the pSecTag2A vector (Invitrogen, Cat # V90020) in frame with the N-terminal IgK signalling sequence. The same strategy was used for the assembly of the expression vector for *C1ql2.K262E* after the mutagenesis (see section 2.13). pSecTag2A was used for control experiments. pSyn5-GFP-Nrxn3 α (25b+), pSyn1-NLS-GFP-Cre and pSyn1-NLS-GFP-Cre^{Y324F} were provided by Dr. Carsten Reißner and Prof. Dr. Markus Missler, Institute of Anatomy and Molecular Neurobiology, University of Münster, Münster (Germany).

2.11 Structural protein modelling

The modelling of C1ql2 was done with the help of Dr. Carsten Reißner from the Institute of Anatomy and Molecular Neurobiology, University of Münster, Münster (Germany). The crystal structure of trimeric C1q-domains of mouse C1ql2 (Ressl et al., 2015) was used and an electrostatic surface map of the trimer was calculated using APBS (Jurrus et al., 2018). Potential electrostatic binding sites to splice insert 25b of Nrxn3 α were predicted. The K262E mutation was introduced using FoldX (foldxsuite.crg.eu) and was chosen in order to generate a negatively charged surface that would potentially be repulsive to Nrxn3 α binding. Final models were visualized with PyMOL (pymol.org).

2.12 C1ql2 mutagenesis

For the introduction of the K262E point mutation, C1ql2-pGEM-Teasy was used as template. Primers were designed with NEBaseChanger (<http://nebasechanger.neb.com/>) (For: 5'-*agaaCTGGACGCGGGAAGGCT*-3'; Rev: 5'-*acgtaGACTTCATCGCCTGAATCCAGGTG*-3';

Eurofins), and mutation was introduced with the Q5 Site-Directed Mutagenesis Kit (New England Biolabs, Cat. #E0554S) according to the manufacturers protocol.

2.13 Primary Hippocampal Cultures

Hippocampi were dissected from P0 mice in HBSS media (Gibco, Cat #14170-088) and transferred on ice in tubes containing HBSS. Once all pups were dissected, the hippocampi were washed 3x with HBSS and then digested for 15 min with HBSS containing 0.1% Trypsin (Gibco, Cat #15090046) in a water bath at 37 °C. The hippocampi were transferred in new tubes containing prewarmed at 37°C MEM media (Gibco, Cat #31095-029) supplemented with 0.6% glucose, 10% FBS, 1% penicillin/streptomycin (Gibco, Cat # 15140122). 4 U/mL DNaseI (Invitrogen, Cat #18047019) was added and the tissue was triturated with a polished Pasteur pipette. Cells were seeded at 1.5×10^5 cells/mL on poly-L-Lysin (Sigma-Aldrich, Cat #P2636) precoated coverslips placed inside 12-well plates (Sarsted, Cat #83.3921300). Cultures were kept at 37 °C under 5% CO₂ atmosphere. After 3 h the plating media was replaced with growth medium containing Neurobasal A (Gibco, Cat #10888-022) supplemented with 2% B27 (Gibco, Cat #17504044), 2mM L-Glutamine (Gibco, Cat #25030149), 1% penicillin/streptomycin, 1% N2 (Gibco, Cat #A1370701) and 0.005% NGF (Gibco, Cat #13290010). The day of plating was considered as 0 days *in vitro* (DIV). At DIV3 and DIV7, 80% of the medium was exchanged with fresh growth medium. At DIV9 the medium was exchanged with penicillin/streptomycin-free growth medium and at DIV10 neurons were transfected using Lipofectamine 2000 (Invitrogen, Cat #11668030). A total of 200 µL transfection mix per well was prepared by first mixing 100 µL Opti-MEM (Gibco, Cat #31985062) with 4 µL Lipofectamin 2000 in one tube and 100 µL Opti-MEM with 3 µg DNA in a different tube. After 5 min both volumes were combined and the mixture was incubated for 20 min at RT. The transfection mix was then added dropwise to the neurons. After 3 h of incubation, the medium was exchanged with fresh growth medium.

2.14 HEK293 Cell Culture

Human embryonic Kidney (HEK) 293 cells (ATCC, Cat #PTA-4488) were maintained in DMEM (Gibco, Cat # 31966047) supplemented with 10% FBS and 1% penicillin/streptomycin at 37 °C under 5% CO₂ atmosphere. 1 day before transfections medium was exchanged with penicillin/streptomycin-free medium. Cells were transfected using Lipofectamine 2000 according to the supplier's instructions on the same day the neurons were transfected. Cells were incubated for at least 24 h before being used in co-culture experiments.

2.15 Neuronal and HEK293 co-culture and immunostaining

Transfected HEK293 cells were washed, dissociated with 0.25% Trypsin, washed and resuspended in neuronal growth medium. 15×10^3 cells were added in each well containing DIV11 transfected neurons. HEK293 cells were co-cultured with the hippocampal primary neurons 2 days (DIV13 for neurons) before proceeding with immunostaining. Coverslips with cultured neurons and HEK293 cells were first fixed with 4% PFA in 1x PBS for 10 min at 4 °C, then washed 3x with 1 mL 1x PBS and blocked with 10% HS in 0.1% PBT-X for 1 h at RT. The cells were incubated o/n at 4 °C with primary antibodies (Table 7). The next day the cells were washed 3x 5 min with 1x PBS and incubated for 90 min at RT with fluorophore-conjugated secondary antibodies (Table 8) and DAPI (1:5000) in 0,1% PBT-X containing 5% HS. Cells were washed 3x 5 min with 1x PBS, rinsed with milliQ-H₂O and mounted on glass slides with Shandon Immu-Mount.

2.16 Image acquisition and analysis

Sectioned hippocampal tissue used for mRNA *in situ* Hybridization was examined and imaged with a DMI6000B microscope (Leica), equipped with a DFC425 C camera (Leica), and using Leica Application Suite V3 Software (Leica). Images were acquired with a 20x objective. Sectioned hippocampal tissue stained with fluorescent probes was examined with a TCS SP5II confocal microscope (Leica) using LAS-X software (Leica). Overview images

of the hippocampus were acquired with a 20x objective. Images for synapse numbers quantification were acquired with a 40x objective at x2 zoom. Images for C1ql2 fluorescence intensity quantification were acquired with a 40x objective. Acquisition settings were kept constant for every sample and condition. ROI selection, intensity measurements and image processing were done on Fiji (Schindelin et al., 2012). HEK293 cells co-cultured with primary neurons were examined and imaged with a TCS SP8 confocal microscope (Leica) using LAS-X software. Images were acquired with a 40x objective at 4x zoom, with constant acquisition settings for every sample and condition. The images were analyzed on Fiji. Transfected HEK293 cells were masked and the area of each mask covered by the chosen stain was measured.

2.17 Quantification and statistical analysis

Data analysis was conducted blind to the experimental treatment. Statistical analysis and graph generation was done using Python 3. If samples met the criteria for normality, two-tailed unpaired t-test to compare two groups and one-way ANOVA for multiple groups were used. For non-normally distributed data, Mann-Whitney u-test was used. Two-way ANOVA was used for examining the influence of two different categorical independent variables. For significant ANOVAs, a post hoc Tukey's multiple-comparisons (Tukey's PHC) test to compare groups (structural and expression data) or a post hoc Bonferonni's comparison test (electrophysiological data) was used. Data are presented as mean±SEM. Significance levels were set as indicated in figures: ns, not significant; *p<0.05; **p<0.01; ***p<0.001.

3 Results

3.1 Rescue of C1ql2 expression in dentate granule cells of *Bcl11b* mutants

3.1.1 AAV-mediated reintroduction of C1ql2 restores expression level in dentate granule cells

In the present study, I used *Bcl11b*^{flox/flox}; *CamKIIa*CreER^{T2} mice that offer a tamoxifen-inducible, forebrain-specific, conditional knock-out (cKO) of *Bcl11b* and were previously described in De Bruyckere et al. (2018). To study the mossy fiber synapses (MFS) after adult ablation of *Bcl11b*, tamoxifen was administered for 5 consecutive days to 2 months old *Bcl11b* cKO mice and control littermates. Previous work from our group has shown that the synaptic organizer C1ql2 is a direct transcriptional target of Bcl11b in the adult dentate granule cells (DGCs). Upon *Bcl11b* deletion, C1ql2 expression is downregulated (De Bruyckere et al., 2018). Two months post mutation induction (m.p.i.) C1ql2 transcript levels, as seen with mRNA ISH on hippocampal sections and quantified by quantitative real-time PCR (qPCR; Figure 6a-b; Control: 1 ± 0.308 ; *Bcl11b* cKO: 0.129 ± 0.003 , mean \pm SEM;), and protein levels, as seen with immunostainings (Figure 6c) were significantly reduced (Koumoundourou et al., 2023). To test whether C1ql2 is also a functional target of Bcl11b at MFS, I reintroduced C1ql2 in the DGCs of *Bcl11b* cKOs by stereotaxically injecting an adeno-associated virus (AAV) expressing GFP and C1ql2. I then examined the MFS for potential improvement of the *Bcl11b* mutant phenotype that included loss of MFS, loss of ultrastructural complexity of mossy fiber boutons (MFBs), misdistribution of synaptic vesicles (SVs) and loss of long-term potentiation (LTP) (De Bruyckere et al., 2018). To exclude that any observed changes in the MFS was due to the stereotaxic surgeries or the virus, I injected into the DG of both control and *Bcl11b* cKO mice an AAV with the same backbone, expressing only GFP (Figure 7; Koumoundourou et al., 2023). AAVs were injected 2 weeks after *Bcl11b* KO induction, a time interval sufficient to allow for the *Bcl11b* mutant phenotype to develop (De Bruyckere et al., 2018). The brains were examined 6 weeks post transduction. AAV-mediated expression of C1ql2 in the DG of *Bcl11b* cKOs fully restored C1ql2 protein levels (Figure 8a-b; Control+EGFP: 1 ± 0.216 , *Bcl11b* cKO+EGFP: 0.2 ± 0.023 ,

Bcl11b cKO+EGFP-2A-C1ql2: 2.44 ± 0.745 , mean \pm SEM; Koumoundourou et al., 2023). Expression pattern of exogenous C1ql2 was similar to that observed in control animals, with C1ql2 localizing at the cell bodies of DGCs and at the stratum lucidum (SL) of CA3, where the MFS are located (Figure 8c; Koumoundourou et al., 2023). To ensure that exogenous C1ql2 was targeted to the MFS, I performed immunohistological stainings for the vesicular glutamate receptor 1 (vGlut1) and Homer scaffold protein 1 (Homer1), that serve as markers for pre- and postsynapse respectively, and could verify that all three proteins colocalized (Figure 8d; Koumoundourou et al., 2023).

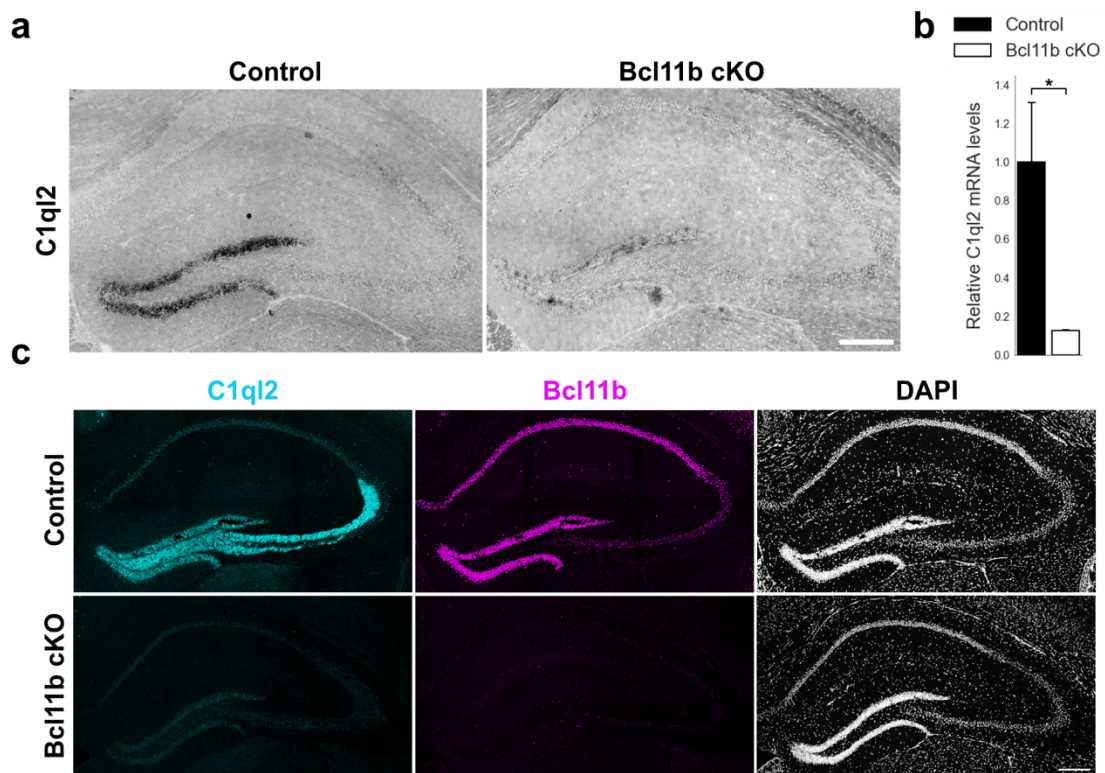


Figure 6. C1ql2 expression in hippocampus upon *Bcl11b* ablation. a) mRNA *in situ* hybridization of *C1ql2* on hippocampal sections. Scale bar: 200 μ m. b) Quantification of *C1ql2* mRNA levels in DGCs. n=4. All data are presented as means; error bars indicate SEM. Unpaired t-test. *p=0.03. c) Hippocampal sections stained for C1ql2 (cyan) and Bcl11b (magenta). Scale bar: 200 μ m. (Adapted from Koumoundourou et al., 2023; Published under CC BY 4.0, <https://creativecommons.org/licenses/by/4.0/>).

3.1.2 Reintroduction of C1ql2 in dentate granule cells of *Bcl11b* mutants rescues synaptic vesicle recruitment at the mossy fiber synapse

Bcl11b cKOs are characterized by misdistribution of SVs, with a smaller number of SVs localizing in the vicinity of the active zones (AZs; De Bruyckere et al., 2018). I used transmission electron microscopy (TEM) to study the distribution of SVs in proximity to the AZs. A scoring system was used for rating synapses based on the number of SVs and their distance from the AZ within the readily releasable pool margins, with higher in score corresponding to more vesicles in closer proximity to the AZ (De Bruyckere et al., 2018). The injection of the EGFP-expressing AAV had no effect on the previously observed phenotype (Figure 9; Koumoundourou et al., 2023). Reintroduction of C1ql2 in *Bcl11b* cKO DGCs was able to fully rescue the SV distribution to control values, as revealed by the average synapse score (Figure 9a-b; Control+EGFP: 3.4 ± 0.012 , *Bcl11b* cKO+EGFP: 2.96 ± 0.037 , *Bcl11b* cKO+EGFP-2A-C1ql2: 3.47 ± 0.043 , mean \pm SEM; Koumoundourou et al., 2023). By analyzing the relative frequency of the individual synapse scores, I was able to show that *Bcl11b* ablation led to an increase in the number of inactive synapses characterized by a synapse score of 0 and reduction of the number of SVs in close proximity to the AZs revealed by a shift to smaller synapse scores. C1ql2 reintroduction restored both the number of active synapses as well as increased the size of the SV pool localizing in close proximity to the active synapses (Figure 9c; Koumoundourou et al., 2023).

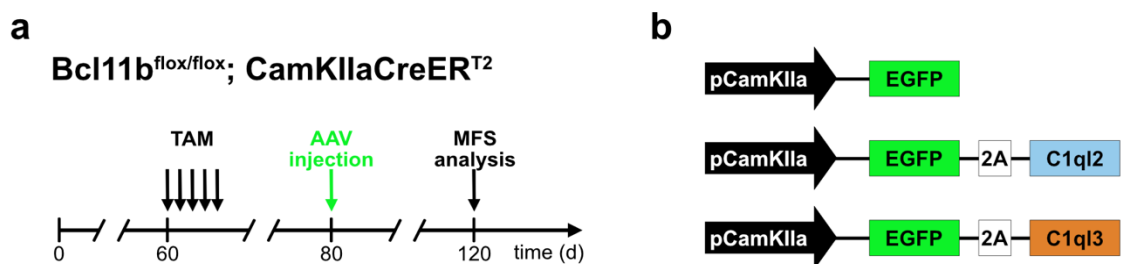


Figure 7. Experimental design for C1ql2 expression rescue. a) Animal model and chronograph of treatments for induction of *Bcl11b* mutation, AAV injection and brain analysis. b) AAV constructs used for rescue of C1ql2 expression and control vectors. TAM: Tamoxifen. (Adapted from Koumoundourou et al., 2023; Published under CC BY 4.0, <https://creativecommons.org/licenses/by/4.0/>).

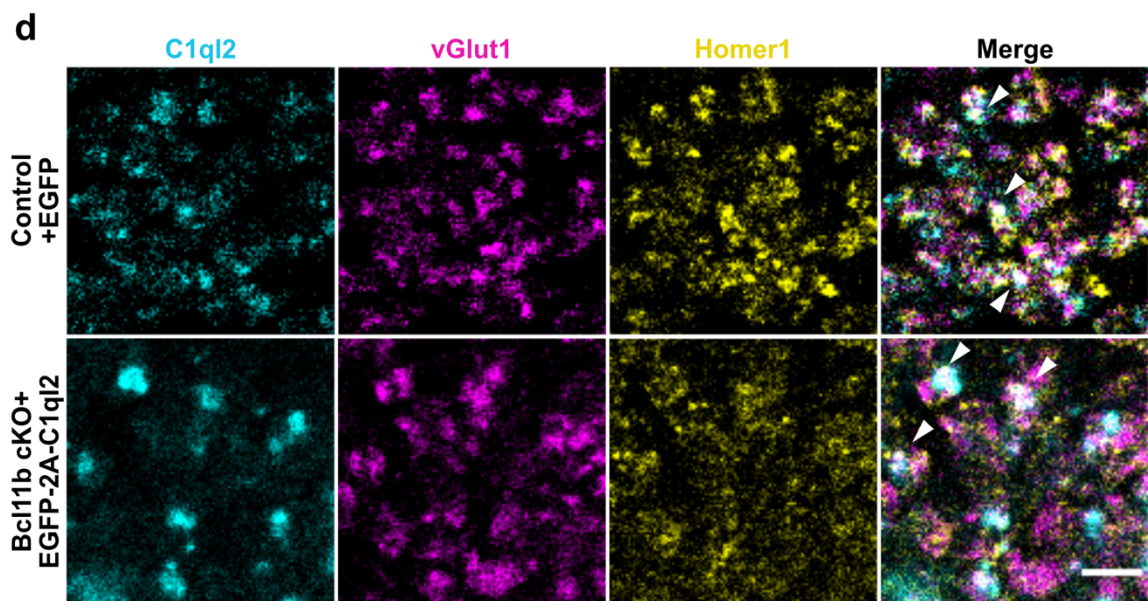
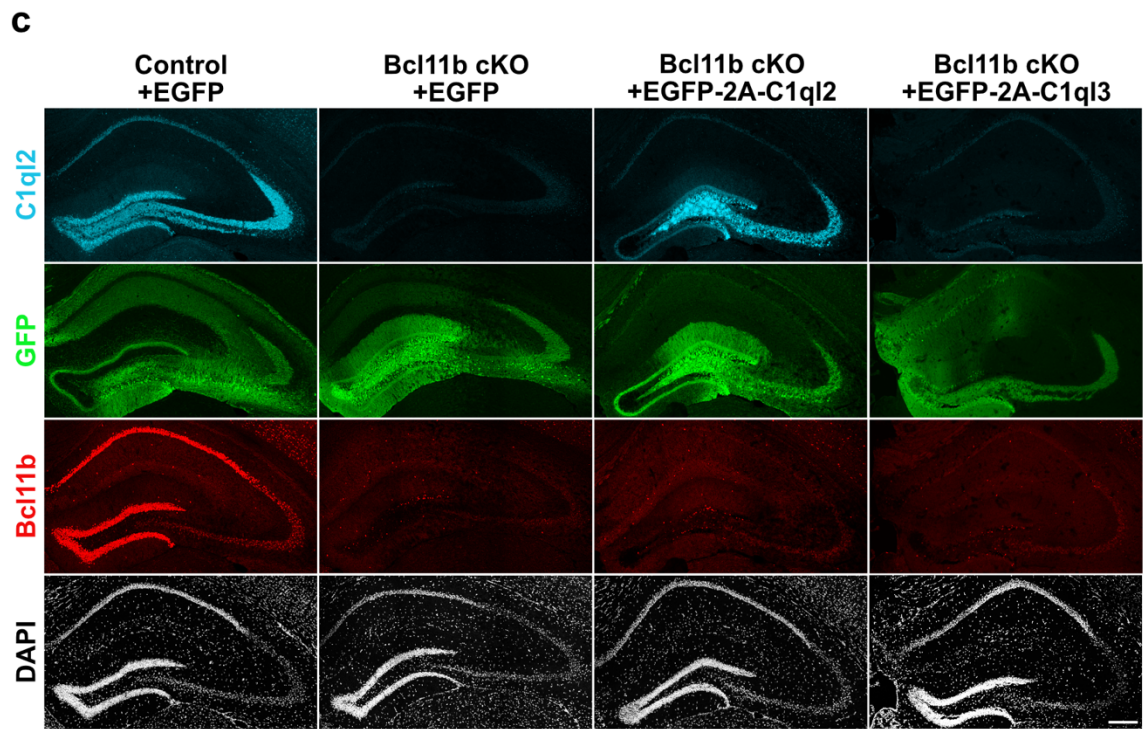
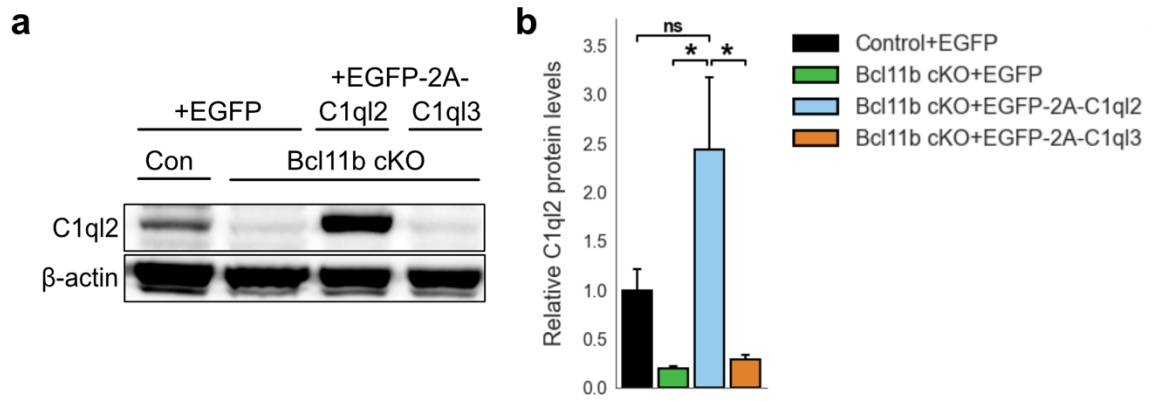


Figure 8. AAV-mediated expression of C1qI2 in *Bcl11b* cKO DGCs restores C1qI2 levels and expression pattern. a) Western blot and b) quantification of C1qI2 protein levels in hippocampal homogenates. n=3. All data are presented as means; error bars indicate SEM. Two-way ANOVA and Tuckey's PHC. *Bcl11b* cKO+EGFP-2A-C1qI2 vs. *Bcl11b* cKO+EGFP: *p=0.015; *Bcl11b* cKO+EGFP-2A-C1qI2 vs. *Bcl11b* cKO+EGFP-2A-C1qI3: *p=0.019; ns, not significant. c) Hippocampal sections stained for C1qI2 (cyan), GFP (green) and *Bcl11b* (red). Scale bar 200 μ m. d) Images from SL of CA3 stained for C1qI2 (cyan), vGluT1 (magenta) and Homer1 (yellow). Arrowheads indicate colocalization of all three proteins. Scale bar: 15 μ m. (Adapted from Koumoundourou et al., 2023; Published under CC BY 4.0, <https://creativecommons.org/licenses/by/4.0/>).

It was previously shown that C1qI2 acts at the MFS together with C1qI3, another member of the C1qI-subfamily. Conditional deletion of either *C1qI2* or *C1qI3* had no overt phenotype at the MFS, while deletion of both resulted in dysfunction of the MFS suggesting the two proteins to have compensatory functions (Matsuda et al., 2016). To that end I examined the expression levels of C1qI3 in my system. qPCR and immunohistochemistry revealed that expression of C1qI3 was unaltered in *Bcl11b* cKOs, revealing that *Bcl11b* controls the transcription of specifically *C1qI2* but not *C1qI3* (Figure 10; Control+EGFP: 1 ± 0.022 , *Bcl11b* cKO+EGFP: 1.09 ± 0.126 , *Bcl11b* cKO+EGFP-2A-C1qI2: 0.87 ± 0.146 , mean \pm SEM; Koumoundourou et al., 2023). To investigate whether C1qI2 specifically was regulating the SV distribution in a *Bcl11b* cKO background, I overexpressed C1qI3 in the DG of *Bcl11b* cKOs (Figure 7; Koumoundourou et al., 2023) and tested whether the excess amount of C1qI3 could compensate for the function of C1qI2 and rescue the SV distribution. Overexpression of C1qI3 did not alter expression of C1qI2 (Figure 8b-c; *Bcl11b* cKO+EGFP-2A-C1qI3: 0.29 ± 0.042 , mean \pm SEM; Koumoundourou et al., 2023). Moreover, C1qI3 overexpression in *Bcl11b* cKO DGCs had no effect on the average synapse score of MFS (Figure 9; *Bcl11b* cKO+EGFP-2A-C1qI3: 2.97 ± 0.062 , mean \pm SEM; Koumoundourou et al., 2023).

To further understand the role of C1qI2 in the recruitment of SVs at the MFS, I quantified the number of docked vesicles on the AZs. Docking is the process during which the vesicle and pre-synaptic membrane line up in a fusion-ready state. Here, only SVs with a distance ≤ 5 nm from the plasma membrane were considered docked (Kusick et al., 2022; Vandael

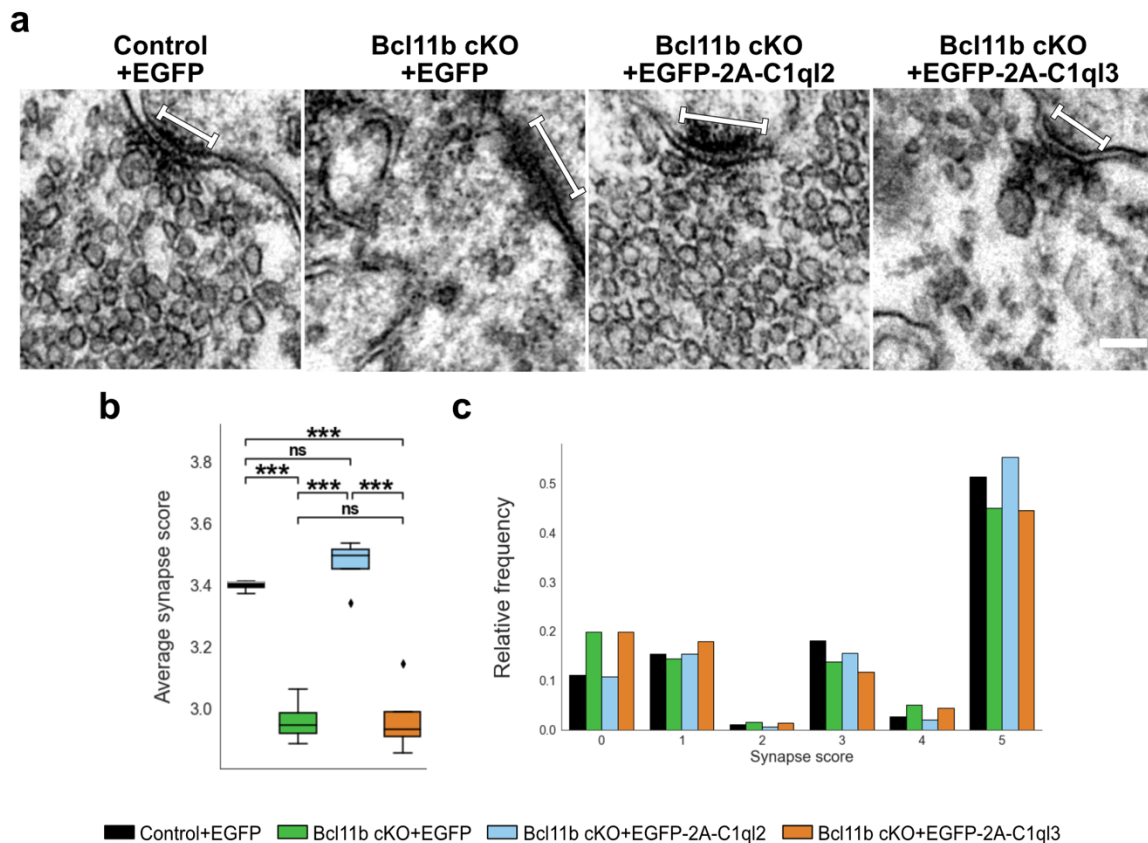


Figure 9. Reintroduction of C1ql2 in *Bcl11b* cKO DGCs rescues synaptic vesicle distribution. a) Electron microscope images of MFS (white bar, presented on the postsynaptic side) and the SVs distributed in the proximity of the AZ. Scale bar: 100 nm. b) Average synapse score. Control+EGFP, n=3; Bcl11b cKO+EGFP, Bcl11b cKO+EGFP-2A-C1ql2, Bcl11b cKO+EGFP-2A-C1ql3, n=4. Two-way ANOVA and Tuckey's PHC. Control+EGFP vs. Bcl11b cKO+EGFP: ***p=0.0002, and vs. Bcl11b cKO+EGFP-2A-C1ql3: ***p=0.0003; Bcl11b cKO+EGFP-2A-C1ql2 vs. Bcl11b cKO+EGFP and vs. Bcl11b cKO+EGFP-2A-C1ql3: ***p<0.0001; ns, not significant. c) Relative frequency of synapse scores. (Adapted from Koumoundourou et al., 2023; Published under CC BY 4.0, <https://creativecommons.org/licenses/by/4.0/>).

et al., 2020). Conditional deletion of *Bcl11b* significantly reduced the number of docked vesicles per 100 nm of AZ at the MFS when compared to control animals, with both a shift in the number of docked vesicles towards lower values and an increase in the number of AZs with no docked vesicles (Figure 11a-c; Koumoundourou et al., 2023). Reintroduction of C1ql2 fully restored the number of docked vesicles to control levels, while overexpression of C1ql3 did not change this *Bcl11b* mutant phenotype (Figure 11a; Control+EGFP: 0.53 ± 0.098 , Bcl11b cKO+EGFP: 0.24 ± 0.038 , Bcl11b cKO+EGFP-2A-C1ql2: 0.51 ± 0.049 , Bcl11b

cKO+EGFP-2A-C1q13: 0.26 ± 0.041 , mean \pm SEM; Koumoundourou et al., 2023). As larger vesicles could potentially carry and release larger amounts of glutamate, I further measured the diameter of the docked vesicles but found no difference upon *Bcl11b* ablation or after C1q12 reintroduction (Figure 11d; Control+EGFP: 36.39 ± 1.75 , Bcl11b cKO+EGFP: 35.18 ± 1.13 , Bcl11b cKO+EGFP-2A-C1q12: 36.35 ± 1.01 , Bcl11b cKO+EGFP-2A-C1q13: 36.65 ± 0.1 , mean \pm SEM; Koumoundourou et al., 2023).

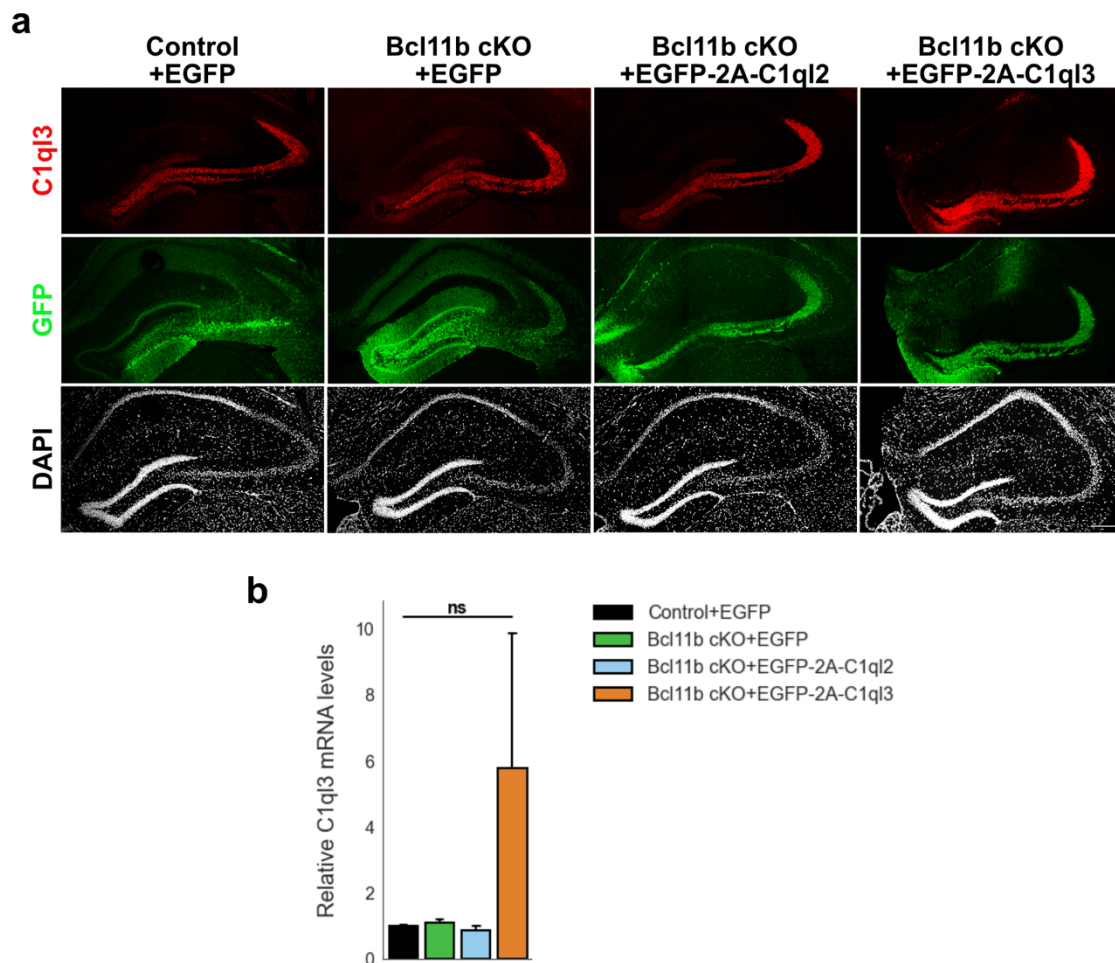


Figure 10. C1q13 expression in DGCs is not altered by *Bcl11b* cKO. a) Hippocampal sections stained for C1q13 (red) and GFP (green). Scale bar 200 μ m. b) Quantification of *C1q13* mRNA levels in DGCs. Control+EGFP, Bcl11b cKO+EGFP, Bcl11b cKO+EGFP-2A-C1q12, n=4; Bcl11b cKO+EGFP-2A-C1q13, n=3. All data are presented as means; error bars indicate SEM. Two-way ANOVA. ns, not significant. (Adapted from Koumoundourou et al., 2023; Published under CC BY 4.0, <https://creativecommons.org/licenses/by/4.0/>).

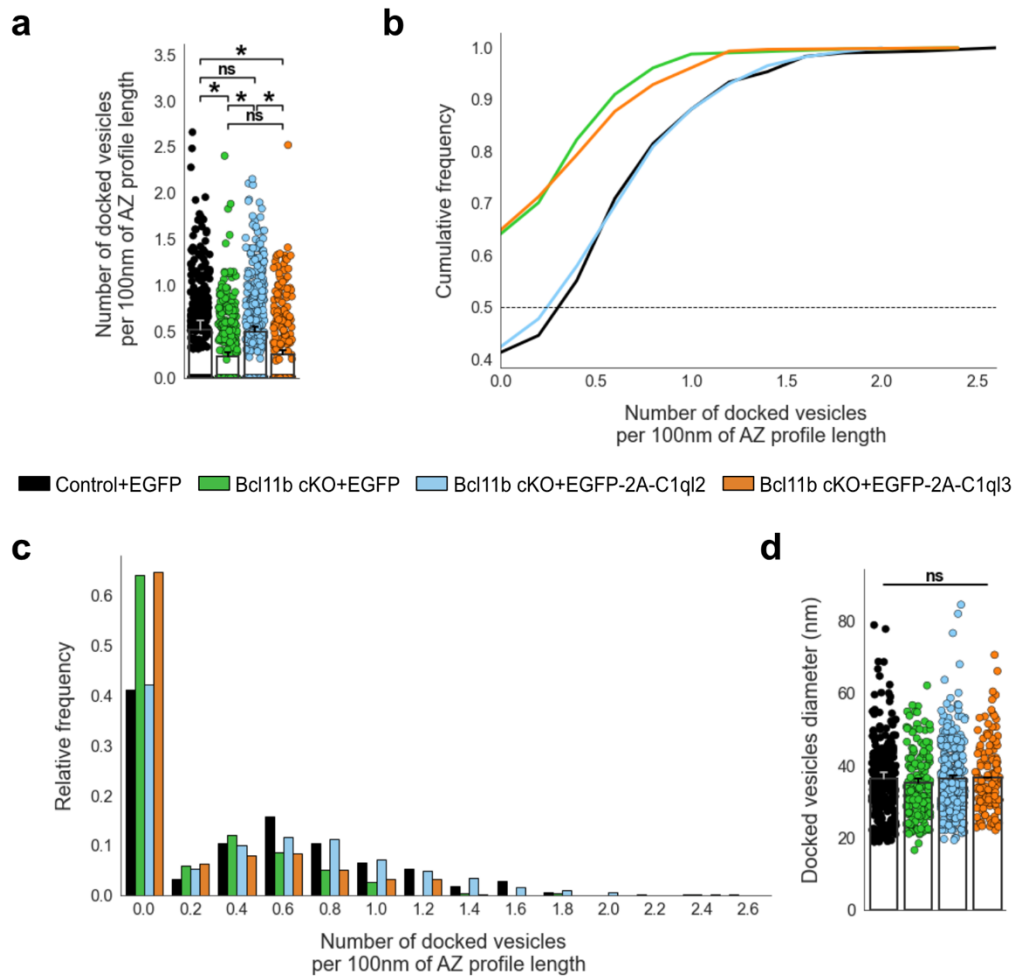


Figure 11. Reintroduction of C1q12 in *Bcl11b* cKO DGCs rescues synaptic vesicle docking. a) Number of docked vesicles per 100 nm AZ profile length. Control+EGFP, Bcl11b cKO+EGFP-2A-C1q13, n=3; Bcl11b cKO+EGFP, Bcl11b cKO+EGFP-2A-C1q12, n=4. All data are presented as means; error bars indicate SEM. Points represent the individual examined AZs and SVs, respectively. Two-way ANOVA and Tuckey's PHC. Control+EGFP vs. Bcl11b cKO+EGFP: *p=0.024, and vs. Bcl11b cKO+EGFP-2A-C1q13: *p=0.045; Bcl11b cKO+EGFP-2A-C1q12 vs. Bcl11b cKO+EGFP: *p=0.026, and vs. Bcl11b cKO+EGFP-2A-C1q13: *p=0.049. b) Cumulative and c) relative frequency of the number of docked vesicles per 100 nm AZ profile length. d) Diameter of docked vesicles. Control+EGFP, Bcl11b cKO+EGFP-2A-C1q13, n=3; Bcl11b cKO+EGFP, Bcl11b cKO+EGFP-2A-C1q12, n=4; Two-way ANOVA. ns, not significant. (Adapted from Koumoundourou et al., 2023; Published under CC BY 4.0, <https://creativecommons.org/licenses/by/4.0/>).

3.1.3 Reintroduction of C1ql2 in dentate granule cells of *Bcl11b* mutants rescues mossy fiber long-term potentiation

Bcl11b is essential for mossy fiber long-term potentiation (MF-LTP), with adult-induced KO of *Bcl11b* leading to a dramatic decline in the MF-LTP (De Bruyckere et al., 2018). To test whether C1ql2 has also a role in the MF-LTP expression, LTP was measured upon reintroduction of C1ql2 in the DGCs of *Bcl11b* cKOs. All LTP experiments and relevant data analyses were performed as part of this study by Märt Rannap from the group of Prof. Dr. Andreas Draguhn at the Institute of Physiology and Pathophysiology, Heidelberg University. LTP was induced at mossy fibers on acute slices with a high-frequency stimulation (HFS). Reintroduction of C1ql2 two weeks after *Bcl11b* mutation induction completely restored the LTP at all time intervals to control levels (Figure 12; 0-10 min: Control+EGFP: 90.4 ± 7.2 , *Bcl11b* cKO+EGFP: 106.1 ± 10.8 , *Bcl11b* cKO+EGFP-2A-C1ql2: 86.5 ± 7.4 , 10-20 min: Control+EGFP: 42.7 ± 3.6 , *Bcl11b* cKO+EGFP: 39.5 ± 4.6 , *Bcl11b* cKO+EGFP-2A-C1ql2: 49.4 ± 5.9 , 20-30 min: Control+EGFP: 52.5 ± 7.6 , *Bcl11b* cKO+EGFP: 24.8 ± 3.2 , *Bcl11b* cKO+EGFP-2A-C1ql2: 47.2 ± 5.7 , 30-40 min: Control+EGFP: 50.1 ± 7.3 , *Bcl11b* cKO+EGFP: 20.3 ± 3.7 , *Bcl11b* Control+EGFP: 52.5 ± 7.6 , *Bcl11b* cKO+EGFP: 24.8 ± 3.2 , *Bcl11b* cKO+EGFP-2A-C1ql2: 47.2 ± 5.7 , 30-40 min: Control+EGFP: 50.1 ± 7.3 , *Bcl11b* cKO+EGFP: 20.3 ± 3.7 , *Bcl11b* cKO+EGFP-2A-C1ql2: 44.9 ± 5.3 , mean \pm SEM; Koumoundourou et al., 2023). C1ql3 overexpression in *Bcl11b* cKO DGCs did not improve the MF-LTP expression at any time-interval highlighting the specificity for this C1ql2 function as well (Figure 12; 0-10 min: Control+EGFP: 90.4 ± 7.2 , *Bcl11b* cKO+EGFP-2A-C1ql3: 104.2 ± 9.9 , 10-20 min: Control+EGFP: 42.7 ± 3.6 , *Bcl11b* cKO+EGFP-2A-C1ql3: 44.4 ± 5.7 , 20-30 min: Control+EGFP: 52.5 ± 7.6 , *Bcl11b* cKO+EGFP-2A-C1ql3: 29.0 ± 2.3 , 30-40 min: Control+EGFP: 50.1 ± 7.3 , *Bcl11b* cKO+EGFP-2A-C1ql3: 22.6 ± 2.4 , mean \pm SEM; Koumoundourou et al., 2023).

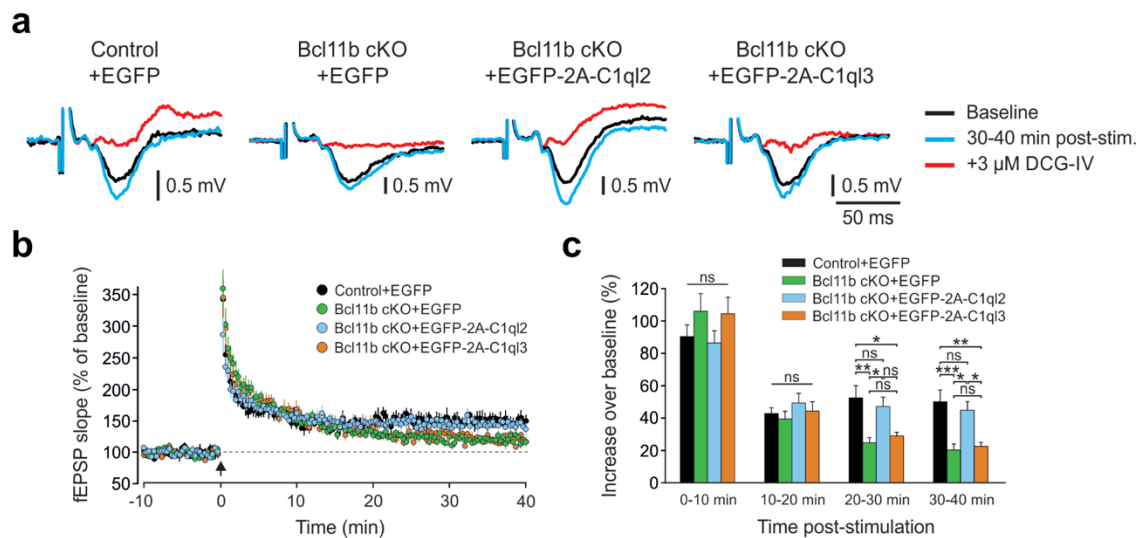


Figure 12. Reintroduction of C1ql2 in *Bcl11b* cKO DGCs rescues long-term potentiation. a) Representative fEPSP traces showing baselines before HFS (black), fEPSP changes 30-40 min after HFS (cyan) and following the application of 3 μ M DCG-IV (red). b) Time course of fEPSP slopes. The black arrow indicates HFS and the dashed line the baseline level. c) Quantification of fEPSP facilitation at four different time intervals after HFS. Changes in fEPSP slope are shown as percentage of the mean baseline fEPSP. Control+EGFP, n=7; Bcl11b cKO+EGFP, Bcl11b cKO+EGFP-2A-C1ql3, n=8; Bcl11b cKO+EGFP-2A-C1ql2, n=6; All data are presented as means; error bars indicate SEM. One-way ANOVA followed by Bonferroni's PHC for each time interval. 20-30 min: Control+EGFP vs. Bcl11b cKO+EGFP: **p=0.002, and vs. Bcl11b cKO+EGFP-2A-C1ql3: *p=0.011; Bcl11b cKO+EGFP-2A-C1ql2 vs. Bcl11b cKO+EGFP: *p=0.023; 30-40 min: Control+EGFP vs. Bcl11b cKO+EGFP: ***p<0.001, and vs. Bcl11b cKO+EGFP-2A-C1ql3: **p=0.002; Bcl11b cKO+EGFP-2A-C1ql2 vs. Bcl11b cKO+EGFP: *p=0.01 and vs. Bcl11b cKO+EGFP-2A-C1ql3: *p=0.0523; ns, not significant. (Adapted from Koumoundourou et al., 2023; Published under CC BY 4.0, <https://creativecommons.org/licenses/by/4.0/>).

3.1.4 Reintroduction of C1ql2 in dentate granule cells of *Bcl11b* mutants does not rescue loss of mossy fiber synapses and of mossy fiber bouton ultrastructural complexity

Conditional deletion of *Bcl11b* in adult DGCs was shown to lead to progressive reduction in the number of MFS and loss of the characteristic structural complexity of MFBs (De Bruyckere et al., 2018). I, therefore, tested whether re-expression of C1ql2 could also rescue these *Bcl11b* mutant phenotypes. The number of the MFS was determined by the colocalization of the pre- and postsynaptic markers for glutamatergic synapses, vGlut1 and Homer1 respectively, at the SL of CA3 (this quantification was performed by Dr. De Bruyckere). Reintroduction of C1ql2 in *Bcl11b* cKO DGCs did not reverse nor slow down the loss of MFS that was on the same level as observed in *Bcl11b* cKOs (Figure 13a; Control+EGFP: 90.65 ± 8.25 , *Bcl11b* cKO+EGFP: 60.68 ± 4.62 , *Bcl11b* cKO+EGFP-2A-C1ql2: 56.84 ± 6.99 , mean \pm SEM; Koumoundourou et al., 2023). Furthermore, the structural complexity of the MFBs, quantified as the ratio of the MFB perimeter to the corresponding area on TEM images, did not change upon rescue of C1ql2 expression (Figure 13b-c; Control+EGFP: 0.0051 ± 0.00031 , *Bcl11b* cKO+EGFP: 0.0042 ± 0.00014 , *Bcl11b* cKO+EGFP-2A-C1ql2: 0.0037 ± 0.00021 , mean \pm SEM; Koumoundourou et al., 2023).

3.2 Reintroduction of C1ql2 in dentate granule cells of *Bcl11b* mutants increases the number of postsynaptic spines containing a spine apparatus

During the examination of MFS with TEM, I also analyzed the contacting postsynaptic spines for possible changes in their structure. I quantified the number of all contacting spines and of invaginated spines per MFB, the surface area covered by the spines, the number of postsynaptic densities (PSDs) per MFB and the length of the PSDs, but found no difference in *Bcl11b* cKO upon injection of control or C1ql2-expressing virus when compared to control mice (Figure 14; Spines/MFB: Control+EGFP: 5.59 ± 0.3 , *Bcl11b* cKO+EGFP: 5.63 ± 0.56 , *Bcl11b* cKO+EGFP-2A-C1ql2: 5.54 ± 0.23 ; Invaginated spines/MFB: Control+EGFP: 3.89 ± 0.3 , *Bcl11b* cKO+EGFP: 3.55 ± 0.42 , *Bcl11b* cKO+EGFP-2A-C1ql2: 3.14 ± 0.33 ; Average spine surface: Control+EGFP: $209 \pm 12 \times 10^3$, *Bcl11b* cKO+EGFP: $217 \pm 8 \times 10^3$, *Bcl11b* cKO+EGFP-2A-C1ql2: $237 \pm 10 \times 10^3$; PSD/MFB: Control+EGFP: 5.57 ± 0.25 , *Bcl11b* cKO+EGFP: 6.21 ± 0.2 , *Bcl11b*

cKO+EGFP-2A-C1qI2: 6.45 ± 0.38 ; PSD length: Control+EGFP: 166 ± 4 , Bcl11b cKO+EGFP: 156 ± 3 , Bcl11b cKO+EGFP-2A-C1qI2: 168 ± 6 , mean \pm SEM).

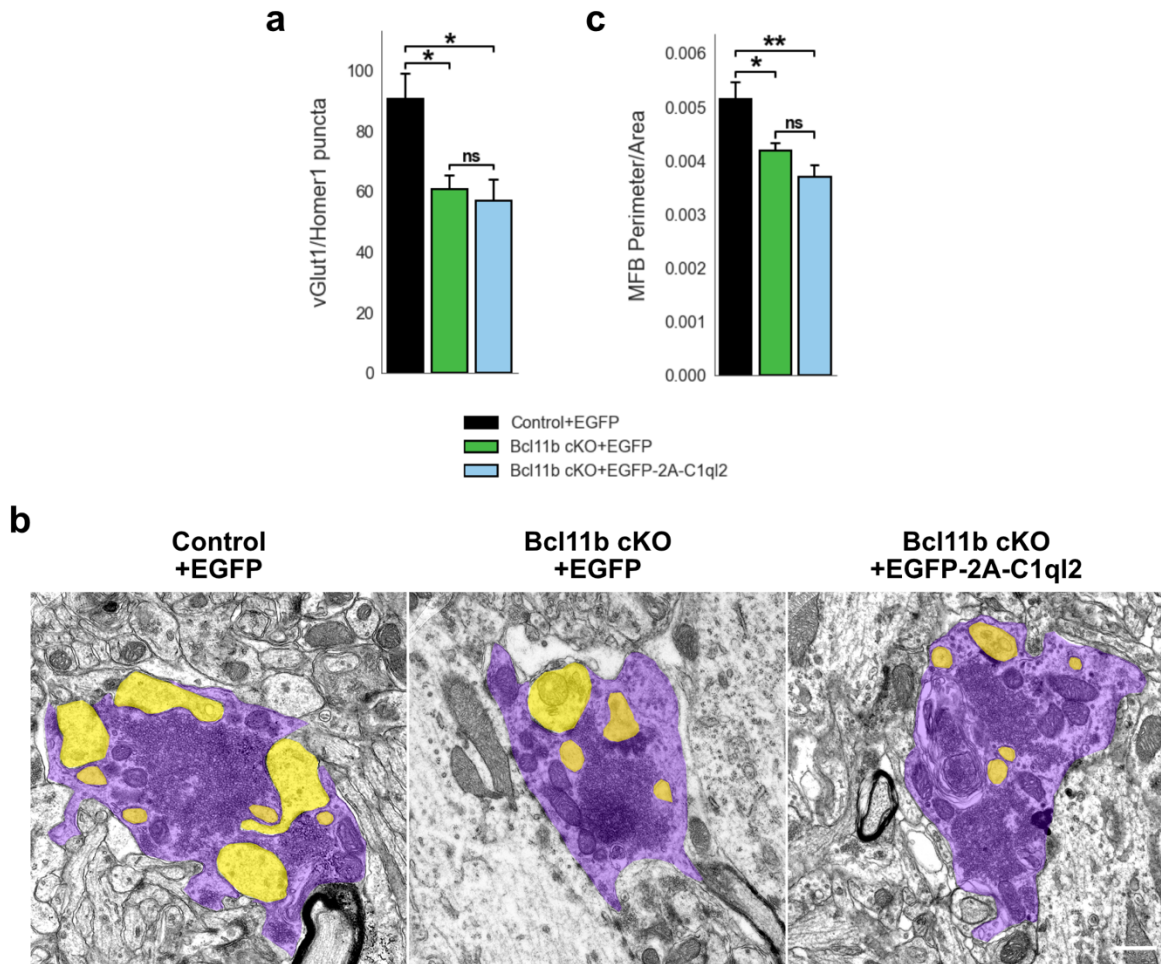


Figure 13. Reintroduction of C1qI2 in *Bcl11b* cKO DGCs does not rescue loss of mossy fiber synapses and mossy fiber bouton complexity. a) vGlut1 and Homer1 double positive puncta in selected CA3 SL ROIs. n=3. All data are presented as means; error bars indicate SEM. Two-way ANOVA and Tuckey's PHC. Control+EGFP vs. Bcl11b cKO+EGFP: *p=0.047, and vs. Bcl11b cKO+EGFP-2A-C1qI2: *p=0.029. b) Electron microscopy images of MFBs (purple) and contacting postsynaptic spines (yellow). Scale bar: 500 nm. c) MFB perimeter-to-area ratio. n=5. All data are presented as means; error bars indicate SEM. Two-way ANOVA and Tuckey's PHC. Control+EGFP vs. Bcl11b cKO+EGFP: *p=0.035, and vs. Bcl11b cKO+EGFP-2A-C1qI2: **p=0.0014; ns, not significant. (Adapted from Koumoundourou et al., 2023; Published under CC BY 4.0, <https://creativecommons.org/licenses/by/4.0/>).

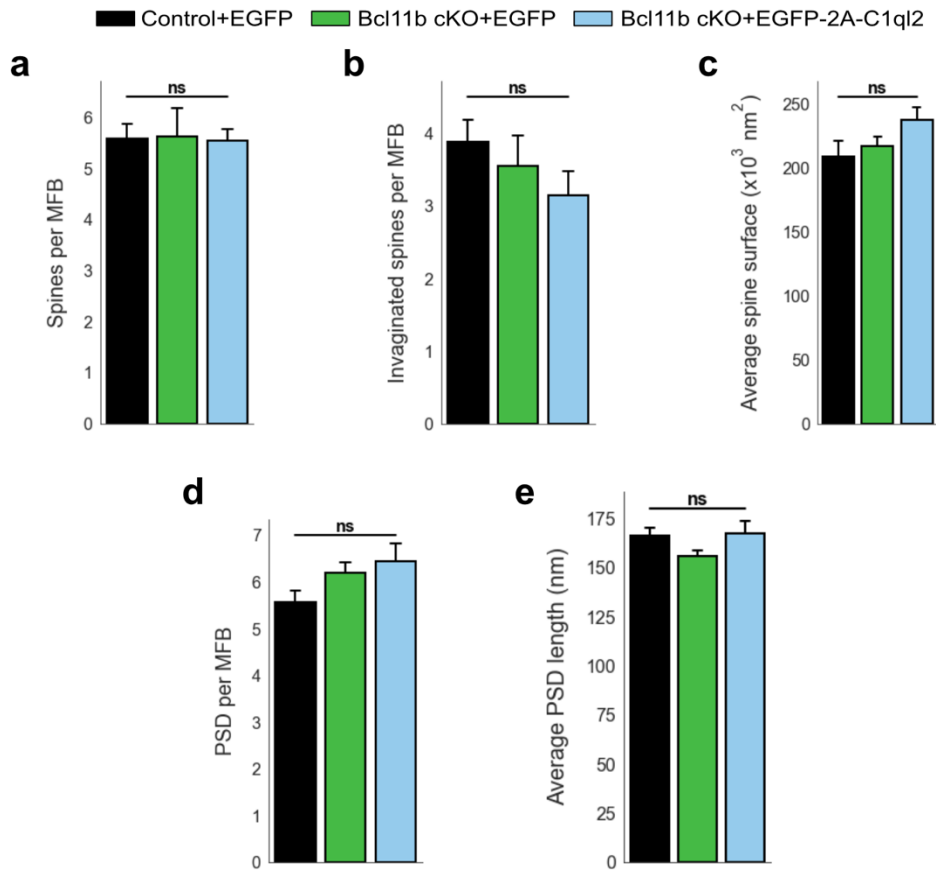


Figure 14. Reintroduction of C1ql2 in *Bcl11b* cKO DGCs has no effect on the number and size of contacted spines and the number and size of postsynaptic densities. a) Average number of spines in contact with a single MFB. b) Average number spines invaginated by a single MFB. c) Average surface area of spines in contact with MFBs. d) Average number of PSDs per MFB. e) Average length of MFS PSDs. For all measurements: Control+EGFP, Bcl11b cKO+EGFP-2A-C1ql2: n=6; Bcl11b cKO+EGFP: n=5. All data are presented as means; error bars indicate SEM. Two-way ANOVA. ns, not significant.

Interestingly, I observed differences in the postsynaptic spine apparatus (SA) of *Bcl11b* cKOs upon reintroduction of C1ql2. The SA is a specialized form of smooth endoplasmic reticulum that is found in subpopulations of mature dendritic spines of cortical and hippocampal neurons (Spacek & Harris, 1997) and has been suggested to act as a reservoir of neurotransmitter receptors (Racca et al., 2000), have a role in local protein synthesis and trafficking (Pierce et al., 2000) and to regulate intraspinal calcium (Segal et al., 2010). Reintroduction of C1ql2 in *Bcl11b* cKO DGCs resulted in an increase in the number of the spines in contact with MFBs containing a SA compared to control animals. Importantly,

ablation of *Bcl11b* did not show changes in the number of contacting spines containing a SA compared to controls. Overexpression of C1ql3 showed no effect on the number of spines containing a SA (Figure 15a-b; Control+EGFP: 10.54 ± 1.83 , *Bcl11b* cKO+EGFP: 13.7 ± 1.7 , *Bcl11b* cKO+EGFP-2A-C1ql2: 18.38 ± 1.92 , *Bcl11b* cKO+EGFP-2A-C1ql3: 11.4 ± 1.96 , mean \pm SEM). Moreover, the SA of *Bcl11b* cKOs with a rescued C1ql2 expression presented with a tendency for increased complexity, quantified as the percentage SA with ≥ 3 dense plates, that was however not statistically significant. *Bcl11b* cKOs did not show any changes in the SA complexity compared to controls. Furthermore, C1ql3 overexpression in *Bcl11b* cKO DGCs had no effect on the SA complexity (Figure 15c; Control+EGFP: 6.53 ± 1.49 , *Bcl11b* cKO+EGFP: 8.65 ± 1.92 , *Bcl11b* cKO+EGFP-2A-C1ql2: 15.4 ± 3.93 , *Bcl11b* cKO+EGFP-2A-C1ql3: 8.5 ± 2.93 , mean \pm SEM). Synaptopodin (Synpo), an actin binding protein, is an essential component of the SA (Deller et al., 2010). To further corroborate that C1ql2 re-expression had an effect on postsynaptic SA, I quantified the fluorescent intensity of Synpo at selected ROIs at the SL of CA3. Reintroduced C1ql2 in *Bcl11b* cKO DGCs tended to increase, however not significantly, the amount of Synpo at the postsynaptic spines of the DG-CA3 connections compared to control and *Bcl11b* cKO animals. No effect on Synpo fluorescence intensity was observed upon *Bcl11b* cKO (Figure 15d-e; Control+EGFP: $30.95 \pm 4.2 \times 10^3$, *Bcl11b* cKO+EGFP: $30.39 \pm 2.74 \times 10^3$, *Bcl11b* cKO+EGFP-2A-C1ql2: $36.22 \pm 1.9 \times 10^3$, mean \pm SEM).

3.3 Overexpression of C1ql2 in dentate granule cells has no effect on mossy fiber synapse

As reintroduction of C1ql2 in *Bcl11b* cKO DGCs was able to reverse the SV misdistribution observed upon *Bcl11b* ablation, I wanted to test whether overexpression of C1ql2 at MFS of animals with a control background could lead to further increase in the recruitment of SV to the proximity of AZs. To do so, I injected C1ql2-expressing AAV in the DG of control animals and compared them to controls receiving the AAV expressing only EGFP. Overexpression of C1ql2 did not affect the SV distribution, with the average synapse score reaching similar levels to controls (Figure 16a; Control+EGFP: 3.4 ± 0.02 , Control+EGFP-2A-C1ql2: 3.41 ± 0.03 , mean \pm SEM; Koumoundourou et al., 2023).

Furthermore, C1ql2 overexpression did not affect the postsynaptic SA with the number of spines contacting MFBs that contain a SA and the complexity of the SA remaining similar to that in control animals (Figure 16b-c; Spines with SA: Control+EGFP: 9.79 ± 1.68 , Control+EGFP-2A-C1ql2: 13.1 ± 1.33 ; SA complexity: Control+EGFP: 6.53 ± 1.49 , Control+EGFP-2A-C1ql2: 6.63 ± 2.48 , mean \pm SEM). As expected, C1ql2 overexpression had no effect on the number of MFS and the complexity of MFBs (Figure 16d-e; Synapse number: Control+EGFP: 90.65 ± 8.25 , Control+EGFP-2A-C1ql2: 77.92 ± 5.49 ; MFB complexity: Control+EGFP: 0.0048 ± 0.00045 , Control+EGFP-2A-C1ql2: 0.0043 ± 0.00028 , mean \pm SEM).

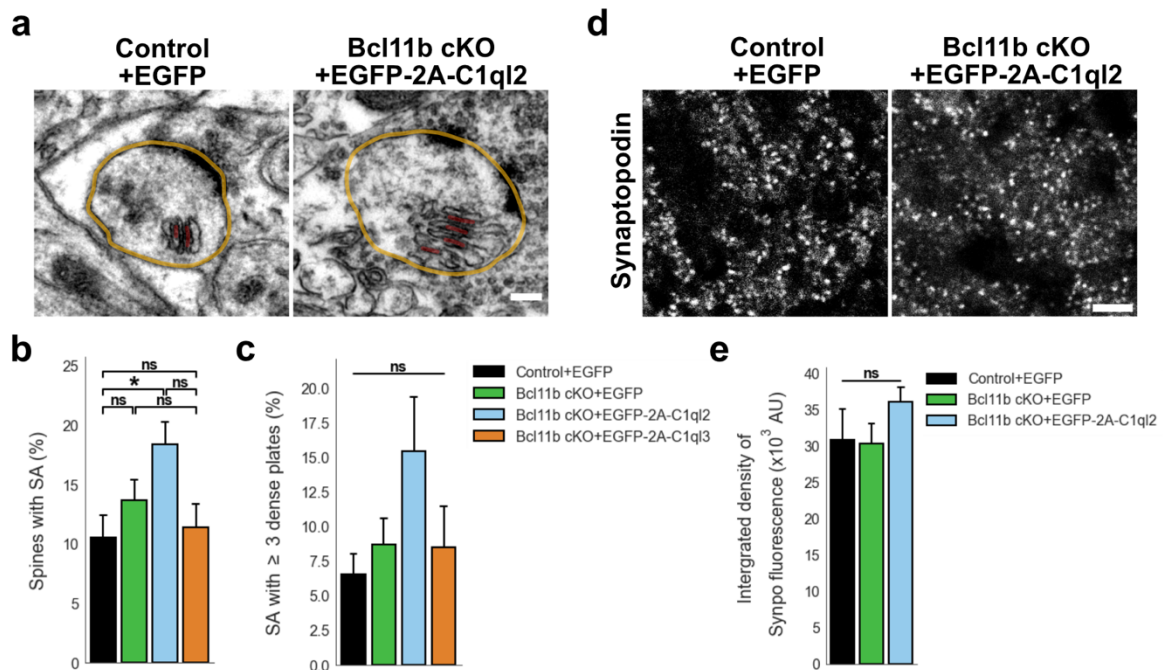


Figure 15. Reintroduction of C1ql2 in *Bcl11b* cKO DGCS affects the postsynaptic spine apparatus.

a) Electron microscopy images of postsynaptic spines (borders marked with yellow line) contacting a MFB that contain a SA. Dense plates of SA highlighted with red lines. Scale bar: 150 nm. b) Percentage of spines in contact with MFBs containing a SA. n=5. All data are presented as means; error bars indicate SEM. Two-way ANOVA with Tukey's PHC. Control+EGFP vs. Bcl11b cKO+EGFP-2A-C1ql2: *p=0.039. c) Percentage of SA with ≥ 3 dense plates. n=5. All data are presented as means; error bars indicate SEM. Two-way ANOVA. d) Confocal images of the SL of CA3 immunostained for Synaptopodin. Scale bar: 5 μ m. e) Integrated density of Synaptopodin fluorescence. n=3. All data are presented as means; error bars indicate SEM. Two-way ANOVA. ns, not significant.

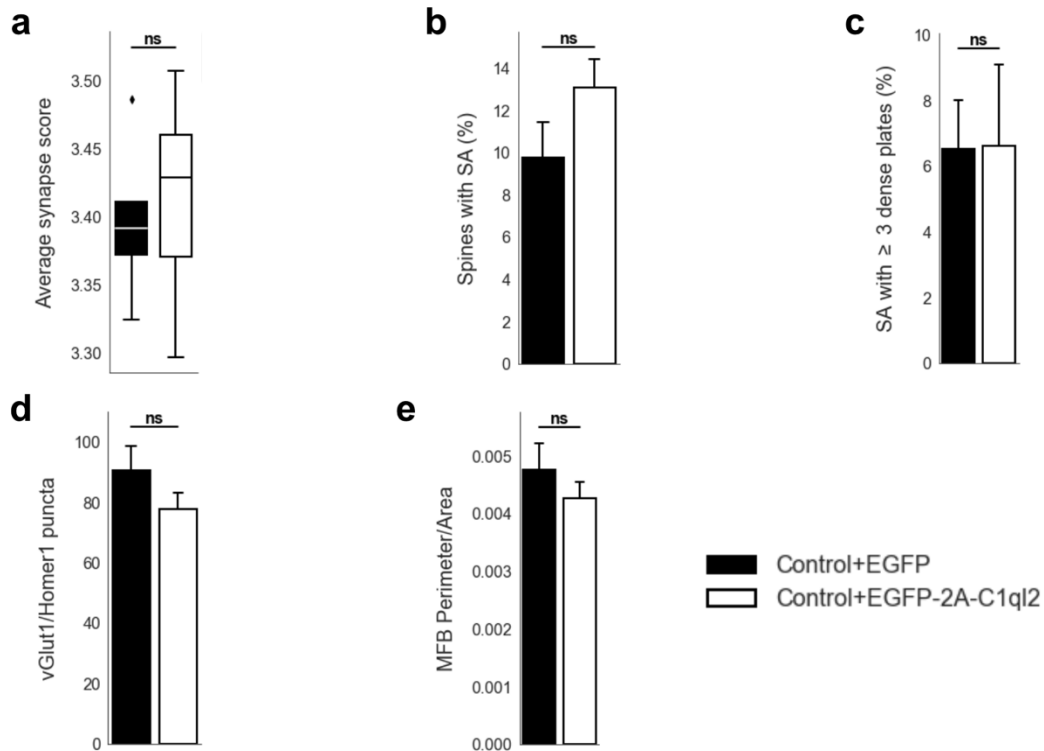


Figure 16. Overexpression of C1ql2 in control DGCs has no effect on the mossy fiber synapse. a) Average synapse score. n=6. Unpaired t-test. b) Percentage of spines in contact with MFBS containing a SA and c) percentage of SAs with ≥ 3 dense plates. n=6. All data are presented as means; error bars indicate SEM. Unpaired t-test. d) vGlut1 and Homer1 double positive puncta in selected CA3 SL ROIs. n=3. All data are presented as means; error bars indicate SEM. Unpaired t-test. e) MFB perimeter-to-area ratio. n=6. All data are presented as means; error bars indicate SEM. ns, not significant. (Adapted from Koumoundourou et al., 2023; Published under CC BY 4.0, <https://creativecommons.org/licenses/by/4.0/>).

3.4 Knock-down of C1ql2 in wild-type dentate granule cells perturbs mossy fiber synapse organization and function

To further corroborate that the observed C1ql2-dependent regulation of SV recruitment and LTP expression at the MFS of *Bcl11b* cKOs was a direct function of C1ql2, I knocked-down *C1ql2* in DGCs of wild-type (WT) mice and analyzed the MFS. Knock-down (KD) of *C1ql2* in DGCs was achieved by stereotaxic injection of an AAV carrying a cassette of 4 short-hairpin RNAs (shRNAs) targeting C1ql2. To eliminate the possibility that any observed effect was due to the stereotaxic surgery or the virus, an AAV with an identical backbone carrying

an shRNA cassette with 4 non-sense (NS) sequences was used as control. The AAVs were injected in the DG of 2-month-old animals, the same timepoint the *Bcl11b* mutation was induced for the initial phenotypic characterization, and were analyzed 2 months later (Figure 17a; Koumoundourou et al., 2023). Compared to control AAV, the AAV targeting *C1ql2* significantly reduced *C1ql2* transcript levels, by approximately 80%, as revealed by qPCR (Figure 17b; +shNS-EGFP: 1 ± 0.07 , +sh*C1ql2*-EGFP: 0.23 ± 0.059 , mean \pm SEM; Koumoundourou et al., 2023), and subsequently protein levels as revealed by immunohistochemistry (Figure 17d; Koumoundourou et al., 2023). The AAV targeting *C1ql2* had no effect on the mRNA and protein levels of *C1ql3* that is a highly homologous to *C1ql2*, demonstrating the specificity of my approach (Figure 17c, e; +shNS-EGFP: 1 ± 0.09 , +sh*C1ql2*-EGFP: 0.986 ± 0.035 , mean \pm SEM; Koumoundourou et al., 2023).

C1ql2 KD led to a misdistribution of the SV in relation to the AZ, with MFS having a lower average synapse score compared to controls (Figure 18a-b, +shNS-EGFP: 3.38 ± 0.069 , +sh*C1ql2*-EGFP: 3.15 ± 0.031 , mean \pm SEM), as well as a reduction in the number of docked vesicles (Figure 18c,e-f; +shNS-EGFP: 0.48 ± 0.04 , +sh*C1ql2*-EGFP: 0.31 ± 0.02 , mean \pm SEM), to a similar extent as observed in *Bcl11b* cKO animals (Koumoundourou et al., 2023). The diameter of the docked vesicles was unchanged (Figure 18d; +shNS-EGFP: 34.28 ± 0.84 , +sh*C1ql2*-EGFP: 35.37 ± 0.21 , mean \pm SEM; Koumoundourou et al., 2023). To test whether the shRNA-mediate KD of *C1ql2* was also sufficient to interfere with MF-LTP expression, LTP recordings were performed by Märt Rannap at the Institute of Physiology and Pathophysiology, Heidelberg University. *C1ql2* KD mice showed a significant loss of LTP when compared to controls, that was detectable as early as 10 min post HFS and got progressively more prominent, similar to *Bcl11b* cKOs (Figure 18g-i; 0-10 min: +shNS-EGFP: 105.0 ± 4.0 , +sh*C1ql2*-EGFP: 94.3 ± 4.5 , 10-20 min: +shNS-EGFP: 56.3 ± 4.5 , +sh*C1ql2*-EGFP: 35.1 ± 2.8 , 20-30 min: +shNS-EGFP: 50.2 ± 4.5 , +sh*C1ql2*-EGFP: 23.4 ± 3.5 , 30-40 min: +shNS-EGFP: 44.6 ± 4.3 , +sh*C1ql2*-EGFP: 20.1 ± 4.1 , mean \pm SEM; Koumoundourou et al., 2023).

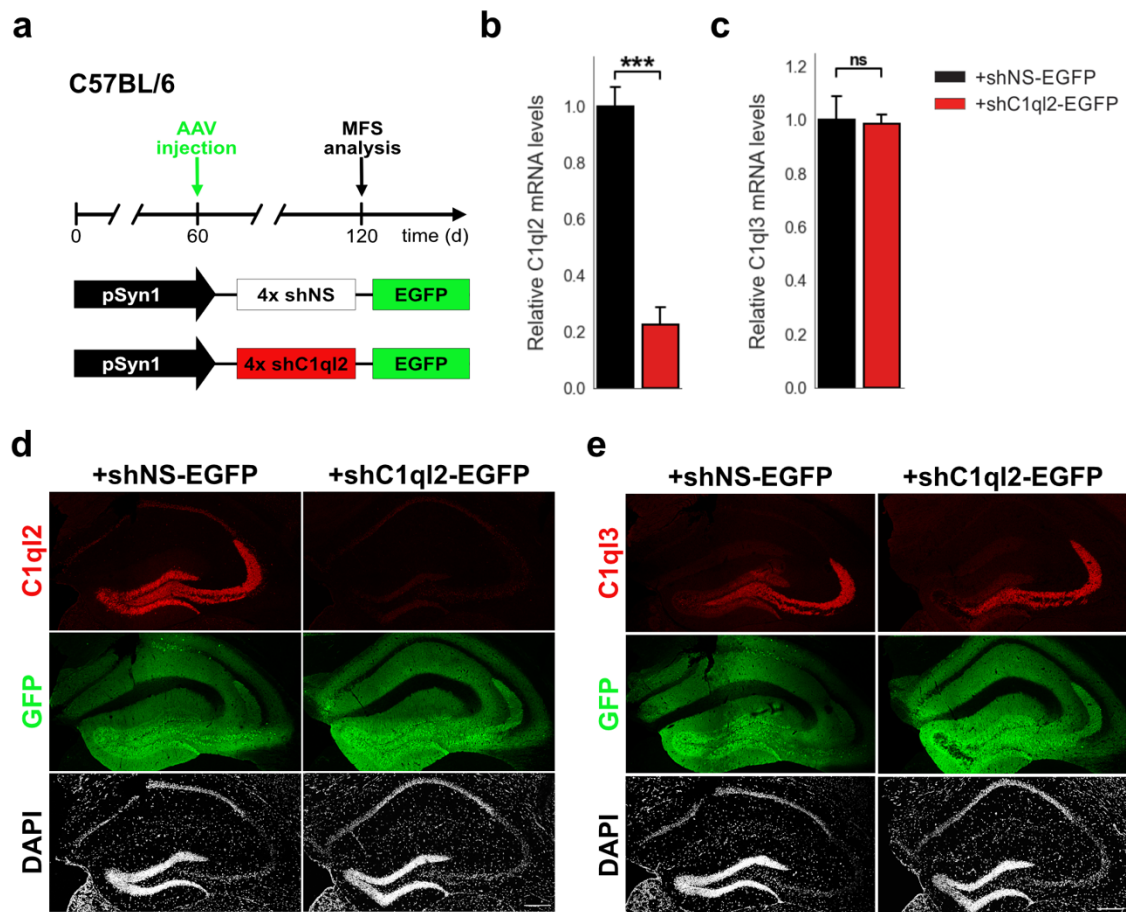


Figure 17. shRNA-mediated targeting of *C1q2* successfully reduces its expression levels. a) Animal model, chronograph of treatment for shRNA-mediated KD of *C1q2* and AAV constructs used. b) Quantification of *C1q2* mRNA and c) *C1q3* mRNA levels. n=4. All data are presented as means; error bars indicate SEM. Unpaired t-test. ***p=0.0002; ns, not significant. d) Hippocampal sections stained for *C1q2* (red) and GFP (green). Scale bar 200 μ m. e) Hippocampal sections stained for *C1q3* (red) and GFP (green). Scale bar 200 μ m. (Adapted from Koumoundourou et al., 2023; Published under CC BY 4.0, <https://creativecommons.org/licenses/by/4.0/>).

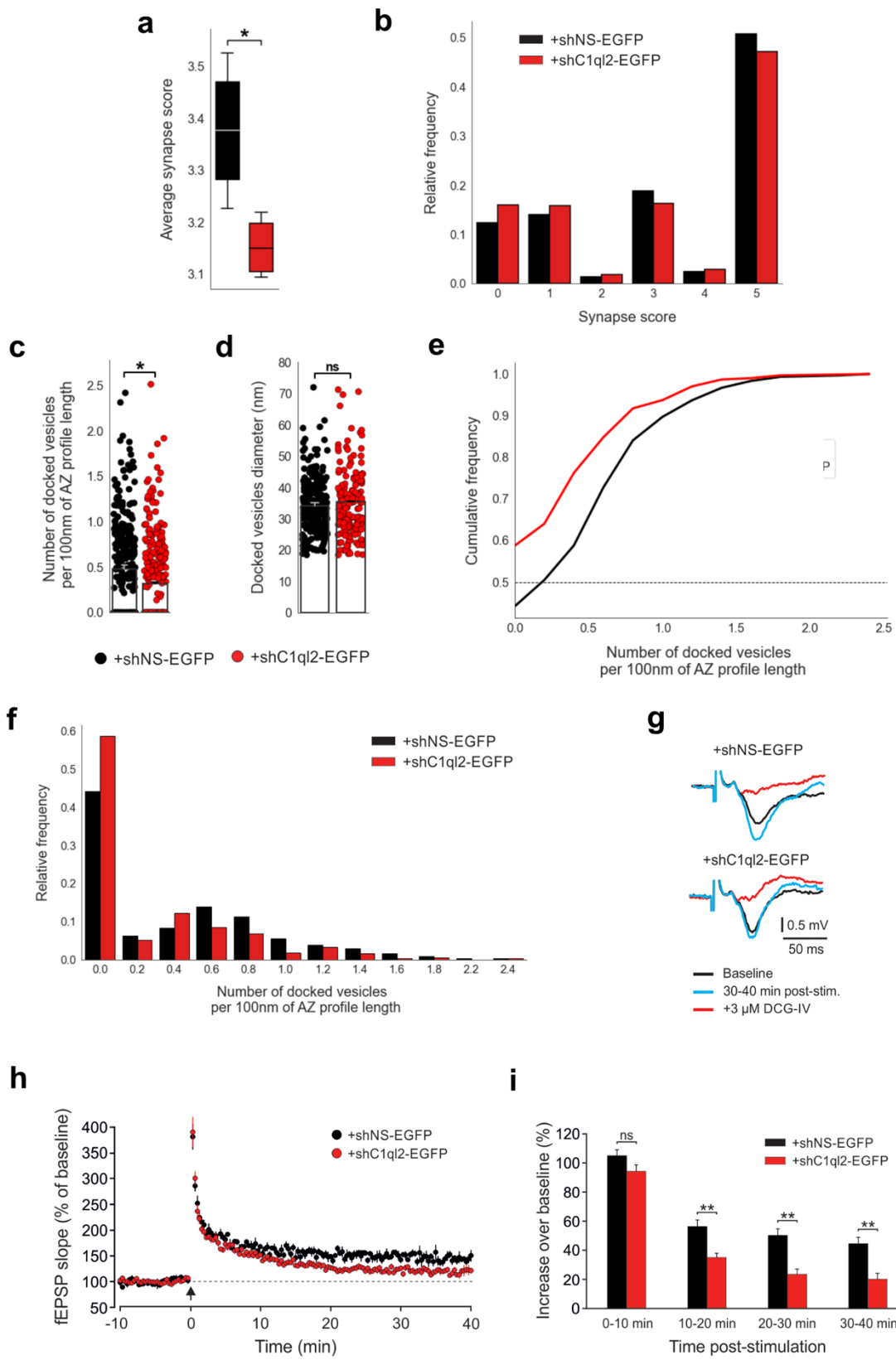


Figure 18. KD of C1qI2 in DGCs of WT mice impairs synaptic vesicle recruitment and long-term potentiation. a) Average synapse score. n=4. Unpaired t-test. *p=0.025. b) Relative frequency of synapse scores. c) Number of docked vesicles per 100 nm AZ profile length. n=3. All data are presented as means; error bars indicate SEM. Points represent the individual examined AZs. Unpaired t-test. *p=0.018. d) Diameter of docked vesicles. n=3. All data are presented as means; error bars indicate SEM. Points represent the individual SVs. e) Cumulative and f) relative frequency of the number of docked vesicles per 100 nm AZ profile length. g) Representative fEPSP traces showing baselines before HFS (black), fEPSP changes 30-40 min after HFS (cyan) and following the application of 3 μ M DCG-IV (red). h) Time course of fEPSP slopes. The black arrow indicates HFS and the dashed line the baseline level. i) Quantification of fEPSP facilitation at four different time intervals after HFS. Changes in fEPSP slope are shown as percentage of the mean baseline fEPSP. +shNS-EGFP, n=6; +shC1qI2-EGFP, n=7. All data are presented as means; error bars indicate SEM. Mann-Whitney U-test for each time interval. 10-20 min: **p=0.0012; 20-30 min: **p=0.0023; 30-40 min: **p=0.0023; ns, not significant. (Adapted from Koumoundourou et al., 2023; Published under CC BY 4.0, <https://creativecommons.org/licenses/by/4.0/>).

3.5 C1qI2-Nrxn3(25b+) is required for synaptic vesicle recruitment at the mossy fiber synapse

3.5.1 C1qI2-Nrxn3(25b+) is required for synaptic vesicle recruitment *in vitro*

To further understand the molecular mechanism through which Bcl11b and C1qI2 exert their function at the MFS, I decided to search for potential interaction partners of C1qI2 that participate in the regulation of SV recruitment and LTP. As both the SV recruitment and the LTP are presynaptic features of MFS (Nicoll & Schmitz, 2005), I hypothesized that C1qI2 upon secretion interacts with presynaptic proteins that send feedback signals to the MFB for the organization of the SV machinery. It was previously shown *in vitro* that C1qI2 binds to the presynaptic Nrxn3 β containing the SS5^{25b} sequence (Nrxn3(25b+)) (Matsuda et al., 2016). To investigate whether C1qI2 binding to Nrxn3(25b+) induces SV recruitment, I designed an *in vitro* assay in which HEK293 cells expressing C1qI2 were co-cultured with primary hippocampal neurons expressing Nrxn3(25b+). I quantified the accumulation of

endogenous neuronal vGlut1, a proxy for SV, at the contact points between the neurons and the HEK293 cells in the presence and absence of C1qI2. To show that the interaction between the two proteins drives the SV accumulation, I created a C1qI2 mutant variant unable to bind to Nrnx3(25b+). Dr. Carsten Reißner from the group of Prof. Dr. Markus Missler at the Institute of Anatomy and Molecular Neurobiology, University of Münster analyzed the electrostatic properties of the solvent-accessible surfaces of the C1q domain of C1qI2 (PDB_ID: 4QPY; Ressler et al., 2015) to identify crucial candidate residues for the interaction of C1qI2 and the 25b+ region of Nrnx3. Lysine262 (K262) is positioned in the center of the area underneath the C1qI2-specific Ca²⁺ and receptor binding loops. Changing this residue to glutamic acid would render a larger area negative, which could potentially repel binding to Nrnx3(25b+) (Figure 19; Koumoundourou et al., 2023).

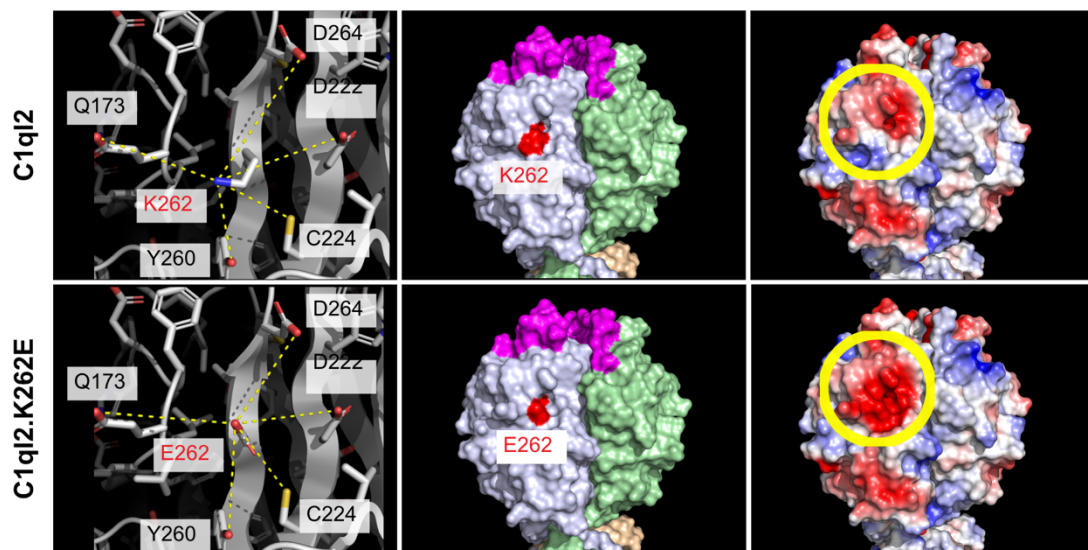


Figure 19. The amino acid substitution K262E changes the surface charge of C1qI2. Trimeric structures of C1qI2 (PDB_ID: 4QPY, upper panels) and the variant C1qI2.K262E (lower panels). Residue 262 is the central residue (red, left & middle panels) of a larger area underneath the C1qI2-specific calcium and receptor binding loops (magenta, middle panel). The mutation K262E alters the charge of that surface area negative (yellow-circled area, right panels) and makes it potentially repulsive to bind Nrnx3(25b+). (Adapted from Koumoundourou et al., 2023; Published under CC BY 4.0, <https://creativecommons.org/licenses/by/4.0/>).

To test whether C1ql2.K262E was indeed unable to bind to Nrnx3(25b+), I first determined the accumulation of neuronal Nrnx3(25b+) at the contact points of neurons with HEK293 cells expressing C1ql2 or C1ql2.K262E. Due to the lack of specific Nrnx3(25b+) antibodies and the generally low level of expression of the different Nrnx3 isoforms, the neurons were transfected with GFP-Nrxn3 α (25b+). I used the extracellularly longer Nrnx3 α isoform as it is expressed on higher levels in the murine DG compared to Nrnx3 β (Uchigashima et al., 2019). Indeed, HEK293 cells expressing C1ql2 induced significantly more Nrnx3 α (25b+) accumulation compared to HEK293 cells transfected with the control construct, calculated by the HEK293 surface area covered by GFP immunoreactivity. C1ql2.K262E-expressing HEK293 cells induced Nrnx3 α (25b+) accumulation to similar levels as the control construct, suggesting that the mutation did not allow the interaction of C1ql2 with Nrnx3(25b+) (Figure 20a-b; myc-tag: 17.29 \pm 2.27, myc-C1ql2: 39.97 \pm 3.99, myc-K262E: 18.84 \pm 5.15, mean \pm SEM; Koumoundourou et al., 2023). Next, I measured the HEK293 area that was covered by vGlut1 immunoreactivity and found that while HEK293 cells expressing C1ql2 accumulated significantly more vGlut1 at contacting neurons compared to C1ql2-negative cells, C1ql2.K262E was unable to induce vGlut1 accumulation (Figure 20c-d; myc-tag: 24.78 \pm 4.99, myc-C1ql2: 40.88 \pm 3.25, myc-K262E: 16.9 \pm 1.2, mean \pm SEM; Koumoundourou et al., 2023).

To further corroborate that the C1ql2-Nrxn3(25b+) interaction is required for the SV recruitment, I co-cultured C1ql2-expressing HEK293 cells with primary hippocampal neurons derived from Nrnx123^{flox/flox} mice (Chen et al., 2017b), that have all three *Nrxn* genes floxed. Neurons were transfected with Cre for pan-*neurexin* KO or with an inactive Cre variant (Klatt et al., 2021) as control. Furthermore, C1ql2-expressing HEK293 cells were co-cultured with *Nrxn*-null neurons co-transfected with GFP-Nrxn3 α (25b+). Indeed, KO of neuronal *Nrxns* significantly reduced the accumulation of vGlut1 on HEK293 cells compared to controls, while the rescue of Nrnx3 α (25b+) expression in *Nrxn*-null neurons was able to induce vGlut1 accumulation (Figure 20e-f; +inactive Cre: 51.66 \pm 5.97, +Cre: 27.83 \pm 2.83, +Cre+Nrxn3 α (25b+): 39.23 \pm 4.3, mean \pm SEM; Koumoundourou et al., 2023).

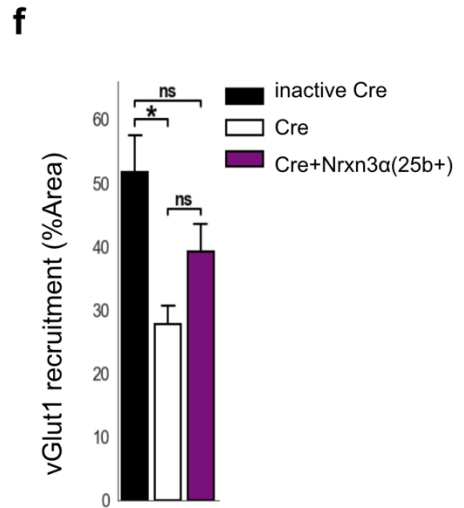
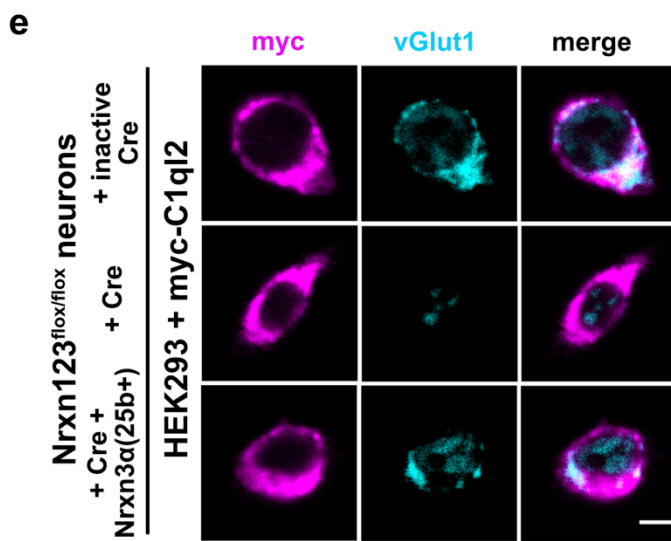
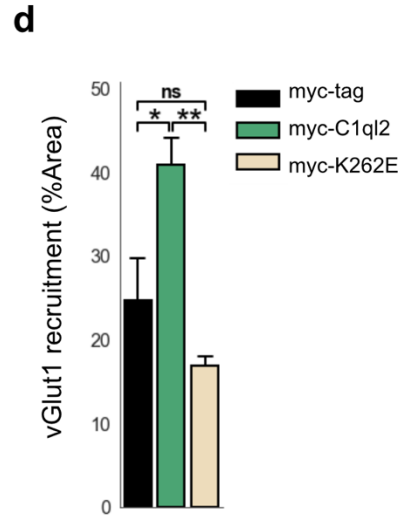
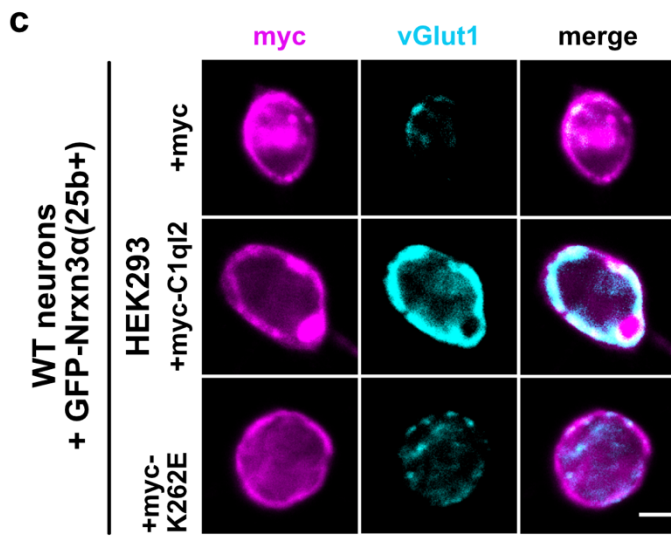
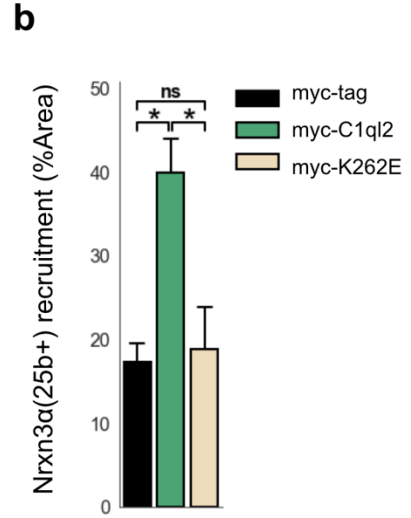
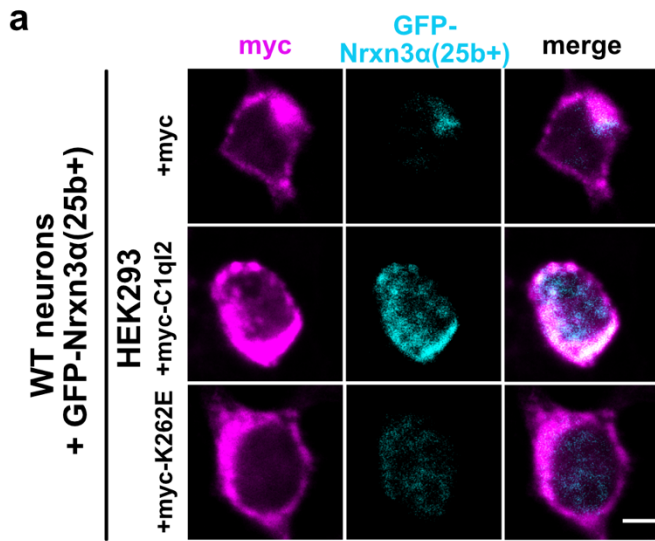


Figure 20. C1ql2-Nrxn3 interaction recruits vGlut1 *in vitro*. a) Immunocytochemistry of HEK293 cells expressing myc-tagged C1ql2, C1ql2.K262E or myc-tag and GFP-Nrxn3 α (25b+) (cyan) from contacting hippocampal neurons. Scale bar: 5 μ m. b) Nrxn3 α (25b+) recruitment by differentially transfected HEK293 cells. n=3. All data are presented as means; error bars indicate SEM. One-way ANOVA and Tuckey's PHC. myc-C1ql2 vs. myc-tag: *p=0.016, and vs. myc-K262E: *p=0.022. c) Immunohistochemistry of HEK293 cells expressing myc-tagged C1ql2, C1ql2.K262E or myc-tag and vGlut1 (cyan) from contacting hippocampal neurons. Scale bar: 5 μ m. d) vGlut1 recruitment by differentially transfected HEK293 cells. n = 3. All data are presented as means; error bars indicate SEM. One-way ANOVA and Tuckey's PHC. myc-C1ql2 vs. myc-tag: *p=0.04, and vs. myc-K262E: **p=0.007. e) Immunocytochemistry of HEK293 cells expressing myc-tagged C1ql2 (magenta) and vGlut1 (cyan) from contacting control, *Nrxn123* KO or *Nrxn123* KO with a Nrxn3 α (25+) rescue hippocampal neurons. Scale bar: 5 μ m. f) vGlut1 recruitment by HEK293 cells in presence or absence of neuronal Nrxns. n = 3. All data are presented as means; error bars indicate SEM. One-way ANOVA and Tuckey's PHC. inactive Cre vs. Cre: *p=0.023, and vs. Cre+ Nrxn3 α (25+): p=0.21; ns: non-significant. (Adapted from Koumoundourou et al., 2023; Published under CC BY 4.0, <https://creativecommons.org/licenses/by/4.0/>).

3.5.2 Introduction of C1ql2.K262E in dentate granule cells of *Bcl11b* mutants does not rescue synaptic vesicle recruitment at the mossy fiber synapse

To analyze the interaction of C1ql2 with Nrnx3(25b+) *in vivo* directly at the MFS, I stereotaxically injected an AAV expressing C1ql2.K262E into the DG of *Bcl11b* cKO, where endogenous C1ql2 is strongly downregulated by the *Bcl11b* ablation (Figure 21a; Koumoundourou et al., 2023). C1ql2.K262E was strongly expressed in *Bcl11b* cKO DGCs as quantified by the protein expression (Figure 21b-c; Control+EGFP: 1 ± 0.42 , *Bcl11b* cKO+EGFP-2A-K262E: 9.68 ± 4.75 , mean \pm SEM; Koumoundourou et al., 2023). Surprisingly, the spatial distribution of the protein within the MF system was changed compared to reintroduced WT C1ql2, with reduced mutant protein signal on the SL of CA3, as observed in immunostainings on hippocampal sections and quantified by the integrated density of the protein fluorescence (Figure 22a-b; *Bcl11b* cKO+EGFP-2A-C1ql2: $9.75 \pm 0.57 \times 10^4$, *Bcl11b* cKO+EGFP-2A-K262E: $5.89 \pm 0.55 \times 10^4$, mean \pm SEM; Koumoundourou et al., 2023). Since C1ql2 forms heteromers with C1ql3 and C1ql3 was also shown to bind to Nrnx3 β (25b+) *in vitro* (Matsuda et al., 2016), I examined also the distribution of C1ql3 but found no obvious changes (Figure 22c; Koumoundourou et al., 2023).

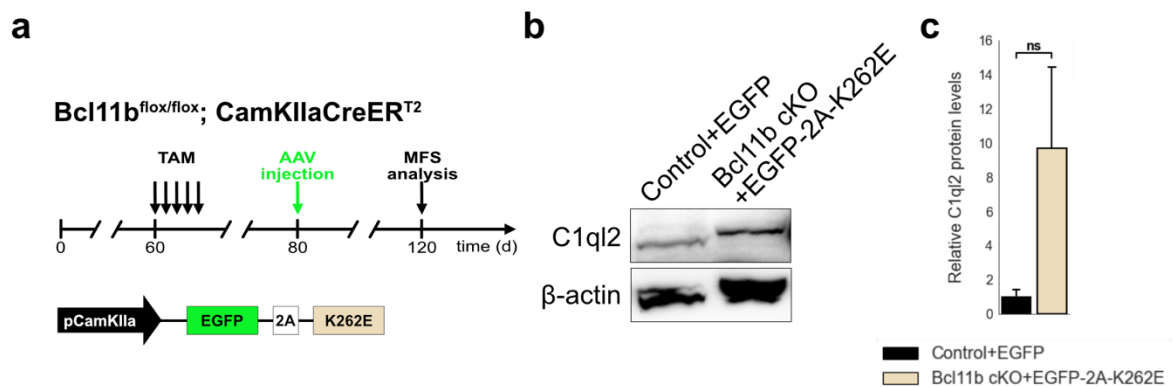


Figure 21. Expression of C1ql2.K262E in *Bcl11b* cKO DGCs. a) Animal model, chronograph of treatment for expression of mutant C1ql2 and AAV constructs used. b) Western blot and c) quantification of C1ql2.K262E protein levels in mouse hippocampal homogenates. n=3. All data are presented as means; error bars indicate SEM. Mann-Whitney U-test. ns, not significant. (Adapted from Koumoundourou et al., 2023; Published under CC BY 4.0, <https://creativecommons.org/licenses/by/4.0/>).

Next, I analyzed the SV distribution and docking to the AZ of MFS of *Bcl11b* cKOs expressing C1ql2.K262E and found that neither the average synapse score (Figure 23a-c; Control+EGFP: 3.39 ± 0.048 , *Bcl11b* cKO+EGFP-2A-K262E: 2.87 ± 0.043 , mean \pm SEM), nor the number of docked vesicles per 100 nm of AZ profile length (Figure 23d,f-g; Control+EGFP: 0.41 ± 0.069 , *Bcl11b* cKO+EGFP-2A-K262E: 0.19 ± 0.035 , mean \pm SEM) were recovered by the mutant C1ql2 protein and both remained significantly lower than in controls and similar to values reported for the *Bcl11b* cKO mice (Koumoundourou et al., 2023). No changes in the diameter of the docked vesicles were observed (Figure 23e; Control+EGFP: 39.06 ± 1.22 , *Bcl11b* cKO+EGFP-2A-K262E: 36.38 ± 2.19 , mean \pm SEM; Koumoundourou et al., 2023). Unexpectedly, introduction of C1ql2.K262E in *Bcl11b* cKO DGCs rescued the MF-LTP expression. Additionally, it caused a significant increase of the fEPSP slope during the induction phase that was not observed upon C1ql2 expression rescue. The LTP measurements were done by Märt Rannap from the group of Prof. Dr. Andreas Draguhn at the Institute of Physiology and Pathophysiology, Heidelberg University (Figure 23h-j; 0-10 min: Control+EGFP: 90.4 ± 7.2 , *Bcl11b* cKO+EGFP-2A-K262E: 155.8 ± 30.3 , 10-20 min: Control+EGFP: 42.7 ± 3.6 , *Bcl11b* cKO+EGFP-2A-K262E: 68.7 ± 17.3 , 20-30 min: Control+EGFP: 52.5 ± 7.6 , *Bcl11b* cKO+EGFP-2A-K262E: 55.9 ± 13.8 , 30-40 min: Control+EGFP: 50.1 ± 7.3 , *Bcl11b* cKO+EGFP-2A-K262E: 47.8 ± 9.3 , mean \pm SEM). 52.5 \pm 7.6, *Bcl11b* cKO+EGFP-2A-K262E: 55.9 ± 13.8 , 30-40 min: Control+EGFP: 50.1 ± 7.3 , *Bcl11b* cKO+EGFP-2A-K262E: 47.8 ± 9.3 , mean \pm SEM; Koumoundourou et al., 2023).

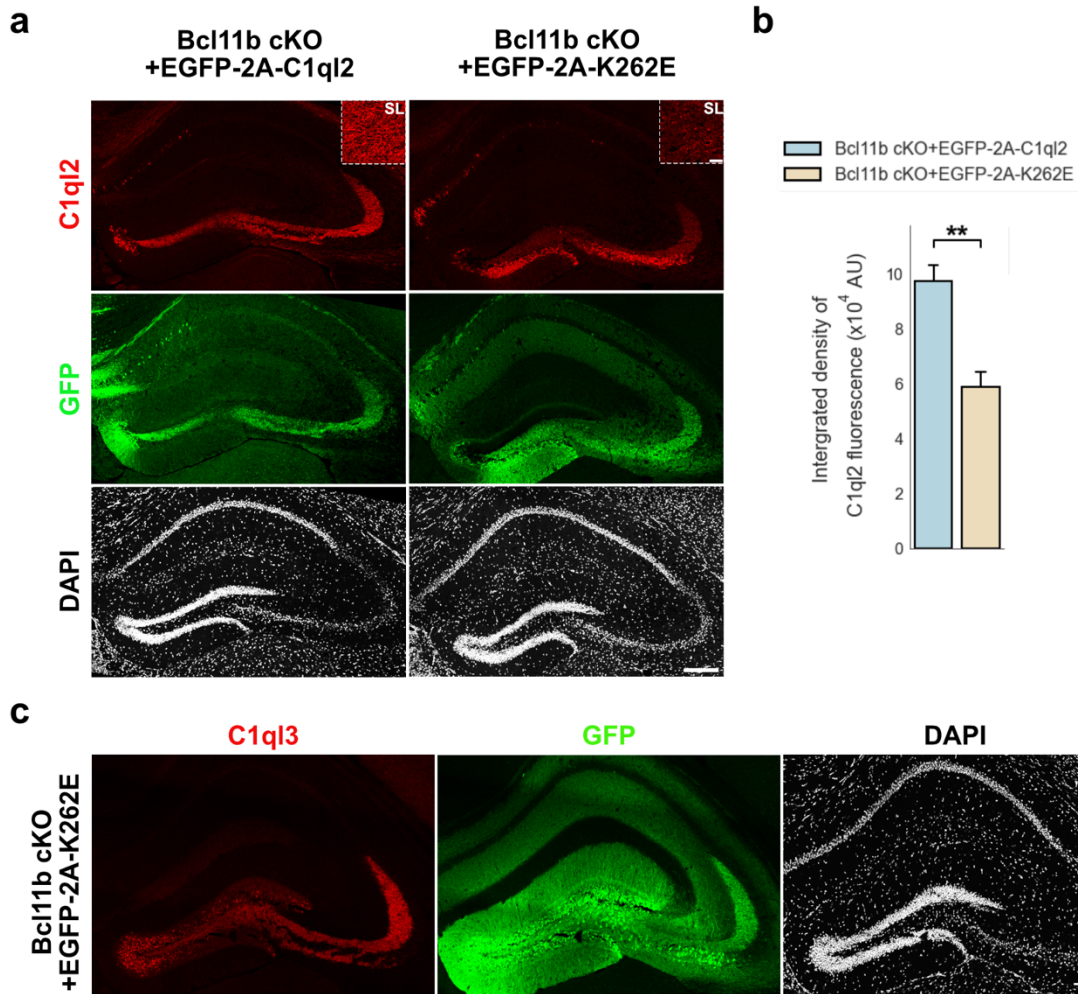


Figure 22. C1qI2.K262E is not targeted to the mossy fiber synapse. a) Hippocampal sections stained for C1qI2 (red) and GFP (green). Scale bar 200 μ m. Upper right corner in C1qI2 panels, depict close-ups from the SL of CA3. Scale bar: 15 μ m. b) Integrated density of C1qI2 fluorescence in the SL of CA3. n=3. All data are presented as means; error bars indicate SEM. Unpaired t-test. **p=0.008. c) Hippocampal section stained for C1qI3 (red) and GFP (green). Scale bar 200 μ m. (Adapted from Koumoundourou et al., 2023; Published under CC BY 4.0, <https://creativecommons.org/licenses/by/4.0/>).

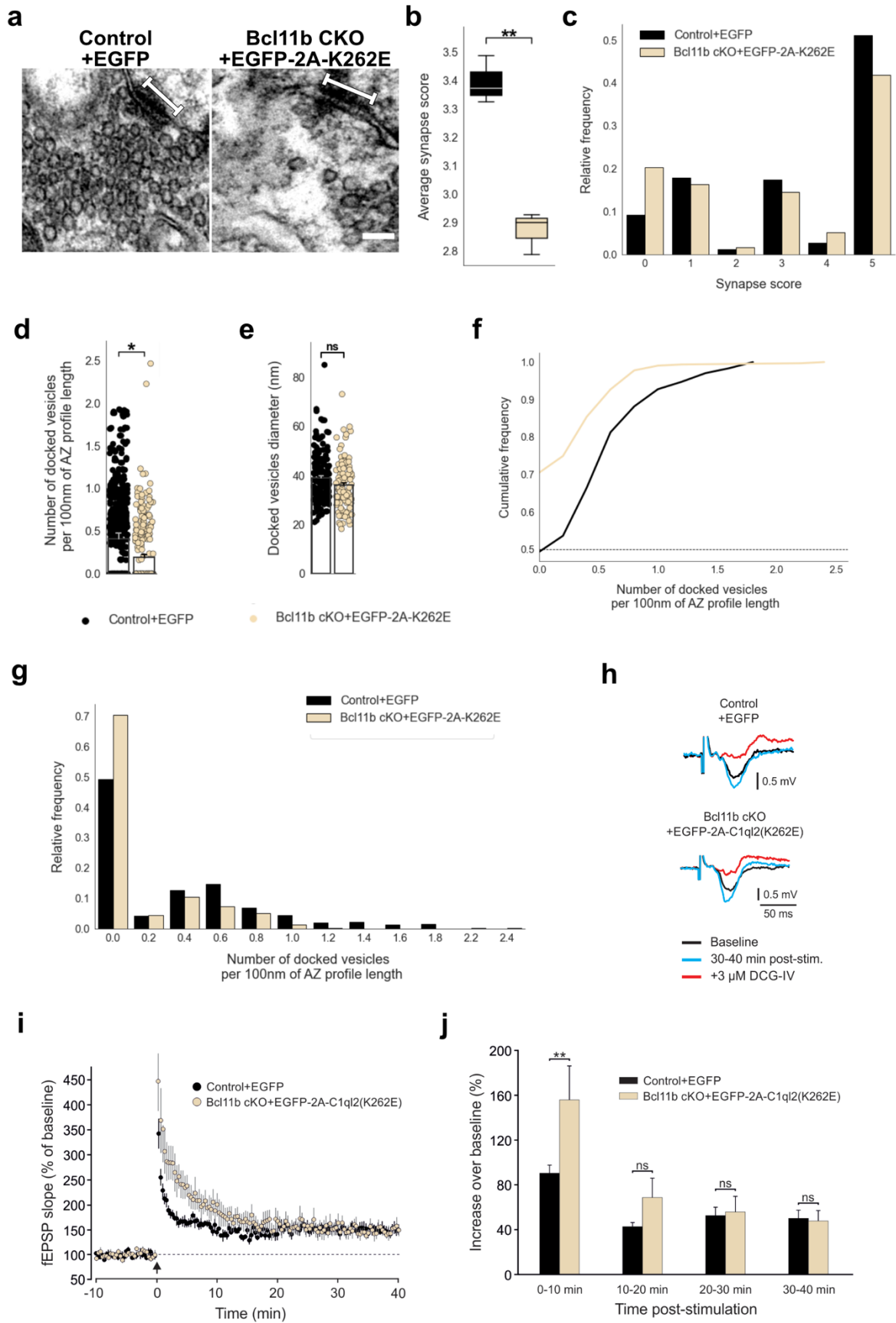


Figure 23. C1ql2-Nrxn3(25b+) interaction is essential for C1ql2 targeting to MFS and SV recruitment. a) Electron microscope images of MFS (white bar, presented on the postsynaptic side) and the SVs distributed in proximity to it. Scale bar: 100 nm. b) Average synapse score. n=3. Unpaired t-test. **p=0.0012. c) Relative frequency of synapse scores. d) Number of docked vesicles per 100 nm AZ profile length. n=3. All data are presented as means; error bars indicate SEM. Points represent the individual examined AZs. Unpaired t-test. *p=0.018. e) Diameter of docked vesicles. n=3. All data are presented as means; error bars indicate SEM. Points represent the individual SVs. f) Cumulative and g) relative frequency of the number of docked vesicles per 100 nm AZ profile length. h) Representative fEPSP traces showing baselines before HFS (black), fEPSP changes 30-40 min after HFS (cyan) and following the application of 3 μ M DCG-IV (red). i) Time course of fEPSP slopes. The black arrow indicates HFS and the dashed line the baseline level. j) Quantification of fEPSP facilitation at four different time intervals after HFS. Changes in fEPSP slope are shown as percentage of the mean baseline fEPSP. Control+EGFP, n=7; Bcl11b cKO+EGFP-2A-K262E, n=5. All data are presented as means; error bars indicate SEM. Mann-Whitney U-test for each time interval. 0-10 min: **p=0.005; ns, not significant. (Adapted from Koumoundourou et al., 2023; Published under CC BY 4.0, <https://creativecommons.org/licenses/by/4.0/>).

3.5.3 Suppression of *Nrxn3* expression in dentate granule cells perturbs synaptic vesicle recruitment at the mossy fiber synapse

To further support that C1ql2-*Nrxn3*(25b+) interaction is essential for SV recruitment at the MFS and for targeting of C1ql2 to the MFS, I disrupted the pathway by removing *Nrxn3* from the DGCs. I used *Nrxn123*^{flox/flox} mice (Chen et al., 2017b) and injected AAVs expressing either Cre to induce the mutation or inactive Cre as control (Klatt et al., 2021) in the DG of 2 months old animals and examined the brains 2 months later (Figure 24a; Koumoundourou et al., 2023). AAV-mediated expression of Cre in DGCs was sufficient to significantly suppress expression of *Nrxn3*, but only mildly reduced *Nrxn1* expression, while *Nrxn2* expression was unchanged (Figure 24b; *Nrxn1*: inactive Cre: 1 ± 0.084 , Cre: 0.714 ± 0.037 ; *Nrxn2*: inactive Cre: 1 ± 0.065 , Cre: 0.771 ± 0.071 ; *Nrxn3*: inactive Cre: 1 ± 0.127 , Cre: 0.381 ± 0.09 , mean \pm SEM; Koumoundourou et al., 2023). *Nrxn123* cKO animals had significantly reduced expression of endogenous C1ql2 at the SL of CA3 compared to controls, as seen on hippocampal sections stained for C1ql2 and quantified by the integrated density of C1ql2 fluorescence (Figure 24c-d; +inactive Cre: 11.65 ± 1.75 , +Cre: 4.71 ± 0.93 , mean \pm SEM; Koumoundourou et al., 2023). To exclude that the observed reduction in C1ql2 localization along the MF tract was due to a general disruption of the circuit and potential loss or reorganization of MFB, the structures that secrete C1ql2, I used ZnT3, a marker for MFB, but observed no overt change in its fluorescence intensity or distribution (Figure 24e; Koumoundourou et al., 2023). The expression pattern of C1ql3 was unchanged (Figure 24f; Koumoundourou et al., 2023). Finally, I examined the MFS by TEM and could show that suppression of *Nrxn3* reduced both the average synapse score (Figure 25a-c; +inactive Cre: 3.11 ± 0.06 ; +Cre: 2.67 ± 0.074 , mean \pm SEM) and the number of docked vesicles (Figure 25d,f-g; +inactive Cre: 0.404 ± 0.035 ; Koumoundourou et al., 2023). The diameter of the docked vesicles was unchanged (Figure 25e; +inactive Cre: 38.38 ± 0.44 ; +Cre: 37.12 ± 0.8 , mean \pm SEM; Koumoundourou et al., 2023).

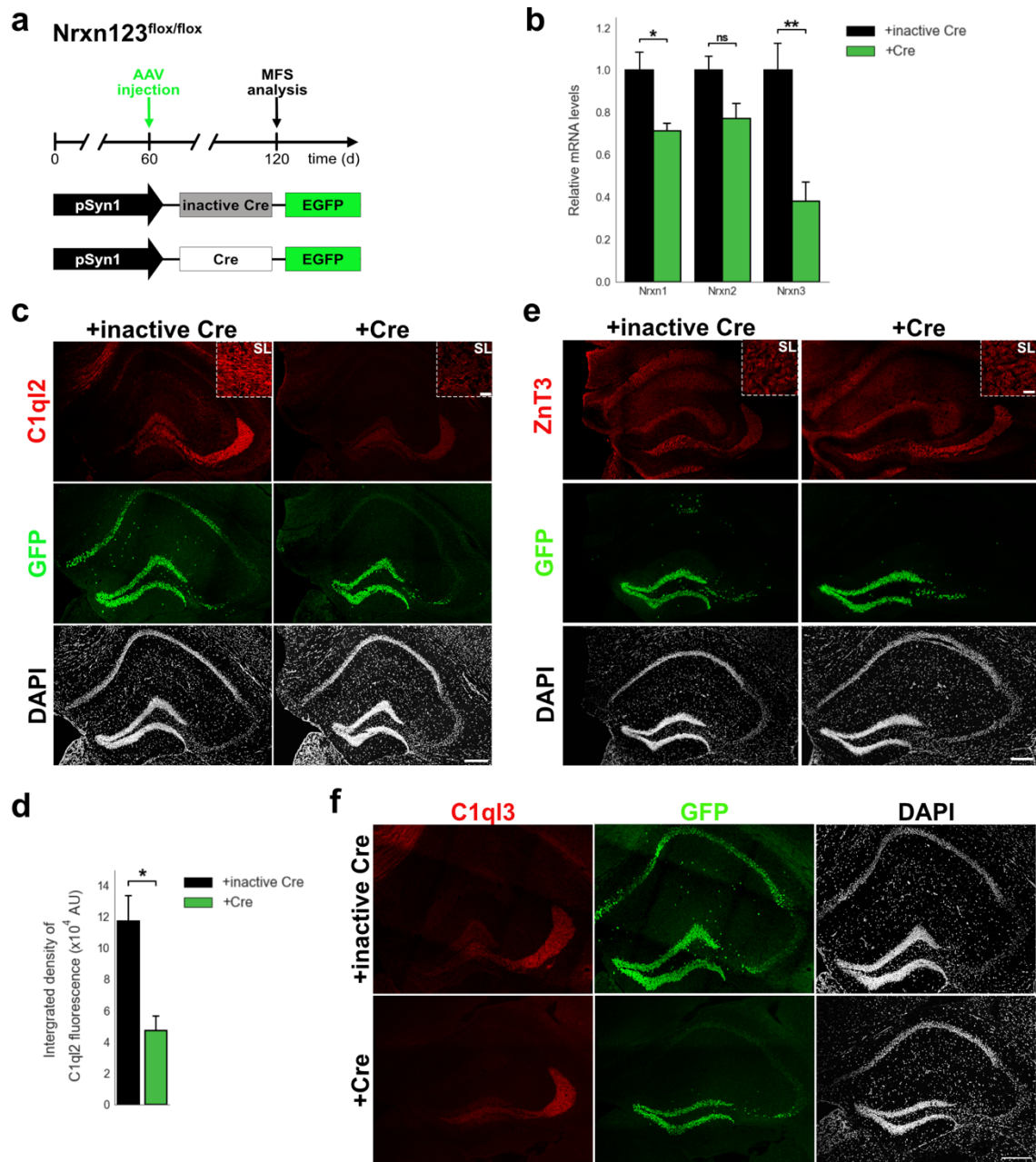


Figure 24. *Nrxn* KO perturbs C1ql2 targeting to mossy fiber synapses. a) Animal model, chronograph of treatment for suppression of *Nrxn3* and AAV constructs used. b) Quantification of *Nrxn3* mRNA levels in DGCs. n=a. All data are presented as means; error bars indicate SEM. Unpaired t-test. *Nrxn1*: *p=0.034; *Nrxn3*: **p=0.007. c) Hippocampal sections stained for C1ql2 (red) and GFP (green). Scale bar 200 μ m. Upper right corner in C1ql2 panels, depict close-ups from the SL of CA3. Scale bar: 15 μ m. d) Integrated density of C1ql2 fluorescence in the SL of CA3. n=3. All data are presented as means; error bars indicate SEM. Unpaired t-test. *p=0.02. e) Hippocampal section stained for ZnT3 (red) and GFP (green). Scale bar 200 μ m. Upper right corner in ZnT3 panels, depict close-ups from the SL of CA3. Scale bar: 15 μ m. f) Hippocampal sections stained for C1ql3 (red) and

GFP (green). Scale bar 200 μm . (Adapted from Koumoundourou et al., 2023; Published under CC BY 4.0, <https://creativecommons.org/licenses/by/4.0/>).

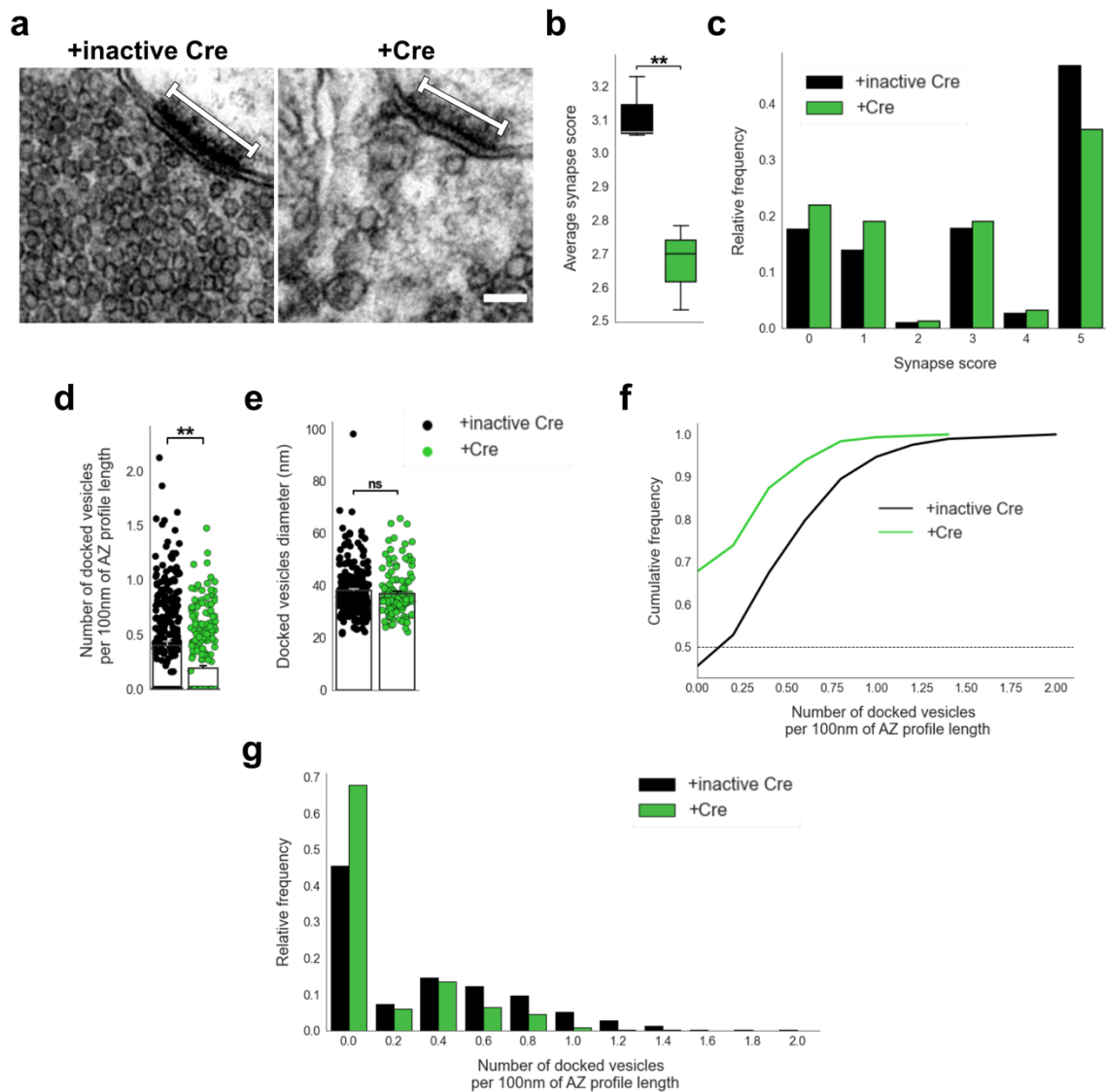


Figure 25. *Nrxn* KO perturbs synaptic vesicle recruitment at mossy fiber synapses. a) Electron microscope images of MFS (white bar, presented on the postsynaptic side) and the SVs distributed in proximity to it. Scale bar: 100 nm. b) Average synapse score. n=3. Unpaired t-test. **p=0.009. c) Relative frequency of synapse scores. d) Number of docked vesicles per 100 nm AZ profile length. n=3. All data are presented as means; error bars indicate SEM. Points represent the individual examined AZs. Unpaired t-test. **p=0.007. e) Diameter of docked vesicles. n=3. All data are presented as means; error bars indicate SEM. Points represent the individual SVs. f) Cumulative and g) relative frequency of the number of docked vesicles per 100 nm AZ profile length. ns, not

significant. (Adapted from Koumoundourou et al., 2023; Published under CC BY 4.0, <https://creativecommons.org/licenses/by/4.0/>).

4 Discussion

In my thesis, I identified a downstream molecular pathway through which *Bcl11b* regulates the function of hippocampal MFS in adult mice. I show that *Bcl11b* exerts part of its functions through its transcriptional target *C1ql2*. Reintroduction of *C1ql2* in DGCs with ablated *Bcl11b* rescues the SV misdistribution and the reduced docking of vesicles to the AZ, as well as the loss of LTP. KD of *C1ql2* in WT DGCs recapitulates the *Bcl11b* mutant phenotype and impairs the SV recruitment and the LTP expression at the MFS. Moreover, I identify that interaction of *C1ql2* with presynaptic *Nrxn3(25b+)* is essential for SV recruitment, but not for LTP expression at the MFS. Interruption of *C1ql2*-*Nrxn3(25b+)* interaction, either by expression of a *C1ql2* variant that does not bind *Nrxn3(25b+)* or by deletion of *Nrxn3*, perturbs SV recruitment both on cultured neurons and in MFS of mice. Finally, I show that *C1ql2*-*Nrxn3(25b+)* interaction is also required for targeting of *C1ql2* to the MFS.

4.1 *Bcl11b* regulates mossy fiber synapse integrity through both *C1ql2*-dependent and -independent mechanisms

It was previously shown that the TF *Bcl11b* is essential for the structural and functional stability of hippocampal MFS. Ablation of *Bcl11b* in the adult hippocampus leads to reduction of MFS number, loss of the MFB complexity, misdistribution of SV, as well as loss of LTP (De Bruyckere et al., 2018). In the same study, several transcriptional targets of *Bcl11b* were identified, among which the secreted synaptic organizer *C1ql2*, that is downregulated in *Bcl11b* mutant DGCs (De Bruyckere et al., 2018). AAV-mediated re-expression of *C1ql2* in *Bcl11b* cKO DGCs rescued part of the *Bcl11b* mutant phenotype at the MFS. Reintroduction of *C1ql2* completely restored the SV localization and docking, as well as the LTP at the MFS. KD of *C1ql2* in WT DGCs was sufficient to impair the SV recruitment and the MF-LTP. These results support *C1ql2* to be a functional target of *Bcl11b* at the MFS. Accumulation and docking of SV at the AZ has been shown to increase the release probability (P_r) of the MF presynapse, the long-term increase of which is

characteristic for MF-LTP (Orlando et al., 2021; Vandael et al., 2020). Indeed, *Bcl11b* cKO and *C1ql2* KD perturbed both SV recruitment to the AZ and LTP at MFS, while reintroduction of *C1ql2* in *Bcl11b* cKO DGCs specifically rescued SV recruitment and LTP. This suggests that *Bcl11b* regulates the functional stability of MFS in a *C1ql2*-dependent manner. It is important to note that the AAV-mediated re-expression of *C1ql2* did not allow for precise restoration of *C1ql2* expression to exact control levels. While not significantly, *C1ql2* levels were higher than those in control animals. Overexpression of *C1ql2* in control animals did not have an effect on the analyzed measures of MFS function, thus the observed effects upon re-expression of *C1ql2* in *Bcl11b* cKO DGCs can be attributed to the physiological function of *C1ql2*. However, *C1ql2* functions that are sensitive to its expression levels cannot be analyzed within this system.

Reintroduction of *C1ql2* in *Bcl11b* cKO DGCs, failed to reverse the overall loss of MFS and the ultrastructural complexity of MFB, suggesting that *Bcl11b* acts on the MFS through *C1ql2*-independent pathways to regulate the structural integrity of the mossy fiber circuit. One of the genes that was deregulated in the DGCs upon *Bcl11b* ablation, and was shown to be a direct transcriptional target of *Bcl11b*, was Semaphorin 5b (*Sema5b*) (De Bruyckere et al., 2018). Several members of the semaphorin family have been shown to affect the structure and function of CNS synapses, with *Sema5b* being implicated in synapse elimination. Overexpression of *Sema5b* in cultured hippocampal neurons and bath application containing the secreted sema domain led to a loss of synaptic sites (O'Connor et al., 2009). *Sema5b*, the expression of which is normally constrained to the subventricular zone of the DG in the postnatal hippocampus, was upregulated in *Bcl11b* cKO DGCs and could thus potentially explain the loss of MFS. To further understand the role of *Sema5b* in MFS maintenance, a similar strategy to the one used for the functional analysis of *C1ql2* could be used.

4.2 A novel function for *C1ql2* at the mossy fiber synapse

The C1q-like protein family comprises of four proteins with distinct expression across the CNS that act as secreted synaptic organizers. *C1ql2* is predominantly expressed by DGCs along with the more broadly expressed *C1ql3*, with both proteins highly localizing at the

mossy fiber system (Iijima et al., 2010; Shimono et al., 2010). It was previously shown that C1ql2 forms functional heteromers with C1ql3 at the MFS cleft, and together they recruit postsynaptic KARs. The same study suggested that the two proteins had compensatory functions, as only the deletion of both *C1ql2* and *-3*, but not that of the individual proteins, impaired MFS function (Matsuda et al., 2016). By reintroducing C1ql2 in *Bcl11b* cKO DGCs and knocking-down *C1ql2* in WT DGCs, I identified a novel function for C1ql2 at the MFS. I was able to show that C1ql2 participates in the presynaptic organization of the MFS, by driving the recruitment of SVs to the AZs, and is necessary for LTP expression, highlighting for the first time C1ql2 as an important component of this synapse type. This was further corroborated by the fact that overexpression of C1ql3 in *Bcl11b* cKO DGCs, that was previously shown to have compensatory functions to C1ql2, did not rescue the mutant phenotype. It is important to note that Matsuda et al., induced the C1ql2 mutation during embryonic development and analyzed mice in early postnatal stages (P12-P20), a time when the development of the mossy fiber circuit is still ongoing (Matsuda et al., 2016). In my work, I analyzed the functions of C1ql2 in the adult hippocampus, by inducing the mutation after the functional maturation of the mossy fiber system. The observed difference in the functions of C1ql2 could therefore be due to a mechanistic turnover upon circuit maturation, while the ability of C1ql3 to compensate for the C1ql2 functions in earlier stages could stem by the increased plasticity and adaptability of the brain during embryonic development.

Overexpression of C1ql2 in DGC had no effect on the SV recruitment compared to control animals, suggesting that some form of homeostasis is taking place on C1ql2 action level. The significant increase in C1ql2 protein levels was not investigated on a subcellular level. Not much is known about the surface presentation and transport of C1ql2 to the MFS and how this process is regulated, thus the possibility that the excess C1ql2 does not reach the synapse cannot be excluded. Moreover, C1ql2 is a secreted protein and its mechanism of action depends on its binding to pre- and postsynaptic partners. Thus, the availability of the interaction partners of C1ql2, or the lack therefore, could prohibit an additional effect by the excess C1ql2. Furthermore, the mechanism behind the SV recruitment to the AZ of MFS is not fully understood, leaving open the possibility that there is a threshold to the amount of SV that can be directed to an AZ at a certain time.

Moreover, I also observed C1ql2 to have an effect on the postsynaptic SA. Reintroduction of C1ql2 in a *Bcl11b* mutant background increased the number of spines in contact with MFB that contained a SA. The organelle also presented with a tendency of increased complexity when compared to control animals. Loss of C1ql2, however, did not have an effect on the SA, suggesting that the observed increase in the number of spines with a SA and the complexity of the SA was an indirect effect. In the *Bcl11b* mutant background a reduced number of MFS were present, possibly creating a need for strengthening of the remaining synapses. It has been shown that the SA is important for synaptic plasticity (Deller et al., 2007; Jedlicka et al., 2008; Segal et al., 2010). Thus, reintroduction of C1ql2 in the remaining MFS and the now renewed ability of the MF system to express LTP could have led the system to enhance the spines with SA to functionally compensate for the reduced number of MFS as a homeostatic process. However, based on the current literature on the SA functions, as well as the role C1ql2 has in synaptic function and the data presented in my thesis, no further conclusions can be drawn.

4.3 C1ql2-Nrxn3(25b+) interaction drives synaptic vesicle recruitment and C1ql2 targeting to the mossy fiber synapse

As both SV recruitment and MF-LTP expression happen at the presynaptic side (Nicoll & Schmitz, 2005), I hypothesized that C1ql2 induces both processes by sending feedback signals through interaction with presynaptic proteins. It was previously shown *in vitro* that C1ql2 interacts with a specific Nrxn3 isoform containing the sequence encoded by exon 25b, Nrxn3(25b+) (Matsuda et al., 2016). The Nrxn protein family is one of the best studied families of synaptic cell adhesion molecules that act as synaptic organizers. In mammals, three genes encode for neurexins: *Nrxn1*, *Nrxn2* and *Nrxn3*. The existence of alternative promoters and multiple splicing sites within the three genes yields the potential to produce an enormous amount of *Nrxn* isoforms, a number that exceeds the 12000 transcript isoforms in mice, the expression of which is brain-region specific (Gomez et al., 2021; Reissner et al., 2013; Schreiner et al., 2014; Treutlein et al., 2014). Nrxn3 is expressed in DGCs (Uchigashima et al., 2019). A number of synaptic proteins have been shown to interact with Nrxns in an isoform specific manner, forming complex interaction networks that

regulate many synaptic functions (Sudhof 2017; 2021). Nrns have been shown to not only control global regulatory functions of the synapse but can also act through distinct, neuron-type specific mechanisms (Missler et al., 2003; Chen et al., 2017b). Several studies have implicated Nrns in the recruitment of SV and dense-core vesicles (Dean et al., 2003; Ferdos et al., 2021; Quinn et al., 2017; Rui et al., 2017). Thus, I analyzed whether C1ql2 controlled SV recruitment through interaction with Nrnx3(25b+). HEK293 cells expressing C1ql2 co-cultured with hippocampal neurons expressing GFP-Nrnx3 α (25b+) induced the accumulation of GFP-Nrnx3 α (25b+) and neuronal vGlut1 at their contact points. However, C1ql2.K262E, a C1ql2 variant that was designed to not interact with Nrnx3(25b+), was unable to cluster GFP-Nrnx3 α (25b+) and vGlut1. Moreover, C1ql2-expressing HEK293 cells did not recruit vGlut1 in contacting hippocampal neurons upon deletion of all three *Nrxns*, while re-expression of Nrnx3 α (25b+) in the neurons was sufficient to rescue the phenotype. The difference in the capability to accumulate Nrnx3(25b+) at contact point of C1ql2 and the non-binding C1ql2 suggests that C1ql2 acts as a nucleator for Nrnx3(25b+). Moreover, the need for the presence of both proteins with binding ability suggests that the direct interaction between C1ql2 and Nrnx3(25b+) drives SV recruitment *in vitro*.

The co-culture system, however, is a highly artificial system and it does not take into account other factors contributing to the same processes that could alter the function of proteins. It is known that synaptic proteins and their signaling are really sensitive to the combination of synaptic proteins in their environment (Misk et al., 2022; Yang et al., 2014). Therefore, I analyzed the role of the C1ql2-Nrnx3(25b+) interaction in the context of SV recruitment *in vivo* at the MF system. Expression of the non-binding C1ql2 in DGCs of *Bcl11b* cKO mice, that do not express endogenous C1ql2, did not rescue the SV recruitment. However, the non-binding C1ql2 variant was not tested for interaction with other binding partners. Thus, it cannot be excluded that the introduced mutation also disrupts other C1ql2 interactions that contribute to the SV recruitment. Repression of *Nrxns* in DGCs recapitulated the impairment of the SV recruitment observed in *Bcl11b* cKO and *C1ql2* KD animals, supporting a role for Nrnx3 in SV recruitment at the MFS. However, due to the lack of specificity in the repression of *Nrxns* in the animal model I used, it cannot be excluded that the observed effect arose from C1ql2-independent Nrnx mechanisms. Rescue of specifically Nrnx3(25b+) in the DGCs of these animals would strengthen the conclusion that C1ql2-Nrnx3(25b+)

interaction is important for SV recruitment. Together, my data indicate that interaction of C1ql2 with Nrnx3(25b+) is necessary for the recruitment of SV at the MFS. The lack of Nrnx-isoform specific antibodies did not allow analysis of the role of C1ql2 in Nrnx3(25b+) accumulation in this system.

C1ql2 is secreted into the synaptic cleft, it is unknown, though, how its secretion is regulated and whether it is targeted to all MFS simultaneously. Interestingly, interruption of the C1ql2-Nrnx3(25b+) interaction *in vivo*, either by expressing a non-binding C1ql2 variant or by deletion of *Nrnx3* in DGCs reduces targeting of C1ql2 to MFS. It was previously shown, that Neurexophilin 1, another secreted protein that interacts with certain Nrnx isoforms, is delivered to the surface only upon interaction with Nrnx (Neupert et al., 2015). A similar mechanism could apply for the targeting of C1ql2 to the MFS, with C1ql2 interacting with Nrnx3(25b+) already at the ER level and being co-transported to the MFS. Once presented to the surface, both axonal and synaptic Nrnx are quite mobile, a property that is enhanced upon increase in activity (Klatt et al., 2021; Neupert et al., 2015). It is thus possible, that C1ql2 and Nrnx3(25b+) participate in a mechanism of self-augmented stabilization at the synapse. C1ql2 requires Nrnx3(25b+) to reach the MFS upon activation. Once at the synapse, C1ql2, that is able to form higher-order oligomers through its C1q domain (Ressl et al., 2015), acts as a nucleator for other mobile C1ql2-Nrnx3(25b+) molecules, creating larger complexes that are stabilized at the MFS. The accumulation of Nrnx3(25b+) at the MFS then drives SV recruitment. As the kinetics of synaptic proteins and their ability to form megaclusters directly connects to their function (Frank & Grant. 2017), it would be interesting to analyze the mechanisms involved in the surface presentation of C1ql2 and its transport to the synapse.

Finally, the importance of the C1ql2-Nrnx3(25b+) interaction in the expression of MF-LTP was analyzed. Surprisingly, expression of C1ql2.K262E in *Bcl11b* cKO DGCs, while not able to rescue SV recruitment, was able to fully rescue MF-LTP. This suggest that C1ql2 regulates MF-LTP through mechanisms independently of the interaction with Nrnx3(25b+) and independently of SV recruitment. Indeed, the increase in P_r at MFS has not only been linked with accumulation of SV but also with accumulation of Ca^{2+} channels at release sites (Fukaya et al., 2021) and their tighter coupling with SV (Midorikawa & Sakaba, 2017). However, MF-LTP upon introduction of C1ql2.K262E was also not completely similar to that in the control

or the C1ql2 rescue situation, but presented with a significant increase in the fEPSP slope during the initial induction phase. It might be possible, that the mutation I introduced to C1ql2 creates a gain-of-function effect, and thus conclusions regarding the mechanisms downstream of C1ql2 in MF-LTP expression cannot yet be drawn.

4.4 Bcl11b/C1ql2/Nrxn3(25b+) in the understanding of neurodevelopmental and neuropsychiatric disorders

The TF Bcl11b has been linked to NDDs (Lessel et al., 2018; Prasad et al., 2020) and neuropsychiatric disorders (Contet et al., 2011; Whitton et al., 2018; Whitton et al., 2016). BCL11B-Related Disorder (BCL11BRD) is a neurodevelopmental disorder associated with mutations in *BCL11B*. Individuals with BCL11BRD present with global neurodevelopmental delay, impaired speech acquisition, learning deficits and autistic features (Eto et al., 2022; Lessel et al., 2018; Prasad et al., 2020; Punwani et al., 2016; Yang et al., 2020; Yu et al., 2023). Moreover, polymorphisms in *BCL11B* have been associated with schizophrenia (Pardinas et al., 2018; Trubetskoy et al., 2022). Increasing evidence demonstrates that NDDs and neuropsychiatric conditions, such as ASD, intellectual disability and schizophrenia, arise from synaptic dysfunction (Hayashi-Takagi, 2017; Lepeta et al., 2016; Zoghbi & Bear, 2012). Physiological synaptic function depends on proper formation, maturation and specification of synapses, processes that are regulated by synaptic proteins and their subsequent molecular machineries. A number of synaptic proteins, including those acting as synaptic organizer, have been already identified to govern synaptic function (de Wit & Ghosh, 2016; O'Rourke et al., 2012; Sudhof 2017). Recent genetic studies have linked genes encoding for synaptic proteins to NDDs and neuropsychiatric disorders (Sudhof 2021; Torres et al., 2017; Wang et al., 2018). Nrxn3 is among the synaptic proteins that have been associated with various such disorders (Kasem et al., 2018; Zhang et al., 2022). Deletions in the *NRXN3* gene locus have been found in individuals with ASD (Vaags et al., 2012), while polymorphisms have been implicated in schizophrenia (Hu et al., 2013). Moreover, single-nucleotide polymorphisms (SNP) were associated with addiction, with one recorded SNP altering the expression of Nrxn3(25b+) (Docampo et al., 2012; Hishimoto et al., 2007). Recent genetic studies have associated *C1QL2* as well with schizophrenia and addiction (Huggett &

Stallings, 2020a; 2020b; Marballi et al., 2022). In my thesis, I identified a functional link between the three proteins, Bcl11b, C1ql2 and Nrnx3, on the synaptic organization of MFS, specifically in the recruitment of SVs to the AZ. Impairments in SV trafficking and changes in release probability have been also implicated in neurological and neuropsychiatric disorders (Egbujo & Bartos, 2019; Lepeta et al., 2016; Zhu et al., 2021). Thus, my work could provide a new entry point in the mechanistic understanding of the pathogenesis of related NDDs and neuropsychiatric disorders.

4.5 Bcl11b- a regulator of synaptic specification and function

Synapses are key sites for information transfer and comprise the communication nodes between neurons. With trillions of synapses performing specific computations simultaneously, the question of how the needed synaptic specificity is achieved has been raised. It has been previously suggested that the unique synaptic properties are defined by synapse-type specific molecular codes, with the synaptic organizer proteins at the center of these codes. The unique combination and the relative expression levels of these proteins allows for precise synaptic function (de Wit & Gosh, 2016; O'Rourke, 2012; Sudhof, 2107). Nrnxns have been considered central effectors of these codes due to their intrinsic diversity and the neuron-subtype-specific expression of the different isoforms (Gomez et al., 2021; Sudhof, 2017; Uchigaschima et al., 2019; Ullrich et al., 1995). C1ql2, on the other hand, is expressed in a restricted number of neuron subtypes (Iijima et al., 2010; Shimono et al., 2010). It is most characteristically expressed by DGCs and secreted in the MFS synaptic cleft, where it acts as a synaptic organizer by recruiting postsynaptic KARs (Matsuda et al., 2016) and, as shown here, by organizing the SV pool at the presynapse through interaction with a specific Nrnx3 isoform and promoting LTP expression. Moreover, MFS are considered to have unique features, such as the characteristic complex structure of the boutons that include multiple release sites, the large pool of releasable SV in the proximity of the AZ and the presynaptically expressed LTP. Here, I demonstrated that C1ql2 is an important component for the expression of some of these features. Thus, C1ql2 is not only part of the molecular code but could be considered a central effector in the MFS specification.

Bcl11b has been demonstrated to have a broad range of functions in the CNS among which neuron differentiation and subtype specification, neurogenesis and cell survival (Arlotta et al., 2005; Enomoto et al., 2011; Nikouei et al., 2016; Simon et al., 2012; 2016). My work provides, for the first time, evidence that Bcl11b directly regulates synapse function. Furthermore, the ability of C1ql2 to establish MFS-specific features, sets Bcl11b as a regulator of neuron subtype-dependent synapse specification. Indications for such a role for Bcl11b can be found in other neuronal populations expressing the TF. It has been shown that in medium spiny neurons (MSN), Bcl11b is important for their differentiation and architectural organization (Arlotta et al., 2008). Transcriptome analysis of MSN upon postnatal deletion of *Bcl11b* revealed that among the deregulated genes, an overrepresentation of genes involved in synaptic organization was apparent (Song et al., 2022). Furthermore, *Bcl11b*-deficient MSN, whilst having physiological morphology and membrane properties, show impaired glutamate-evoked Ca²⁺ signaling and DRD1-mediated modulation of glutamate-evoked currents, features characteristic for MSN postsynapse (Fjodorova et al., 2022). Investigating the role of Bcl11b in synaptic function in other neuronal populations expressing this TF should thus be considered, especially due to its correlation with neurological disorders characterized by synaptic dysfunction.

5 Summary

Synaptic function is determined by the unique combination of synaptic proteins and their relative expression levels. Alterations in the protein composition of the synapse can lead to synaptic dysfunction that has been associated with several neurodevelopmental and neuropsychiatric disorders. Understanding the molecular basis of synaptic function and its regulation could, thus, provide insight into the pathomechanisms of such disorders. *Bcl11b*, a transcription factor associated with various neurodevelopmental and neuropsychiatric disorders characterized by synaptic dysfunction, has been shown to control the structural and functional integrity of the mossy fiber synapses in the adult murine hippocampus. In my thesis, I explore the mechanisms through which *Bcl11b* regulates structural and functional integrity in these synapses. Here, I demonstrate that *C1ql2*, a direct transcriptional target of *Bcl11b* at the dentate gyrus that is downregulated upon *Bcl11b* ablation, is also a functional target of *Bcl11b*. Reintroduction of *C1ql2* with stereotaxic injection of AAV expression vectors in dentate granule cells two weeks post *Bcl11b* mutation induction, was able to rescue the distribution and docking of synaptic vesicles at the active zones of mossy fiber synapses, as well as to restore the long-term potentiation, features that were impaired by the loss of *Bcl11b*. The regulation of these synaptic properties was specific for *C1ql2*, as overexpression of *C1ql3* in *Bcl11b* mutant dentate granule cells, a protein that was thought to compensate for *C1ql2* function, was unable to rescue the *Bcl11b*-mutant phenotypes. Furthermore, knock-down of *C1ql2* in the dentate granule cells, was sufficient to perturb synaptic vesicle recruitment and long-term potentiation to a similar extent to that observed upon *Bcl11b* ablation. To better understand how *C1ql2* exerts these functions, I analysed the previously speculated interaction between *C1ql2* and a specific Neurexin 3 isoform. By perturbing the *C1ql2*-Neurexin 3 interaction, either by expressing a *C1ql2* variant that is unable to bind to Neurexin 3 or by deleting *Neurexin 3*, I was able to show in co-cultures of non-neuronal cells with hippocampal neurons that *C1ql2* promotes accumulation of Neurexin 3, and that their interaction is essential for synaptic vesicle recruitment. Moreover, I could demonstrate a role of the interaction between *C1ql2* and Neurexin 3 *in vivo* directly at the mossy fiber synapses. Expression of the non-binding *C1ql2* variant in *Bcl11b* mutant dentate granules

cells did not rescue the synaptic vesicle recruitment. Repression of *Neurexin 3* expression in the dentate gyrus impaired the synaptic vesicle recruitment to a similar extent as observed in *Bcl11b* mutant and *C1ql2* knock-down animals. Additionally, I observed that interruption of the C1ql2-Neurexin 3 interaction negatively affects the targeting of C1ql2 at the mossy fiber synapse.

Taken together, my data identify Bcl11b/C1ql2/Neurexin 3 as a regulatory pathway in the function of mature mossy fiber synapses. This could provide new insight in the mechanistic understanding of the pathogenesis of related neurodevelopmental and neuropsychiatric disorders.

6 References

1. Abulaiti, X., Wang, A., Zhang, H., Su, H., Gao, R., Chen, J., Gao, S., & Li, L. (2022). Disrupted mossy fiber connections from defective embryonic neurogenesis contribute to SOX11-associated schizophrenia. *Cell Mol Life Sci*, 79(3), 180. <https://doi.org/10.1007/s00018-022-04206-4>
2. Acsády, L., Kamondi, A., Sík, A., Freund, T., & Buzsáki, G. (1998). GABAergic Cells Are the Major Postsynaptic Targets of Mossy Fibers in the Rat Hippocampus. *J Neurosci*, 18(9), 3386-3403. <https://doi.org/10.1523/JNEUROSCI.18-09-03386.1998>
3. Ahmed, I., Sbodio, J. I., Harraz, M. M., Tyagi, R., Grima, J. C., Albacarys, L. K., Hubbi, M. E., Xu, R., Kim, S., Paul, B. D., & Snyder, S. H. (2015). Huntington's disease: Neural dysfunction linked to inositol polyphosphate multikinase. *Proc Natl Acad Sci U S A*, 112(31), 9751-9756. <https://doi.org/10.1073/pnas.1511810112>
4. Amaral, D. G., & Dent, J. A. (1981). Development of the mossy fibers of the dentate gyrus: I. A light and electron microscopic study of the mossy fibers and their expansions. *J Comp Neurol*, 195(1), 51-86. <https://doi.org/10.1002/cne.901950106>
5. Amaral, D. G., Ishizuka, N., & Claiborne, B. (1990). Neurons, numbers and the hippocampal network. *Prog Brain Res*, 83, 1-11. [https://doi.org/10.1016/s0079-6123\(08\)61237-6](https://doi.org/10.1016/s0079-6123(08)61237-6)
6. Amaral, D. G., Scharfman, H. E., & Lavenex, P. (2007). The dentate gyrus: fundamental neuroanatomical organization (dentate gyrus for dummies). *Prog Brain Res*, 163, 3-22. [https://doi.org/10.1016/S0079-6123\(07\)63001-5](https://doi.org/10.1016/S0079-6123(07)63001-5)
7. Amaral, D. G., & Witter, M. P. (1989). The three-dimensional organization of the hippocampal formation: A review of anatomical data. *Neuroscience*, 31(3), 571-591. [https://doi.org/10.1016/0306-4522\(89\)90424-7](https://doi.org/10.1016/0306-4522(89)90424-7)
8. Andersen, P. (1975). Organization of hippocampal neurons and their interconnections. . In R. L. Isaacson & K. H. Pribram (Eds.), *The Hippocampus* (Vol. 1, pp. 155-175). Plenum Press. https://link.springer.com/chapter/10.1007/978-1-4684-2976-3_7

9. Andersen, P., Morris, R., Amaral, D., Bliss, T., & O'Keefe, J. (2006). The Hippocampal Formation. In *The Hippocampus Book* (1 ed., pp. 3-8). Oxford University Press. https://books.google.de/books?id=hSs_RETUVIIC
10. Arikath, J., & Reichardt, L. F. (2008). Cadherins and catenins at synapses: roles in synaptogenesis and synaptic plasticity. *Trends Neurosci*, *31*(9), 487-494. <https://doi.org/10.1016/j.tins.2008.07.001>
11. Arlotta, P., Molyneaux, B. J., Chen, J., Inoue, J., Kominami, R., & Macklis, J. D. (2005). Neuronal subtype-specific genes that control corticospinal motor neuron development in vivo. *Neuron*, *45*(2), 207-221. <https://doi.org/10.1016/j.neuron.2004.12.036>
12. Arlotta, P., Molyneaux, B. J., Jabaudon, D., Yoshida, Y., & Macklis, J. D. (2008). CtIP2 controls the differentiation of medium spiny neurons and the establishment of the cellular architecture of the striatum. *J Neurosci*, *28*(3), 622-632. <https://doi.org/10.1523/JNEUROSCI.2986-07.2008>
13. Atwood, H. L., & Karunanithi, S. (2002). Diversification of synaptic strength: presynaptic elements. *Nat Rev Neurosci*, *3*(7), 497-516. <https://doi.org/10.1038/nrn876>
14. Avram, D., Fields, A., Pretty On Top, K., Nevriy, D. J., Ishmael, J. E., & Leid, M. (2000). Isolation of a novel family of C(2)H(2) zinc finger proteins implicated in transcriptional repression mediated by chicken ovalbumin upstream promoter transcription factor (COUP-TF) orphan nuclear receptors. *J Biol Chem*, *275*(14), 10315-10322. <https://doi.org/10.1074/jbc.275.14.10315>
15. Avram, D., Fields, A., Senawong, T., Topark-Ngarm, A., & Leid, M. (2002). COUP-TF (chicken ovalbumin upstream promoter transcription factor)-interacting protein 1 (CTIP1) is a sequence-specific DNA binding protein *Biochem J*, *368*(Pt 2), 555-563. <https://doi.org/10.1042/BJ20020496>
16. Babb, T. L., Kupfer, W. R., Pretorius, J. K., Crandall, P. H., & Levesque, M. F. (1991). Synaptic reorganization by mossy fibers in human epileptic fascia dentata. *Neuroscience*, *42*(2), 351-363. [https://doi.org/10.1016/0306-4522\(91\)90380-7](https://doi.org/10.1016/0306-4522(91)90380-7)

17. Bartos, M., Vida, I., & Jonas, P. (2007). Synaptic mechanisms of synchronized gamma oscillations in inhibitory interneuron networks. *Nat Rev Neurosci*, *8*(1), 45-56. <https://doi.org/10.1038/nrn2044>
18. Bashir, Z. I., Bortolotto, Z. A., Davies, C. H., Berretta, N., Irving, A. J., Seal, A. J., Henley, J. M., Jane, D. E., Watkins, J. C., & Collingridge, G. L. (1993). Induction of LTP in the hippocampus needs synaptic activation of glutamate metabotropic receptors. *Nature*, *363*, 347-350. <https://doi.org/10.1038/363347a0>
19. Baude, A., Nusser, Z., Molnár, E., McIlhinney, R. A. J., & Somogyi, P. (1995). High-resolution immunogold localization of AMPA type glutamate receptor subunits at synaptic and non-synaptic sites in rat hippocampus. *Neuroscience*, *69*(4), 1031-1055. [https://doi.org/10.1016/0306-4522\(95\)00350-R](https://doi.org/10.1016/0306-4522(95)00350-R)
20. Bayes, A., van de Lagemaat, L. N., Collins, M. O., Croning, M. D., Whittle, I. R., Choudhary, J. S., & Grant, S. G. (2011). Characterization of the proteome, diseases and evolution of the human postsynaptic density. *Nat Neurosci*, *14*(1), 19-21. <https://doi.org/10.1038/nn.2719>
21. Bennett, M. V. L., & Zukin, R. S. (2004). Electrical Coupling and Neuronal Synchronization in the Mammalian Brain. *Neuron*, *41*(11), 495-511. [https://doi.org/10.1016/S0896-6273\(04\)00043-1](https://doi.org/10.1016/S0896-6273(04)00043-1)
22. Blackstad, T. W., Brink, K., Hem, J., & Jeune, B. (1970). Distribution of hippocampal mossy fibers in the rat. An experimental study with silver impregnation methods. *J Comp Neurol*, *138*(4), 433-449. <https://doi.org/10.1002/cne.901380404>
23. Blümcke, I., Behle, K., Malitschek, B., Kuhn, R., Knöpfel, T., Wolf, H. K., & Wiestler, O. D. (1996). Immunohistochemical distribution of metabotropic glutamate receptor subtypes mGluR1b, mGluR2/3, mGluR4a and mGluR5 in human hippocampus. *Brain Res*, *736*(1-2), 217-226. [https://doi.org/10.1016/0006-8993\(96\)00697-X](https://doi.org/10.1016/0006-8993(96)00697-X)
24. Bocchiaro, C. M., & Feldman, J. L. (2004). Synaptic activity-independent persistent plasticity in endogenously active mammalian motoneurons. *Proc Natl Acad Sci U S A*, *101*(12), 4292-4295. <https://doi.org/10.1073/pnas.0305712101>
25. Bolliger, M. F., Martinelli, D. C., & Sudhof, T. C. (2011). The cell-adhesion G protein-coupled receptor BAI3 is a high-affinity receptor for C1q-like proteins. *Proc Natl Acad Sci U S A*, *108*(6), 2534-2539. <https://doi.org/10.1073/pnas.1019577108>

26. Bortolotto, Z. A., Clarke, V. R. J., Delany, C. M., Parry, M. C., Smolders, I., Vignes, M., Ho, K. H., Miu, P., Brinton, B. T., Fantaske, R., Odgen, A., Gates, M., Ornstein, P. L., Lodge, D., Bleakman, D., & Collingridge, G. L. (1999). Kainate receptors are involved in synaptic plasticity. *Nature*, *402*, 297-301. <https://doi.org/10.1038/46290>
27. Breustedt, J., & Schmitz, D. (2004). Assessing the role of GLUK5 and GLUK6 at hippocampal mossy fiber synapses. *J Neurosci*, *24*(45), 10093-10098. <https://doi.org/10.1523/JNEUROSCI.3078-04.2004>
28. Breustedt, J., Vogt, K. E., Miller, R. J., Nicoll, R. A., & Schmitz, D. (2003). Alpha1E-containing Ca²⁺ channels are involved in synaptic plasticity. *Proc Natl Acad Sci U S A*, *100*(21). <https://doi.org/10.1073/pnas.2035117100>
29. Buckmaster, P. S., Strowbridge, B. W., Kunkel, D. D., Schmiede, D. L., & Schwartzkroin, P. A. (1992). Mossy cell axonal projections to the dentate gyrus molecular layer in the rat hippocampal slice. *Hippocampus*, *2*(4), 349-362. <https://doi.org/10.1002/hipo.450020403>
30. Budde, T., Minta, A., White, J. A., & Kay, A. R. (1997). Imaging free zinc in synaptic terminals in live hippocampal slices. *Neuroscience*, *79*(2), 347-358. [https://doi.org/10.1016/S0306-4522\(96\)00695-1](https://doi.org/10.1016/S0306-4522(96)00695-1)
31. Cai, S., Kalisky, T., Sahoo, D., Dalerba, P., Feng, W., Lin, Y., Qian, D., Kong, A., Yu, J., Wang, F., Chen, E. Y., Scheeren, F. A., Kuo, A. H., Sikandar, S. S., Hisamori, S., van Weele, L. J., Heiser, D., Sim, S., Lam, J., . . . Clarke, M. F. (2017). A Quiescent Bcl11b High Stem Cell Population Is Required for Maintenance of the Mammary Gland. *Cell Stem Cell*, *20*(2), 247-260 e245. <https://doi.org/10.1016/j.stem.2016.11.007>
32. Castillo, P. E., Malenka, R. C., & Nicoll, R. A. (1997). Kainate receptors mediate a slow postsynaptic current in hippocampal CA3 neurons. *Nature*, *388*, 182-186. <https://doi.org/10.1038/40645>
33. Chafetz, R. S., Nahm, W. K., & Noebels, J. L. (1995). Aberrant expression of neuropeptide Y in hippocampal mossy fibers in the absence of local cell injury following the onset of spike-wave synchronization. *Brain Res. Mol.*, *31*(1-2), 111-121. [https://doi.org/10.1016/0169-328X\(95\)00041-P](https://doi.org/10.1016/0169-328X(95)00041-P)

34. Chandy, J., Pierce, J. P., & Milner, T. A. (1995). Rat hippocampal mossy fibers contain cholecystinin-like immunoreactivity. *Anat Rec*, 243(4), 519-523. <https://doi.org/10.1002/ar.1092430415>
35. Che, F., Tie, X., Lei, H., Zhang, X., Duan, M., Zhang, L., & Yang, Y. (2022). Identification of two novel variants of the BCL11B gene in two Chinese pedigrees associated with neurodevelopmental disorders. *Front Mol Neurosci*, 15, 927357. <https://doi.org/10.3389/fnmol.2022.927357>
36. Chen, L. F., Zhou, A. S., & West, A. E. (2017a). Transcribing the connectome: roles for transcription factors and chromatin regulators in activity-dependent synapse development. *J Neurophysiol*, 118(2), 755-770. <https://doi.org/10.1152/jn.00067.2017>
37. Chen, L. Y., Jiang, M., Zhang, B., Gokce, O., & Sudhof, T. C. (2017b). Conditional Deletion of All Neurexins Defines Diversity of Essential Synaptic Organizer Functions for Neurexins. *Neuron*, 94(3), 611-625 e614. <https://doi.org/10.1016/j.neuron.2017.04.011>
38. Chicurel, M. E., & Harris, K. M. (1992). Three-dimensional analysis of the structure and composition of CA3 branched dendritic spines and their synaptic relationships with mossy fiber boutons in the rat hippocampus. *J Comp Neurol*, 325(2), 169-182. <https://doi.org/10.1002/cne.903250204>
39. Choquet, D., & Triller, A. (2013). The dynamic synapse. *Neuron*, 80(3), 691-703. <https://doi.org/10.1016/j.neuron.2013.10.013>
40. Chou, S. J., & Tole, S. (2019). Lhx2, an evolutionarily conserved, multifunctional regulator of forebrain development. *Brain Res*, 1705, 1-14. <https://doi.org/10.1016/j.brainres.2018.02.046>
41. Christopherson, K. S., Ullian, E. M., Stokes, C. C., Mallowney, C. E., Hell, J. W., Agah, A., Lawler, J., Mosher, D. F., Bornstein, P., & Barres, B. A. (2005). Thrombospondins are astrocyte-secreted proteins that promote CNS synaptogenesis. *Cell*, 120(3), 421-433. <https://doi.org/10.1016/j.cell.2004.12.020>
42. Cismasiu, V. B., Adamo, K., Gecewicz, J., Duque, J., Lin, Q., & Avram, D. (2005). BCL11B functionally associates with the NuRD complex in T lymphocytes to repress targeted promoter. *Oncogene*, 24(45), 6753-6764. <https://doi.org/10.1038/sj.onc.1208904>

43. Cismasiu, V. B., Ghanta, S., Duque, J., Albu, D. I., Chen, H. M., Kasturi, R., & Avram, D. (2006). BCL11B participates in the activation of IL2 gene expression in CD4+ T lymphocytes. *Blood*, *108*(8), 2695-2702. <https://doi.org/10.1182/blood-2006-05-021790>
44. Claiborne, B. J., Amaral, D. G., & Cowan, W. M. (1986). A light and electron microscopic analysis of the mossy fibers of the rat dentate gyrus. *J Comp Neurol*, *246*(4), 435-458. <https://doi.org/10.1002/cne.902460403>
45. Colom, L. V., Castaneda, M. T., Reyna, T., Hernandez, S., & Garrido-Sanabria, E. (2005). Characterization of medial septal glutamatergic neurons and their projection to the hippocampus. *Synapse*, *58*(3), 151-164. <https://doi.org/10.1002/syn.20184>
46. Commons, K. G., & Milner, T. A. (1995). Ultrastructural heterogeneity of enkephalin-containing terminals in the rat hippocampal formation. *J Comp Neurol*, *358*(3), 324-342. <https://doi.org/10.1002/cne.903580303>
47. Conquet, F., Bashir, Z. I., Davies, C. H., Daniel, H., Ferraguti, F., Bordi, F., Franz-Bacon, K., Reggiani, A., Matarese, V., Condé, F., Collingridge, G. L., & Crépel, F. (1994). Motor deficit and impairment of synaptic plasticity in mice lacking mGluR1. *Nature*, *372*, 237-243. <https://doi.org/10.1038/372237a0>
48. Contet, C., Gardon, O., Filliol, D., Becker, J. A., Koob, G. F., & Kieffer, B. L. (2011). Identification of genes regulated in the mouse extended amygdala by excessive ethanol drinking associated with dependence. *Addict Biol*, *16*(4), 615-619. <https://doi.org/10.1111/j.1369-1600.2010.00304.x>
49. Contractor, A., Swanson, G., & Heinemann, S. F. (2001). Kainate Receptors Are Involved in Short- and Long-Term Plasticity at Mossy Fiber Synapses in the Hippocampus. *Neuron*, *29*(1), 209-216. [https://doi.org/10.1016/S0896-6273\(01\)00191-X](https://doi.org/10.1016/S0896-6273(01)00191-X)
50. Crawford, I. L., & Connor, J. D. (1973). Localization and Release of Glutamic Acid in Relation to the Hippocampal Mossy Fibre Pathway. *Nature*, *244*, 442-443. <https://doi.org/10.1038/244442a0>
51. De Bruyckere, E., Simon, R., Nestel, S., Heimrich, B., Katzel, D., Egorov, A. V., Liu, P., Jenkins, N. A., Copeland, N. G., Schwegler, H., Draguhn, A., & Britsch, S. (2018). Stability and Function of Hippocampal Mossy Fiber Synapses Depend on

<https://doi.org/10.3389/fnmol.2018.00103>

52. de Wit, J., & Ghosh, A. (2016). Specification of synaptic connectivity by cell surface interactions. *Nat Rev Neurosci*, 17(1), 22-35. <https://doi.org/10.1038/nrn.2015.3>
53. De Roo, M., Klauser, P., Garcia, P. M., Poglia, L., & Muller, D. (2008). Spine dynamics and synapse remodeling during LTP and memory processes. *Prog Brain Res*, 169, 199-207. [https://doi.org/10.1016/S0079-6123\(07\)00011-8](https://doi.org/10.1016/S0079-6123(07)00011-8)
54. Dean, C. S., F.G.; Choh, J.; DeMaria, S.; Berger, J.; Isacoff, E.; Scheiffele, P. (2003). Neurexin mediates the assembly of presynaptic terminals. *Nat Neurosci*, 6(7), 708-716. <https://doi.org/10.1038/nn1074>.
55. Deller, T., Bas Orth, C., Del Turco, D., Vlachos, A., Burbach, G. J., Drakew, A., Chabanis, S., Korte, M., Schwegler, H., Haas, C. A., & Frotscher, M. (2007). A role for synaptopodin and the spine apparatus in hippocampal synaptic plasticity. *Ann Anat*, 189(1), 5-16. <https://doi.org/10.1016/j.aanat.2006.06.013>
56. Deller, T., Merten, T., Roth, S. U., Mundel, P., & Frotscher, M. (2000). Actin-associated protein synaptopodin in the rat hippocampal formation: Localization in the spine neck and close association with the spine apparatus of principal neurons. *The Journal of Comparative Neurology*, 418(2), 164-181. [https://doi.org/10.1002/\(sici\)1096-9861\(20000306\)418:2<164::Aid-cne4>3.0.Co;2-0](https://doi.org/10.1002/(sici)1096-9861(20000306)418:2<164::Aid-cne4>3.0.Co;2-0)
57. Desplats, P. A., Lambert, J. R., & Thomas, E. A. (2008). Functional roles for the striatal-enriched transcription factor, Bcl11b, in the control of striatal gene expression and transcriptional dysregulation in Huntington's disease. *Neurobiol Dis*, 31(3), 298-308. <https://doi.org/10.1016/j.nbd.2008.05.005>
58. Dietrich, D., Kirschstein, T., Kukley, M., Pereverzev, A., von der Brélie, C., Schneider, T., & Beck, H. (2003). Functional specialization of presynaptic Cav2.3 Ca²⁺ channels. *Neuron*, 39(3), 483-496. [https://doi.org/10.1016/s0896-6273\(03\)00430-6](https://doi.org/10.1016/s0896-6273(03)00430-6)
59. Docampo, E., Ribases, M., Gratacos, M., Bruguera, E., Cabezas, C., Sanchez-Mora, C., Nieva, G., Puente, D., Argimon-Pallas, J. M., Casas, M., Rabionet, R., & Estivill, X. (2012). Association of neurexin 3 polymorphisms with smoking behavior. *Genes Brain Behav*, 11(6), 704-711. <https://doi.org/10.1111/j.1601-183X.2012.00815.x>

60. Duman, J. G., Tu, Y. K., & Tolia, K. F. (2016). Emerging Roles of BAI Adhesion-GPCRs in Synapse Development and Plasticity. *Neural Plast*, 2016, 8301737. <https://doi.org/10.1155/2016/8301737>
61. Elgueta, C., & Bartos, M. (2019). Dendritic inhibition differentially regulates excitability of dentate gyrus parvalbumin-expressing interneurons and granule cells. *Nat Commun*, 10(1), 5561. <https://doi.org/10.1038/s41467-019-13533-3>
62. Enomoto, T., Ohmoto, M., Iwata, T., Uno, A., Saitou, M., Yamaguchi, T., Kominami, R., Matsumoto, I., & Hirota, J. (2011). Bcl11b/Ctip2 controls the differentiation of vomeronasal sensory neurons in mice. *J Neurosci*, 31(28), 10159-10173. <https://doi.org/10.1523/JNEUROSCI.1245-11.2011>
63. Erdmann, G., Schutz, G., & Berger, S. (2007). Inducible gene inactivation in neurons of the adult mouse forebrain. *BMC Neurosci*, 8, 63. <https://doi.org/10.1186/1471-2202-8-63>
64. Eto, K., Machida, O., Yanagishita, T., Shimojima Yamamoto, K., Chiba, K., Aihara, Y., Hasegawa, Y., Nagata, M., Ishihara, Y., Miyashita, Y., Asano, Y., Nagata, S., & Yamamoto, T. (2022). Novel BCL11B truncation variant in a patient with developmental delay, distinctive features, and early craniosynostosis. *Hum Genome Var*, 9(1), 43. <https://doi.org/10.1038/s41439-022-00220-x>
65. Feil, S., Vatcheva, N., & Feil, R. (2009). Inducible Cre Mice. In R. Kühn & W. Wurst (Eds.), *Gene Knockout Protocols* (Second ed., Vol. 530, pp. 343-363). Humana Press.
66. Ferdos, S., Brockhaus, J., Missler, M., & Rohlmann, A. (2021). Deletion of beta-Neurexins in Mice Alters the Distribution of Dense-Core Vesicles in Presynapses of Hippocampal and Cerebellar Neurons. *Front Neuroanat*, 15, 757017. <https://doi.org/10.3389/fnana.2021.757017>
67. Fjodorova, M., Noakes, Z., De La Fuente, D. C., Errington, A. C., & Li, M. (2022). Dysfunction of cAMP–Protein Kinase A–Calcium Signaling Axis in Striatal Medium Spiny Neurons: A Role in Schizophrenia and Huntington’s Disease Neuropathology. *Biological Psychiatry Global Open Science*. <https://doi.org/10.1016/j.bpsgos.2022.03.010>
68. Flavell, S. W., Kim, T. K., Gray, J. M., Harmin, D. A., Hemberg, M., Hong, E. J., Markenscoff-Papadimitriou, E., Bear, D. M., & Greenberg, M. E. (2008). Genome-wide

- analysis of MEF2 transcriptional program reveals synaptic target genes and neuronal activity-dependent polyadenylation site selection. *Neuron*, 60(6), 1022-1038.
<https://doi.org/10.1016/j.neuron.2008.11.029>
69. Foster, M., & Sherrington, C. S. (1897). The Central Nervous System. In A Textbook of Physiology (Seventh ed.). MacMillan & Co Ltd.
 70. Fox, M. A., & Umemori, H. (2006). Seeking long-term relationship: axon and target communicate to organize synaptic differentiation. *J Neurochem*, 97(5), 1215-1231.
<https://doi.org/10.1111/j.1471-4159.2006.03834.x>
 71. Frank, R. A., & Grant, S. G. (2017). Supramolecular organization of NMDA receptors and the postsynaptic density. *Curr Opin Neurobiol*, 45, 139-147.
<https://doi.org/10.1016/j.conb.2017.05.019>
 72. Frerking, M., Wondolowski, J. (2008). Regulation of Neurotransmitter Release by Presynaptic Receptors. In: Wang, ZW. (eds) Molecular Mechanisms of Neurotransmitter Release. Contemporary Neuroscience. Humana Press, Totowa, NJ.
https://doi.org/10.1007/978-1-59745-481-0_14
 73. Fukata, Y., Adesnik, H., Iwanaga, T., Brecht, D. S., Nicoll, R. A., & Fukata, M. (2006). Epilepsy-Related Ligand/Receptor Complex LGI1 and ADAM22 Regulate Synaptic Transmission. *Science*, 313(5794), 1792-1795.
<https://doi.org/10.1126/science.1129947>
 74. Fukaya, R., Maglione, M., Sigrist, S. J., & Sakaba, T. (2021). Rapid Ca²⁺ channel accumulation contributes to cAMP-mediated increase in transmission at hippocampal mossy fiber synapses. *Proc Natl Acad Sci U S A*, 118(9).
<https://doi.org/10.1073/pnas.2016754118>
 75. Gall, C., Lauterborn, J., Isackson, P., & White, J. (1990). Seizures, neuropeptide regulation, and mRNA expression in the hippocampus. *Prog Brain Res*, 83, 371-390.
[https://doi.org/10.1016/s0079-6123\(08\)61263-7](https://doi.org/10.1016/s0079-6123(08)61263-7)
 76. Golonzhka, O., Metzger, D., Bornert, J. M., Bay, B. K., Gross, M. K., Kioussi, C., & Leid, M. (2009). Ctip2/Bcl11b controls ameloblast formation during mammalian odontogenesis. *Proc Natl Acad Sci U S A*, 106(11), 4278-4283.
<https://doi.org/10.1073/pnas.0900568106>

77. Gomez, A. M., Traunmuller, L., & Scheiffele, P. (2021). Neurexins: molecular codes for shaping neuronal synapses. *Nat Rev Neurosci*, 22(3), 137-151. <https://doi.org/10.1038/s41583-020-00415-7>
78. Grant, S. G. (2012). Synaptopathies: diseases of the synaptome. *Curr Opin Neurobiol*, 22(3), 522-529. <https://doi.org/10.1016/j.conb.2012.02.002>
79. Grant, S. G. N. (2019). Synapse diversity and synaptome architecture in human genetic disorders. *Hum Mol Genet*, 28(R2), R219-R225. <https://doi.org/10.1093/hmg/ddz178>
80. Guang, S., Pang, N., Deng, X., Yang, L., He, F., Wu, L., Chen, C., Yin, F., & Peng, J. (2018). Synaptopathology Involved in Autism Spectrum Disorder. *Front Cell Neurosci*, 12, 470. <https://doi.org/10.3389/fncel.2018.00470>
81. Hannou, L., Roy, P. G., Ballester Roig, M. N., & Mongrain, V. (2020). Transcriptional control of synaptic components by the clock machinery. *Eur J Neurosci*, 51(1), 241-267. <https://doi.org/10.1111/ejn.14294>
82. Harris, E. W., & Cotman, C. W. (1986). Long-term potentiation of guinea pig mossy fiber responses is not blocked by N-methyl d-aspartate antagonists. *Neurosci Lett*, 70(1), 132-137. [https://doi.org/10.1016/0304-3940\(86\)90451-9](https://doi.org/10.1016/0304-3940(86)90451-9)
83. Hayashi-Takagi, A. (2017). Synapse pathology and translational applications for schizophrenia. *Neurosci Res*, 114, 3-8. <https://doi.org/10.1016/j.neures.2016.09.001>
84. Hazan, L., & Ziv, N. E. (2020). Activity Dependent and Independent Determinants of Synaptic Size Diversity. *J Neurosci*, 40(14), 2828-2848. <https://doi.org/10.1523/JNEUROSCI.2181-19.2020>
85. Henze, D. A., McMahon, D. B. T., Harris, K. M., & Barrionuevo, G. (2002). Giant miniature EPSCs at the hippocampal mossy fiber to CA3 pyramidal cell synapse are monoquantal. *J Neurophysiol*, 87(1), 15-29. <https://doi.org/10.1152/jn.00394.2001>
86. Hishimoto, A., Liu, Q. R., Drgon, T., Pletnikova, O., Walther, D., Zhu, X. G., Troncoso, J. C., & Uhl, G. R. (2007). Neurexin 3 polymorphisms are associated with alcohol dependence and altered expression of specific isoforms. *Hum Mol Genet*, 16(23), 2880-2891. <https://doi.org/10.1093/hmg/ddm247>
87. Hruska, M., & Dalva, M. B. (2012). Ephrin regulation of synapse formation, function and plasticity. *Mol Cell Neurosci*, 50(1), 35-44. <https://doi.org/10.1016/j.mcn.2012.03.004>

88. Hsia, A. Y., Salin, P. A., Castillo, P. E., Aiba, A., Abeliovich, A., Tonegawa, S., & Nicoll, R. A. (1995). Evidence against a role for metabotropic glutamate receptors in mossy fiber LTP: the use of mutant mice and pharmacological antagonists. *Neuropharmacology*, *34*(11). [https://doi.org/10.1016/0028-3908\(95\)00115-m](https://doi.org/10.1016/0028-3908(95)00115-m)
89. Huang, X., Du, X., & Li, Y. (2012). The role of BCL11B in hematological malignancy. *Exp Hematol Oncol*, *1*, 22. <https://doi.org/10.1186/2162-3619-1-22>
90. Huang, Y. Y., Li, X. C., & Kandel, E. R. (1994). cAMP contributes to mossy fiber LTP by initiating both a covalently mediated early phase and macromolecular synthesis-dependent late phase. *Cell*, *79*(1), 69-79. [https://doi.org/10.1016/0092-8674\(94\)90401-4](https://doi.org/10.1016/0092-8674(94)90401-4)
91. Huggett, S. B., & Stallings, M. C. (2020a). Cocaine'omics: Genome-wide and transcriptome-wide analyses provide biological insight into cocaine use and dependence. *Addict Biol*, *25*(2), e12719. <https://doi.org/10.1111/adb.12719>
92. Huggett, S. B., & Stallings, M. C. (2020b). Genetic Architecture and Molecular Neuropathology of Human Cocaine Addiction. *J Neurosci*, *40*(27), 5300-5313. <https://doi.org/10.1523/JNEUROSCI.2879-19.2020>
93. Iijima, T., Miura, E., Watanabe, M., & Yuzaki, M. (2010). Distinct expression of C1q-like family mRNAs in mouse brain and biochemical characterization of their encoded proteins. *Eur J Neurosci*, *31*(9), 1606-1615. <https://doi.org/10.1111/j.1460-9568.2010.07202.x>
94. Ito, I., & Sugiyama, H. (1991). Roles of glutamate receptors in long-term potentiation at hippocampal mossy fiber synapses. *Neuroreport*, *2*(6), 333-336. <https://doi.org/10.1097/00001756-199106000-00008>
95. Jaffe, D., & Johnston, D. (1990). Induction of long-term potentiation at hippocampal mossy-fiber synapses follows a Hebbian rule. *J Neurophysiol*, *64*(3), 948-960. <https://doi.org/10.1152/jn.1990.64.3.948>
96. Jedlicka, P., Vlachos, A., Schwarzacher, S. W., & Deller, T. (2008). A role for the spine apparatus in LTP and spatial learning. *Behav Brain Res*, *192*(1), 12-19. <https://doi.org/10.1016/j.bbr.2008.02.033>

97. Jonas, P., Major, G., & Sakmann, B. (1993). Quantal components of unitary EPSCs at the mossy fibre synapse on CA3 pyramidal cells of rat hippocampus. *J Physiol*, 472, 615-663. <https://doi.org/10.1113/jphysiol.1993.sp019965>
98. Kakegawa, W., Yamada, N., Iino, M., Kameyama, K., Umeda, T., Tsuzuki, K., & Ozawa, S. (2002). Postsynaptic expression of a new calcium pathway in hippocampal CA3 neurons and its influence on mossy fiber long-term potentiation. *J Neurosci*, 22(11), 4312-4320. <https://doi.org/10.1523/JNEUROSCI.22-11-04312.2002>
99. Kamiya, H., & Ozawa, S. (1999). Dual mechanism for presynaptic modulation by axonal metabotropic glutamate receptor at the mouse mossy fibre-CA3 synapse. *J Physiol*, 518(Pt 2), 497-506. <https://doi.org/10.1111/j.1469-7793.1999.0497p.x>
100. Kasem, E., Kurihara, T., & Tabuchi, K. (2018). Neurexins and neuropsychiatric disorders. *Neurosci Res*, 127, 53-60. <https://doi.org/10.1016/j.neures.2017.10.012>
101. Kim, S., Jang, H. J., Myung, W., Kim, K., Cha, S., Lee, H., Cho, S. K., Kim, B., Ha, T. H., Kim, J. W., Kim, D. K., Stahl, E. A., & Won, H. H. (2019). Heritability estimates of individual psychological distress symptoms from genetic variation. *J Affect Disord*, 252, 413-420. <https://doi.org/10.1016/j.jad.2019.04.011>
102. Kirchner, J. H., Euler, L., & Gjorgjieva, J. (2023). Dendritic growth and synaptic organization from activity-independent cues and local activity-dependent plasticity. *Elife*, 12:RP87527. <https://doi.org/10.7554/eLife.87527.1>
103. Kisaretova, P., Tsybko, A., Bondar, N., & Reshetnikov, V. (2023). Molecular Abnormalities in BTBR Mice and Their Relevance to Schizophrenia and Autism Spectrum Disorders: An Overview of Transcriptomic and Proteomic Studies. *Biomedicines*, 11(2). <https://doi.org/10.3390/biomedicines11020289>
104. Kiss-Toth, A., Dobson, L., Peterfia, B., Angyan, A. F., Ligeti, B., Lukacs, G., & Gaspari, Z. (2019). Occurrence of Ordered and Disordered Structural Elements in Postsynaptic Proteins Supports Optimization for Interaction Diversity. *Entropy (Basel)*, 21(8). <https://doi.org/10.3390/e21080761>
105. Klatt, O., Repetto, D., Brockhaus, J., Reissner, C., El Khallouqi, A., Rohlmann, A., Heine, M., & Missler, M. (2021). Endogenous beta-neurexins on axons and within synapses show regulated dynamic behavior. *Cell Rep*, 35(11), 109266. <https://doi.org/10.1016/j.celrep.2021.109266>

106. Kolomeets, N. S., Orlovskaya, D. D., Rachmanova, V. I., & Uranova, N. A. (2005). Ultrastructural alterations in hippocampal mossy fiber synapses in schizophrenia: a postmortem morphometric study. *Synapse*, 57(1), 47-55. <https://doi.org/10.1002/syn.20153>
107. Kolomeets, N. S., Orlovskaya, D. D., & Uranova, N. A. (2007). Decreased numerical density of CA3 hippocampal mossy fiber synapses in schizophrenia. *Synapse*, 61(8), 615-621. <https://doi.org/10.1002/syn.20405>
108. Koumoundourou, A., Rannap M., De Bruyckere, E., Nestel, S., Reißner, C., Egorov, A. V., Liu, P., Missler, M., Heimrich, B., Draguhn, A., Britsch, S. (2023). Regulation of hippocampal mossy fiber-CA3 synapse function by a Bcl11b/C1ql2/Nrxn3(25b+) pathway. *eLife*, 12:RP89854. <https://doi.org/10.7554/eLife.89854.1>
109. Kunkle, B. W., Jaworski, J., Barral, S., Vardarajan, B., Beecham, G. W., Martin, E. R., Cantwell, L. S., Partch, A., Bird, T. D., Raskind, W. H., DeStefano, A. L., Carney, R. M., Cuccaro, M., Vance, J. M., Farrer, L. A., Goate, A. M., Foroud, T., Mayeux, R. P., Schellenberg, G. D., . . . Pericak-Vance, M. A. (2016). Genome-wide linkage analyses of non-Hispanic white families identify novel loci for familial late-onset Alzheimer's disease. *Alzheimers Dement*, 12(1), 2-10. <https://doi.org/10.1016/j.jalz.2015.05.020>
110. Kusick, G. F., Ogunmowo, T. H., & Watanabe, S. (2022). Transient docking of synaptic vesicles: Implications and mechanisms. *Curr Opin Neurobiol*, 74, 102535. <https://doi.org/10.1016/j.conb.2022.102535>
111. Kyrylkova, K., Kyryachenko, S., Biehs, B., Klein, O., Kioussi, C., & Leid, M. (2012). BCL11B regulates epithelial proliferation and asymmetric development of the mouse mandibular incisor. *PLoS One*, 7(5), e37670. <https://doi.org/10.1371/journal.pone.0037670>
112. Lanore, F., Labrousse, V. F., Szabo, Z., Normand, E., Blanchet, C., & Mulle, C. (2012). Deficits in morphofunctional maturation of hippocampal mossy fiber synapses in a mouse model of intellectual disability. *J Neurosci*, 32(49), 17882-17893. <https://doi.org/10.1523/JNEUROSCI.2049-12.2012>
113. Lautz, J. D., Tsegay, K. B., Zhu, Z., Gniffke, E. P., Welsh, J. P., & Smith, S. E. P. (2021). Synaptic protein interaction networks encode experience by assuming stimulus-

- specific and brain-region-specific states. *Cell Rep*, 37(9), 110076. <https://doi.org/10.1016/j.celrep.2021.110076>
114. Leid, M., Ishmael, J. E., Avram, D., Shepherd, D., Fraulob, V., & Dolle, P. (2004). CTIP1 and CTIP2 are differentially expressed during mouse embryogenesis. *Gene Expr Patterns*, 4(6), 733-739. <https://doi.org/10.1016/j.modgep.2004.03.009>
115. Lennon, M. J., Jones, S. P., Lovelace, M. D., Guillemin, G. J., & Brew, B. J. (2016). Bcl11b: A New Piece to the Complex Puzzle of Amyotrophic Lateral Sclerosis Neuropathogenesis? *Neurotox Res*, 29(2), 201-207. <https://doi.org/10.1007/s12640-015-9573-5>
116. Lepeta, K., Lourenco, M. V., Schweitzer, B. C., Martino Adami, P. V., Banerjee, P., Catuara-Solarz, S., de La Fuente Revenga, M., Guillem, A. M., Haidar, M., Ijomone, O. M., Nadorp, B., Qi, L., Perera, N. D., Refsgaard, L. K., Reid, K. M., Sabbar, M., Sahoo, A., Schaefer, N., Sheean, R. K., . . . Seidenbecher, C. (2016). Synaptopathies: synaptic dysfunction in neurological disorders - A review from students to students. *J Neurochem*, 138(6), 785-805. <https://doi.org/10.1111/jnc.13713>
117. Lessel, D., Gehbauer, C., Bramswig, N. C., Schluth-Bolard, C., Venkataramanappa, S., van Gassen, K. L. I., Hempel, M., Haack, T. B., Baresic, A., Genetti, C. A., Funari, M. F. A., Lessel, I., Kuhlmann, L., Simon, R., Liu, P., Denecke, J., Kuechler, A., de Kruijff, I., Shoukier, M., . . . Kubisch, C. (2018). BCL11B mutations in patients affected by a neurodevelopmental disorder with reduced type 2 innate lymphoid cells. *Brain*, 141(8), 2299-2311. <https://doi.org/10.1093/brain/awy173>
118. Li, P., Burke, S., Wang, J., Chen, X., Ortiz, M., Lee, S. C., Lu, D., Campos, L., Goulding, D., Ng, B. L., Dougan, G., Huntly, B., Gottgens, B., Jenkins, N. A., Copeland, N. G., Colucci, F., & Liu, P. (2010). Reprogramming of T cells to natural killer-like cells upon Bcl11b deletion. *Science*, 329(5987), 85-89. <https://doi.org/10.1126/science.1188063>.
119. López-García, J. C., Arancio, O., Kandel, E. R., & Baranes, D. (1996). A presynaptic locus for long-term potentiation of elementary synaptic transmission at mossy fiber synapses in culture. *Proc Natl Acad Sci U S A*, 93(10), 4712-4717. <https://doi.org/10.1073/pnas.93.10.4712>

120. Lopez-Rojas, J., de Solis, C. A., Leroy, F., Kandel, E. R., & Siegelbaum, S. A. (2022). A direct lateral entorhinal cortex to hippocampal CA2 circuit conveys social information required for social memory. *Neuron*, *110*(9), 1559-1572 e1554. <https://doi.org/10.1016/j.neuron.2022.01.028>
121. Maass, W., & Zador, A. M. (1999). Dynamic Stochastic Synapses as Computational Units. *Neural Comput.*, *11*(4), 903-917. <https://doi.org/10.1162/089976699300016494>
122. Madisen, L., Zwingman, T. A., Sunkin, S. M., Oh, S. W., Zariwala, H. A., Gu, H., Ng, L. L., Palmiter, R. D., Hawrylycz, M. J., Jones, A. R., Lein, E. S., & Zeng, H. (2010). A robust and high-throughput Cre reporting and characterization system for the whole mouse brain. *Nat Neurosci*, *13*(1), 133-140. <https://doi.org/10.1038/nn.2467>
123. Manzoni, O. J., Weisskopf, M. G., & Nicoll, R. A. (1994). MCPG antagonizes metabotropic glutamate receptors but not long-term potentiation in the hippocampus. *Eur J Neurosci*, *6*(6), 1050-1054. <https://doi.org/10.1111/j.1460-9568.1994.tb00599.x>
124. Marballi, K. K., Alganem, K., Brunwasser, S. J., Barkatullah, A., Meyers, K. T., Campbell, J. M., Ozols, A. B., McCullumsmith, R. E., & Gallitano, A. L. (2022). Identification of activity-induced Egr3-dependent genes reveals genes associated with DNA damage response and schizophrenia. *Transl Psychiatry*, *12*(1), 320. <https://doi.org/10.1038/s41398-022-02069-8>
125. Martin, E. A., Muralidhar, S., Wang, Z., Cervantes, D. C., Basu, R., Taylor, M. R., Hunter, J., Cutforth, T., Wilke, S. A., Ghosh, A., & Williams, M. E. (2015). The intellectual disability gene Kirrel3 regulates target-specific mossy fiber synapse development in the hippocampus. *Elife*, *4*, e09395. <https://doi.org/10.7554/eLife.09395>
126. Matsuda, K., Budisantoso, T., Mitakidis, N., Sugaya, Y., Miura, E., Kakegawa, W., Yamasaki, M., Konno, K., Uchigashima, M., Abe, M., Watanabe, I., Kano, M., Watanabe, M., Sakimura, K., Aricescu, A. R., & Yuzaki, M. (2016). Transsynaptic Modulation of Kainate Receptor Functions by C1q-like Proteins. *Neuron*, *90*(4), 752-767. <https://doi.org/10.1016/j.neuron.2016.04.001>
127. McGinty, J. F., Henriksen, S. J., Goldstein, A., Terenius, L., & Bloom, F. E. (1983). Dynorphin is contained within hippocampal mossy fibers: Immunochemical

- alterations after kainic acid administration and colchicine-induced neurotoxicity. *Proc Natl Acad Sci U S A*, 80, 589-593. <https://doi.org/10.1073/pnas.80.2.589>
128. Medeiros A. T., Gratz S.J., Delgado A., Ritt J.T., O'Connor-Giles K. M. (2023) Molecular and organizational diversity intersect to generate functional synaptic heterogeneity within and between excitatory neuronal subtypes. *eLife*, 12:RP88412 <https://doi.org/10.7554/eLife.88412.1>
129. Meftah, S., & Gan, J. (2023). Alzheimer's disease as a synaptopathy: Evidence for dysfunction of synapses during disease progression. *Front Synaptic Neurosci*, 15, 1129036. <https://doi.org/10.3389/fnsyn.2023.1129036>
130. Mello, L. E., Cavalheiro, E. A., Tan, A. M., Kupfer, W. R., Pretorius, J. K., Babb, T. L., & Finch, D. M. (1993). Circuit mechanisms of seizures in the pilocarpine model of chronic epilepsy: cell loss and mossy fiber sprouting. *Epilepsia*, 34(6), 985-995. <https://doi.org/10.1111/j.1528-1157.1993.tb02123.x>.
131. Mellor, J., & Nicoll, R. A. (2001). Hippocampal mossy fiber LTP is independent of postsynaptic calcium. *Nat Neurosci*, 4, 125-126. <https://doi.org/10.1038/83941>
132. Meng, J. L., Wang, Y., Carrillo, R. A., & Heckscher, E. S. (2020). Temporal transcription factors determine circuit membership by permanently altering motor neuron-to-muscle synaptic partnerships. *Elife*, 9. <https://doi.org/10.7554/eLife.56898>
133. Midorikawa, M., & Sakaba, T. (2017). Kinetics of Releasable Synaptic Vesicles and Their Plastic Changes at Hippocampal Mossy Fiber Synapses. *Neuron*, 96(5), 1033-1040 e1033. <https://doi.org/10.1016/j.neuron.2017.10.016>
134. Miski, M., Keomley-Horvath, B. M., Rakoczi Megyerine, D., Csikasz-Nagy, A., & Gaspari, Z. (2022). Diversity of synaptic protein complexes as a function of the abundance of their constituent proteins: A modeling approach. *PLoS Comput Biol*, 18(1), e1009758. <https://doi.org/10.1371/journal.pcbi.1009758>
135. Missler, M., Sudhof, T. C., & Biederer, T. (2012). Synaptic cell adhesion. *Cold Spring Harb Perspect Biol*, 4(4), a005694. <https://doi.org/10.1101/cshperspect.a005694>
136. Missler, M., Zhang, W., Rohlmann, A., Kattenstroth, G., Hammer, R. E., Gottmann, K., & Sudhof, T. C. (2003). Alpha-neurexins couple Ca²⁺ channels to synaptic vesicle exocytosis. *Nature*, 423(6943), 939-948. <https://doi.org/10.1038/nature01755>

137. Naber, P. A., Lopes da Silva, F. H., & Witter, M. P. (2001). Reciprocal connections between the entorhinal cortex and hippocampal fields CA1 and the subiculum are in register with the projections from CA1 to the subiculum. *Hippocampus*, 11(2), 99-104. <https://doi.org/10.1002/hipo.1028>
138. Neupert, C., Schneider, R., Klatt, O., Reissner, C., Repetto, D., Biermann, B., Niesmann, K., Missler, M., & Heine, M. (2015). Regulated Dynamic Trafficking of Neurexins Inside and Outside of Synaptic Terminals. *J Neurosci*, 35(40), 13629-13647. <https://doi.org/10.1523/JNEUROSCI.4041-14.2015>
139. Newman, Z. L., Bakshinskaya, D., Schultz, R., Kenny, S. J., Moon, S., Aghi, K., Stanley, C., Marnani, N., Li, R., Bleier, J., Xu, K., & Isacoff, E. Y. (2022). Determinants of synapse diversity revealed by super-resolution quantal transmission and active zone imaging. *Nat Commun*, 13(1), 229. <https://doi.org/10.1038/s41467-021-27815-2>
140. Nicoll, R. A., & Schmitz, D. (2005). Synaptic plasticity at hippocampal mossy fibre synapses. *Nat Rev Neurosci*, 6(11), 863-876. <https://doi.org/10.1038/nrn1786>
141. Nikouei, K., Munoz-Manchado, A. B., & Hjerling-Leffler, J. (2016). BCL11B/CTIP2 is highly expressed in GABAergic interneurons of the mouse somatosensory cortex. *J Chem Neuroanat*, 71, 1-5. <https://doi.org/10.1016/j.jchemneu.2015.12.004>
142. Nusser, Z. (2018). Creating diverse synapses from the same molecules. *Curr Opin Neurobiol*, 51, 8-15. <https://doi.org/10.1016/j.conb.2018.01.001>
143. O'Connor, T. P., Cockburn, K., Wang, W., Tapia, L., Currie, E., & Bamji, S. X. (2009). Semaphorin 5B mediates synapse elimination in hippocampal neurons. *Neural Dev*, 4, 18. <https://doi.org/10.1186/1749-8104-4-18>
144. O'Rourke, N. A., Weiler, N. C., Micheva, K. D., & Smith, S. J. (2012). Deep molecular diversity of mammalian synapses: why it matters and how to measure it. *Nat Rev Neurosci*, 13(6), 365-379. <https://doi.org/10.1038/nrn3170>
145. Orlando, M., Dvorzhak, A., Bruentgens, F., Maglione, M., Rost, B. R., Sigrist, S. J., Breustedt, J., & Schmitz, D. (2021). Recruitment of release sites underlies chemical presynaptic potentiation at hippocampal mossy fiber boutons. *PLoS Biol*, 19(6), e3001149. <https://doi.org/10.1371/journal.pbio.3001149>
146. Orvis, J., Albertin, C. B., Shrestha, P., Chen, S., Zheng, M., Rodriguez, C. J., Tallon, L. J., Mahurkar, A., Zimin, A. V., Kim, M., Liu, K., Kandel, E. R., Fraser, C. M., Sossin, W., &

- Abrams, T. W. (2022). The evolution of synaptic and cognitive capacity: Insights from the nervous system transcriptome of *Aplysia*. *Proc Natl Acad Sci U S A*, *119*(28), e2122301119. <https://doi.org/10.1073/pnas.2122301119>
147. Pardinas, A. F., Holmans, P., Pocklington, A. J., Escott-Price, V., Ripke, S., Carrera, N., Legge, S. E., Bishop, S., Cameron, D., Hamshere, M. L., Han, J., Hubbard, L., Lynham, A., Mantripragada, K., Rees, E., MacCabe, J. H., McCarroll, S. A., Baune, B. T., Breen, G., . . . Walters, J. T. R. (2018). Common schizophrenia alleles are enriched in mutation-intolerant genes and in regions under strong background selection. *Nat Genet*, *50*(3), 381-389. <https://doi.org/10.1038/s41588-018-0059-2>
148. Pasquier, D. A., & Reinoso-Suarez, F. (1978). The topographic organization of hypothalamic and brain stem projections to the hippocampus. *Brain Research Bulletin*, *3*(4). [https://doi.org/10.1016/0361-9230\(78\)90106-5](https://doi.org/10.1016/0361-9230(78)90106-5)
149. Patton, P. E., & McNaughton, B. (1995). Connection matrix of the hippocampal formation: I. The dentate gyrus. *Hippocampus*, *5*(4), 245-286. <https://doi.org/10.1002/hipo.450050402>
150. Paul, A., Crow, M., Raudales, R., He, M., Gillis, J., & Huang, Z. J. (2017). Transcriptional Architecture of Synaptic Communication Delineates GABAergic Neuron Identity. *Cell*, *171*(3), 522-539 e520. <https://doi.org/10.1016/j.cell.2017.08.032>
151. Perez-Nieves, N., Leung, V. C. H., Dragotti, P. L., & Goodman, D. F. M. (2021). Neural heterogeneity promotes robust learning. *Nat Commun*, *12*(1), 5791. <https://doi.org/10.1038/s41467-021-26022-3>
152. Pierce, J. P., van Leyen, K., & McCarthy, J. B. (2000). Translocation machinery for synthesis of integral membrane and secretory proteins in dendritic spines. *Nat Neurosci*, *3*, 311-313. <https://doi.org/10.1038/73868>
153. Prasad, M., Balci, T. B., Prasad, C., Andrews, J. D., Lee, R., Jurkiewicz, M. T., Napier, M. P., Colaiacovo, S., Guillen Sacoto, M. J., & Karp, N. (2020). BCL11B-related disorder in two canadian children: Expanding the clinical phenotype. *Eur J Med Genet*, *63*(9), 104007. <https://doi.org/10.1016/j.ejmg.2020.104007>
154. Punwani, D., Zhang, Y., Yu, J., Cowan, M. J., Rana, S., Kwan, A., Adhikari, A. N., Lizama, C. O., Mendelsohn, B. A., Fahl, S. P., Chellappan, A., Srinivasan, R., Brenner, S. E., Wiest, D. L., & Puck, J. M. (2016). Multisystem Anomalies in Severe Combined

- Immunodeficiency with Mutant BCL11B. *N Engl J Med*, 375(22), 2165-2176.
<https://doi.org/10.1056/NEJMoa1509164>
155. Quinn, D. P., Kolar, A., Wigerius, M., Gomm-Kolisko, R. N., Atwi, H., Fawcett, J. P., & Krueger, S. R. (2017). Pan-neurexin perturbation results in compromised synapse stability and a reduction in readily releasable synaptic vesicle pool size. *Sci Rep*, 7, 42920. <https://doi.org/10.1038/srep42920>
156. Racca, C., Stephenson, F. A., Streit, P., Roberts, J. D. B., & Somogyi, P. (2000). NMDA Receptor Content of Synapses in Stratum Radiatum of the Hippocampal CA1 Area. *J Neurosci*, 20(7), 2512-2522. <https://doi.org/10.1523/JNEUROSCI.20-07-02512.2000>
157. Reimann, M. W., Horlemann, A. L., Ramaswamy, S., Muller, E. B., & Markram, H. (2017). Morphological Diversity Strongly Constrains Synaptic Connectivity and Plasticity. *Cereb Cortex*, 27(9), 4570-4585. <https://doi.org/10.1093/cercor/bhx150>
158. Reissner, C., Runkel, F., & Missler, M. (2013). Neurexins. *Genome Biol*, 14(9), 213. <https://doi.org/10.1186/gb-2013-14-9-213>.
159. Represa, A., Tremblay, E., & Ben-Ari, Y. (1987). Kainate binding sites in the hippocampal mossy fibers: Localization and plasticity. *Neuroscience*, 20(3), 739-748. [https://doi.org/10.1016/0306-4522\(87\)90237-5](https://doi.org/10.1016/0306-4522(87)90237-5)
160. Ressler, S., Vu, B. K., Vivona, S., Martinelli, D. C., Sudhof, T. C., & Brunger, A. T. (2015). Structures of C1q-like proteins reveal unique features among the C1q/TNF superfamily. *Structure*, 23(4), 688-699. <https://doi.org/10.1016/j.str.2015.01.019>
161. Richter, J. D., & Klann, E. (2009). Making synaptic plasticity and memory last: mechanisms of translational regulation. *Genes Dev*, 23(1), 1-11. <https://doi.org/10.1101/gad.1735809>
162. Roig Adam, A., Martinez-Lopez, J. A., van der Spek, S. J. F., consortium, S., Sullivan, P. F., Smit, A. B., Verhage, M., & Hjerling-Leffler, J. (2023). Transcriptional diversity in specific synaptic gene sets discriminates cortical neuronal identity. *Biol Direct*, 18(1), 22. <https://doi.org/10.1186/s13062-023-00372-y>
163. Rollenhagen, A., Satzler, K., Rodriguez, E. P., Jonas, P., Frotscher, M., & Lubke, J. H. (2007). Structural determinants of transmission at large hippocampal mossy fiber synapses. *J Neurosci*, 27(39), 10434-10444. <https://doi.org/10.1523/JNEUROSCI.1946-07.2007>

164. Rui, M., Qian, J., Liu, L., Cai, Y., Lv, H., Han, J., Jia, Z., & Xie, W. (2017). The neuronal protein Neurexin directly interacts with the Scribble-Pix complex to stimulate F-actin assembly for synaptic vesicle clustering. *J Biol Chem*, *292*(35), 14334-14348. <https://doi.org/10.1074/jbc.M117.794040>
165. Salin, P. A., Scanziani, M., Malenka, R. C., & Nicoll, R. A. (1996). Distinct short-term plasticity at two excitatory synapses in the hippocampus. *Proc Natl Acad Sci U S A*, *93*, 13304-13309. <https://doi.org/10.1073/pnas.93.23.13304>
166. Sandler, R., & Smith, A. D. (1991). Coexistence of GABA and glutamate in mossy fiber terminals of the primate hippocampus: an ultrastructural study. *J Comp Neurol*, *303*(2), 177-192. <https://doi.org/10.1002/cne.903030202>
167. Santos-Terra, J., Deckmann, I., Fontes-Dutra, M., Schwingel, G. B., Bambini-Junior, V., & Gottfried, C. (2021). Transcription factors in neurodevelopmental and associated psychiatric disorders: A potential convergence for genetic and environmental risk factors. *Int J Dev Neurosci*, *81*(7), 545-578. <https://doi.org/10.1002/jdn.10141>
168. Satterwhite, E., Somoki, T., Willis, T. G., Harder, L., Nowak, R., Arriola, E. L., Liu, H., Price, H. P., Gesk, S., Steinemann, D., Schlegelberger, B., Oscier, D. G., Siebert, R., Tucker, P. W., & Dyer, M. J. S. (2001). The BCL11 gene family: involvement of BCL11A in lymphoid malignancies. *Neoplasia*, *98*(12), 3414-3420. <https://doi.org/10.1182/blood.V98.12.3413>
169. Scharkowski, F., Frotscher, M., Lutz, D., Korte, M., & Michaelsen-Preusse, K. (2018). Altered Connectivity and Synapse Maturation of the Hippocampal Mossy Fiber Pathway in a Mouse Model of the Fragile X Syndrome. *Cereb Cortex*, *28*(3), 852-867. <https://doi.org/10.1093/cercor/bhw408>
170. Schindelin, J., Arganda-Carreras, I., Frise, E., Kaynig, V., Longair, M., Pietzsch, T., Preibisch, S., Rueden, C., Saalfeld, S., Schmid, B., Tinevez, J. Y., White, D. J., Hartenstein, V., Eliceiri, K., Tomancak, P., & Cardona, A. (2012). Fiji: an open-source platform for biological-image analysis. *Nat Methods*, *9*(7), 676-682. <https://doi.org/10.1038/nmeth.2019>
171. Schlimgen, A. K., Helms, J. A., Vogel, H., & Perin, M. S. (1995). Neuronal pentraxin, a secreted protein with homology to acute phase proteins of the immune system. *Neuron*, *14*(3), 519-526. [https://doi.org/10.1016/0896-6273\(95\)90308-9](https://doi.org/10.1016/0896-6273(95)90308-9)

172. Schmittgen, T. D., & Livak, K. J. (2008). Analyzing real-time PCR data by the comparative C(T) method. *Nat Protoc*, 3(6), 1101-1108. <https://doi.org/10.1038/nprot.2008.73>
173. Schmitz, D., Mellor, J., Frerking, M., & Nicoll, R. A. (2001). Presynaptic kainate receptors at hippocampal mossy fiber synapses. *Proc Natl Acad Sci U S A*, 98(20), 11003-11008. <https://doi.org/10.1073/pnas.191351498>
174. Schreiner, D., Nguyen, T. M., Russo, G., Heber, S., Patrignani, A., Ahrne, E., & Scheiffele, P. (2014). Targeted combinatorial alternative splicing generates brain region-specific repertoires of neuroligins. *Neuron*, 84(2), 386-398. <https://doi.org/10.1016/j.neuron.2014.09.011>
175. Schwarzer, C., & Sperk, G. (1995). Hippocampal granule cells express glutamic acid decarboxylase-67 after limbic seizures in the rat. *Neuroscience*, 69(3), 705-709. [https://doi.org/10.1016/0306-4522\(95\)00348-M](https://doi.org/10.1016/0306-4522(95)00348-M)
176. Segal, M., Vlachos, A., & Korkotian, E. (2010). The spine apparatus, synaptopodin, and dendritic spine plasticity. *Neuroscientist*, 16(2), 125-131. <https://doi.org/10.1177/1073858409355829>
177. Sgritta, M., Vignoli, B., Pimpinella, D., Griguoli, M., Santi, S., Bialowas, A., Wiera, G., Zacchi, P., Malerba, F., Marchetti, C., Canossa, M., & Cherubini, E. (2023). Impaired synaptic plasticity in an animal model of autism exhibiting early hippocampal GABAergic-BDNF/TrkB signaling alterations. *iScience*, 26(1), 105728. <https://doi.org/10.1016/j.isci.2022.105728>
178. Shao, Z., Yang, Y., & Hu, Z. (2022). Editorial: Regulation of synaptic structure and function. *Front Mol Neurosci*, 15, 1060367. <https://doi.org/10.3389/fnmol.2022.1060367>
179. Shen, K., & Scheiffele, P. (2010). Genetics and cell biology of building specific synaptic connectivity. *Annu Rev Neurosci*, 33, 473-507. <https://doi.org/10.1146/annurev.neuro.051508.135302>
180. Sheng, M., Sabatini, B. L., & Sudhof, T. C. (2012). *The Synapse*. Cold Spring Harbor Laboratory Press.
181. Shimono, C., Manabe, R., Yamada, T., Fukuda, S., Kawai, J., Furutani, Y., Tsutsui, K., Ikenaka, K., Hayashizaki, Y., & Sekiguchi, K. (2010). Identification and characterization

- of nCLP2, a novel C1q family protein expressed in the central nervous system. *J Biochem*, 147(4), 565-579. <https://doi.org/10.1093/jb/mvp203>
182. Siegel, S. J., Brose, N., Janssen, W. G., Gasic, G. P., Jahn, R., Heinemann, S. F., & Morrison, J. H. (1994). Regional, cellular, and ultrastructural distribution of N-methyl-D-aspartate receptor subunit 1 in monkey hippocampus. *Proc Natl Acad Sci U S A*, 91(2), 564-568. <https://doi.org/10.1073/pnas.91.2.564>
183. Simon, R., Baumann, L., Fischer, J., Seigfried, F. A., De Bruyckere, E., Liu, P., Jenkins, N. A., Copeland, N. G., Schwegler, H., & Britsch, S. (2016). Structure-function integrity of the adult hippocampus depends on the transcription factor Bcl11b/Ctip2. *Genes Brain Behav*, 15(4), 405-419. <https://doi.org/10.1111/gbb.12287>
184. Simon, R., Brylka, H., Schwegler, H., Venkataramanappa, S., Andratschke, J., Wiegrefe, C., Liu, P., Fuchs, E., Jenkins, N. A., Copeland, N. G., Birchmeier, C., & Britsch, S. (2012). A dual function of Bcl11b/Ctip2 in hippocampal neurogenesis. *EMBO J*, 31(13), 2922-2936. <https://doi.org/10.1038/emboj.2012.142>
185. Sloviter, R. S., Dichter, M. A., Rachinsky, T. L., Dean, E., Goodman, J. H., Sollas, A. L., & Martin, D. L. (1996). Basal expression and induction of glutamate decarboxylase GABA in excitatory granule cells of the rat and monkey hippocampal dentate gyrus. *The Journal of Comparative Neurology*, 373(4), 593-618. [https://doi.org/10.1002/\(sici\)1096-9861\(19960930\)373:4<593::Aid-cne8>3.0.Co;2-x](https://doi.org/10.1002/(sici)1096-9861(19960930)373:4<593::Aid-cne8>3.0.Co;2-x)
186. Song, S., Creus Muncunill, J., Galicia Aguirre, C., Tshilenge, K. T., Hamilton, B. W., Gerencser, A. A., Benlhabib, H., Cirnaru, M. D., Leid, M., Mooney, S. D., Ellerby, L. M., & Ehrlich, M. E. (2022). Postnatal Conditional Deletion of Bcl11b in Striatal Projection Neurons Mimics the Transcriptional Signature of Huntington's Disease. *Biomedicines*, 10(10). <https://doi.org/10.3390/biomedicines10102377>
187. Sorokina, O., McLean, C., Croning, M. D. R., Heil, K. F., Wysocka, E., He, X., Sterratt, D., Grant, S. G. N., Simpson, T. I., & Armstrong, J. D. (2021). A unified resource and configurable model of the synapse proteome and its role in disease. *Scientific Reports*, 11(1). <https://doi.org/10.1038/s41598-021-88945-7>
188. Spacek, J., & Harris, K. M. (1997). Three-Dimensional Organization of Smooth Endoplasmic Reticulum in Hippocampal CA1 Dendrites and Dendritic Spines of the

- Immature and Mature Rat. *J Neurosci*, 17(1), 190-203.
<https://doi.org/10.1523/JNEUROSCI.17-01-00190.1997>
189. Spoto, G., Valentini, G., Saia, M. C., Butera, A., Amore, G., Salpietro, V., Nicotera, A. G., & Di Rosa, G. (2022). Synaptopathies in Developmental and Epileptic Encephalopathies: A Focus on Pre-synaptic Dysfunction. *Front Neurol*, 13, 826211.
<https://doi.org/10.3389/fneur.2022.826211>
190. Sudhof, T. C. (2008). Neuroligins and neurexins link synaptic function to cognitive disease. *Nature*, 455(7215), 903-911. <https://doi.org/10.1038/nature07456>
191. Sudhof, T. C. (2017). Synaptic Neurexin Complexes: A Molecular Code for the Logic of Neural Circuits. *Cell*, 171(4), 745-769. <https://doi.org/10.1016/j.cell.2017.10.024>
192. Sudhof, T. C. (2021). The cell biology of synapse formation. *J Cell Biol*, 220(7).
<https://doi.org/10.1083/jcb.202103052>
193. Sutula, T., Cascino, G., Cavazos, J., Parada, I., & Ramirez, L. (1989). Mossy fiber synaptic reorganization in the epileptic human temporal lobe. *Ann Neurol*, 26(3), 321-330.
<https://doi.org/10.1002/ana.410260303>
194. Szirmai, I., Buzsaki, G., & Kamondi, A. (2012). 120 years of hippocampal Schaffer collaterals. *Hippocampus*, 22(7), 1508-1516. <https://doi.org/10.1002/hipo.22001>
195. Takahashi, H., & Craig, A. M. (2013). Protein tyrosine phosphatases PTPdelta, PTPsigma, and LAR: presynaptic hubs for synapse organization. *Trends Neurosci*, 36(9), 522-534. <https://doi.org/10.1016/j.tins.2013.06.002>
196. Tamamaki, N., & Nojyo, Y. (1993). Projection of the entorhinal layer II neurons in the rat as revealed by intracellular pressure-injection of neurobiotin. *Hippocampus*, 3(4), 471-480. <https://doi.org/10.1002/hipo.450030408>
197. Tong, G., Malenka, R. C., & Nicoll, R. A. (1996). Long-Term Potentiation in Cultures of Single Hippocampal Granule Cells: A Presynaptic Form of Plasticity. *Neuron*, 16(6), 1147-1157. [https://doi.org/10.1016/S0896-6273\(00\)80141-5](https://doi.org/10.1016/S0896-6273(00)80141-5)
198. Torres, V. I., Vallejo, D., & Inestrosa, N. C. (2017). Emerging Synaptic Molecules as Candidates in the Etiology of Neurological Disorders. *Neural Plast*, 2017, 8081758.
<https://doi.org/10.1155/2017/8081758>

199. Treutlein, B., Gokce, O., Quake, S. R., & Sudhof, T. C. (2014). Cartography of neurexin alternative splicing mapped by single-molecule long-read mRNA sequencing. *Proc Natl Acad Sci U S A*, *111*(13), E1291-1299. <https://doi.org/10.1073/pnas.1403244111>
200. Trubetskoy, V., Pardinas, A. F., Qi, T., Panagiotaropoulou, G., Awasthi, S., Bigdeli, T. B., Bryois, J., Chen, C. Y., Dennison, C. A., Hall, L. S., Lam, M., Watanabe, K., Frei, O., Ge, T., Harwood, J. C., Koopmans, F., Magnusson, S., Richards, A. L., Sidorenko, J., . . . Schizophrenia Working Group of the Psychiatric Genomics, C. (2022). Mapping genomic loci implicates genes and synaptic biology in schizophrenia. *Nature*, *604*(7906), 502-508. <https://doi.org/10.1038/s41586-022-04434-5>
201. Uchigashima, M., Cheung, A., Suh, J., Watanabe, M., & Futai, K. (2019). Differential expression of neurexin genes in the mouse brain. *J Comp Neurol*, *527*(12), 1940-1965. <https://doi.org/10.1002/cne.24664>
202. Ullrich, B., Ushkaryov, Y. A., & Sudhof, T. C. (1995). Cartography of neurexins: More than 1000 isoforms generated by alternative splicing and expressed in distinct subsets of neurons. *Neuron*, *14*(3), 497-507. [https://doi.org/10.1016/0896-6273\(95\)90306-2](https://doi.org/10.1016/0896-6273(95)90306-2)
203. Um, J. W., & Ko, J. (2013). LAR-RPTPs: synaptic adhesion molecules that shape synapse development. *Trends Cell Biol*, *23*(10), 465-475. <https://doi.org/10.1016/j.tcb.2013.07.004>
204. Unroe, K. A., Glover, M. E., Shupe, E. A., Feng, N., & Clinton, S. M. (2021). Perinatal SSRI Exposure Disrupts G Protein-coupled Receptor BAI3 in Developing Dentate Gyrus and Adult Emotional Behavior: Relevance to Psychiatric Disorders. *Neuroscience*, *471*, 32-50. <https://doi.org/10.1016/j.neuroscience.2021.07.007>
205. Urban, N. N., & Barrionuevo, G. (1996). Induction of Hebbian and Non-Hebbian Mossy Fiber Long-Term Potentiation by Distinct Patterns of High-Frequency Stimulation. *J Neurosci*, *16*(13), 4293-4299. <https://doi.org/10.1523/JNEUROSCI.16-13-04293.1996>
206. Vaags, A. K., Lionel, A. C., Sato, D., Goodenberger, M., Stein, Q. P., Curran, S., Ogilvie, C., Ahn, J. W., Drmic, I., Senman, L., Chrysler, C., Thompson, A., Russell, C., Prasad, A., Walker, S., Pinto, D., Marshall, C. R., Stavropoulos, D. J., Zwaigenbaum, L., . . . Scherer, S. W. (2012). Rare deletions at the neurexin 3 locus in autism spectrum disorder. *Am J Hum Genet*, *90*(1), 133-141. <https://doi.org/10.1016/j.ajhg.2011.11.025>

207. Valor, L. M., Charlesworth, P., Humphreys, M., Andreson, C. N. G., & Grant, S. G. N. (2007). Network activity-independent coordinated gene expression program for synapse assembly. *Proc Natl Acad Sci U S A*, *104*(11), 4658-4663. <https://doi.org/10.1073/pnas.0609071104>
208. van Strien, N. M., Cappaert, N. L., & Witter, M. P. (2009). The anatomy of memory: an interactive overview of the parahippocampal-hippocampal network. *Nat Rev Neurosci*, *10*(4), 272-282. <https://doi.org/10.1038/nrn2614>
209. Vandael, D., Borges-Merjane, C., Zhang, X., & Jonas, P. (2020). Short-Term Plasticity at Hippocampal Mossy Fiber Synapses Is Induced by Natural Activity Patterns and Associated with Vesicle Pool Engram Formation. *Neuron*, *107*(3), 509-521 e507. <https://doi.org/10.1016/j.neuron.2020.05.013>
210. Viana da Silva, S., Zhang, P., Haberl, M. G., Labrousse, V., Grosjean, N., Blanchet, C., Frick, A., & Mulle, C. (2019). Hippocampal Mossy Fibers Synapses in CA3 Pyramidal Cells Are Altered at an Early Stage in a Mouse Model of Alzheimer's Disease. *J Neurosci*, *39*(21), 4193-4205. <https://doi.org/10.1523/JNEUROSCI.2868-18.2019>
211. Wakabayashi, Y., Watanabe, H., Inoue, J., Takeda, N., Sakata, J., Mishima, Y., Hitomi, J., Yamamoto, T., Utsuyama, M., Niwa, O., Aizawa, S., & Kominami, R. (2003). Bcl11b is required for differentiation and survival of $\alpha\beta$ T lymphocytes. *Nat Immunol*, *4*, 533-5339. <https://doi.org/10.1038/ni927>
212. Wang, S. S. H., Held, R. G., Wong, M. Y., Liu, C., Karakhanyan, A., & Kaeser, P. S. (2016). Fusion Competent Synaptic Vesicles Persist upon Active Zone Disruption and Loss of Vesicle Docking. *Neuron*, *91*(4), 777-791. <https://doi.org/10.1016/j.neuron.2016.07.005>
213. Wang, X., Christian, K. M., Song, H., & Ming, G. L. (2018). Synaptic dysfunction in complex psychiatric disorders: from genetics to mechanisms. *Genome Med*, *10*(1), 9. <https://doi.org/10.1186/s13073-018-0518-5>
214. Wenzel, H. J., Cole, T. B., Born, D. E., Schwartzkroin, P. A., & Palmiter, R. D. (1997). Ultrastructural localization of zinc transporter-3 (ZnT-3) to synaptic vesicle membranes within mossy fiber boutons in the hippocampus of mouse and monkey. *Proc Natl Acad Sci U S A*, *94*(23), 12676-12681. <https://doi.org/10.1073/pnas.94.23.12676>

215. Whitton, L., Cosgrove, D., Clarkson, C., Harold, D., Kendall, K., Richards, A., Mantripragada, K., Owen, M. J., O'Donovan, M. C., Walters, J., Hartmann, A., Konte, B., Rujescu, D., Wtccc, Gill, M., Corvin, A., Rea, S., Donohoe, G., & Morris, D. W. (2016). Cognitive analysis of schizophrenia risk genes that function as epigenetic regulators of gene expression. *Am J Med Genet B Neuropsychiatr Genet*, *171*(8), 1170-1179. <https://doi.org/10.1002/ajmg.b.32503>
216. Wilke, S. A., Raam, T., Antonios, J. K., Bushong, E. A., Koo, E. H., Ellisman, M. H., & Ghosh, A. (2014). Specific disruption of hippocampal mossy fiber synapses in a mouse model of familial Alzheimer's disease. *PLoS One*, *9*(1), e84349. <https://doi.org/10.1371/journal.pone.0084349>
217. Witter, M. P. (2007). The perforant path: projections from the entorhinal cortex to the dentate gyrus. *Prog Brain Res*, *163*, 43-61. [https://doi.org/10.1016/S0079-6123\(07\)63003-9](https://doi.org/10.1016/S0079-6123(07)63003-9)
218. Witter, M. P., Naber, P. A., van Haeften, T., Machielsen, W. C., Rombouts, S. A., Barkhof, F., Scheltens, P., & Lopes da Silva, F. H. (2000). Cortico-hippocampal communication by way of parallel parahippocampal-subicular pathways. *Hippocampus*, *10*(4), 398-410. [https://doi.org/10.1002/1098-1063\(2000\)10:4<398::AID-HIPO6>3.0.CO;2-K](https://doi.org/10.1002/1098-1063(2000)10:4<398::AID-HIPO6>3.0.CO;2-K)
219. Wolff, J. R., & Missler, M. (1992). Synaptic reorganization in developing and adult nervous systems. *Ann Anat*, *174*(5), 393-403. [https://doi.org/10.1016/s0940-9602\(11\)80257-8](https://doi.org/10.1016/s0940-9602(11)80257-8)
220. Wyss, J. M., Swanson, L. W., & M., C. W. (1979). Evidence for an Input to the Molecular Layer and the stratum granulosum of the Dentate Gyrus from the Supramammillary Region of the Hypothalamus. *Anat Embryol*, *156*, 165-176. <https://doi.org/10.1007/BF00300012>
221. Xiang, Z., Greenwood, A. C., Kairiss, E. W., & Brown, T. H. (1994). Quantal mechanism of long-term potentiation in hippocampal mossy-fiber synapses. *J Neurophysiol*, *71*(6), 2552-2556. <https://doi.org/10.1152/jn.1994.71.6.2552>
222. Yang, S., Kang, Q., Hou, Y., Wang, L., Li, L., Liu, S., Liao, H., Cao, Z., Yang, L., & Xiao, Z. (2020). Mutant BCL11B in a Patient With a Neurodevelopmental Disorder and T-Cell Abnormalities. *Front Pediatr*, *8*, 544894. <https://doi.org/10.3389/fped.2020.544894>

223. Yang, X., Hou, D., Jiang, W., & Zhang, C. (2014). Intercellular protein-protein interactions at synapses. *Protein Cell*, 5(6), 420-444. <https://doi.org/10.1007/s13238-014-0054-z>
224. Yap, E. L., & Greenberg, M. E. (2018). Activity-Regulated Transcription: Bridging the Gap between Neural Activity and Behavior. *Neuron*, 100(2), 330-348. <https://doi.org/10.1016/j.neuron.2018.10.013>
225. Yeckel, M. F., Kapur, A., & Johnston, D. (1999). Multiple forms of LTP in hippocampal CA3 neurons use a common postsynaptic mechanism. *Nat Neurosci*, 2, 625-633. <https://doi.org/10.1038/10180>
226. Yu, T. P., & Brown, T. H. (1994). Three-dimensional quantification of mossy-fiber presynaptic boutons in living hippocampal slices using confocal microscopy. *Synapse*, 18(3), 190-197. <https://doi.org/10.1002/syn.890180304>
227. Yu, Y., Jia, X., Yin, H., Jiang, H., Du, Y., Yang, F., Yang, Z., & Li, H. (2023). A novel variant in BCL11B in an individual with neurodevelopmental delay: A case report. *Mol Genet Genomic Med*, e2132. <https://doi.org/10.1002/mgg3.2132>
228. Yuzaki, M. (2008). Cbln and C1q family proteins: new transneuronal cytokines. *Cell Mol Life Sci*, 65(11), 1698-1705. <https://doi.org/10.1007/s00018-008-7550-3>
229. Yuzaki, M. (2017). The C1q complement family of synaptic organizers: not just complementary. *Curr Opin Neurobiol*, 45, 9-15. <https://doi.org/10.1016/j.conb.2017.02.002>
230. Zador, A. M. (2000). The basic unit of computation. *Nat Neurosci*, 3, 1167. <https://doi.org/10.1038/81432>
231. Zalutsky, R. A., & Nicoll, R. A. (1990). Comparison of two forms of long-term potentiation in single hippocampal neurons. *Science*, 248(4963), 1619-1624. <https://doi.org/10.1126/science.2114039>
232. Zhang, R., Jiang, H., Liu, Y., & He, G. (2022). Structure, function, and pathology of Neurexin-3. *Genes & Diseases*. 10(5), 1908-1919. <https://doi.org/10.1016/j.gendis.2022.04.008>
233. Zhang, Y. F., Xiong, T. Q., Tan, B. H., Song, Y., Li, S. L., Yang, L. B., & Li, Y. C. (2014). Pilocarpine-induced epilepsy is associated with actin cytoskeleton reorganization in

the mossy fiber-CA3 synapses. *Epilepsy Res*, 108(3), 379-389.
<https://doi.org/10.1016/j.eplepsyres.2014.01.016>

234. Zhu, F., Cizeron, M., Qiu, Z., Benavides-Piccione, R., Kopanitsa, M. V., Skene, N. G., Koniaris, B., DeFelipe, J., Fransen, E., Komiyama, N. H., & Grant, S. G. N. (2018). Architecture of the Mouse Brain Synaptome. *Neuron*, 99(4), 781-799 e710.
<https://doi.org/10.1016/j.neuron.2018.07.007>
235. Zhu, L. J., Zhang, C., & Chen, C. (2021). Research progress on the vesicle cycle and neurological disorders. *J Pharm Pharm Sci.*, 24, 400-402.
<https://doi.org/10.18433/jpps31458>.
236. Zoghbi, H. Y., & Bear, M. F. (2012). Synaptic dysfunction in neurodevelopmental disorders associated with autism and intellectual disabilities. *Cold Spring Harb Perspect Biol*, 4(3). <https://doi.org/10.1101/cshperspect.a009886>

Declaration

I hereby declare that I wrote the present dissertation with the topic: "**The transcription factor Bcl11b regulates the function of adult hippocampal mossy fiber synapses through a C1ql2/Nrxn3 pathway**" independently and used no other aids than those cited. In each individual case, I have clearly identified the source of the passages that are taken word for word or paraphrased from other works.

I also hereby declare that I have carried out my scientific work according to the principles of good scientific practice in accordance with the current „Satzung der Universität Ulm zur Sicherung guter wissenschaftlicher Praxis“ [Rules of the University of Ulm for Assuring Good Scientific Practice].

Ulm, 22.11.23

Artemis Koumoundourou

Education

Apr 2019 –

Doctoral studies in the International Graduate School in Molecular Medicine, Ulm University (Germany)

Oct 2015 – Aug 2017

Master of Science in Cellular & Molecular Neuroscience, Graduate Training Center of Neuroscience, Eberhard Karls University of Tübingen (Germany)

Sep 2011 – Jul 2015

Bachelor in Molecular Biology and Genetics, Department of Molecular Biology and Genetics, School of Health, Democritus University of Thrace, Alexandroupolis (Greece)

Experience

Oct 2018 – Dec 2023

Graduate Research Assistant in the Institute of Molecular and Cellular Anatomy, Ulm University (Germany)



Advisor

Prof. Dr. Stefan Britsch



Doctoral Thesis Project

The role of transcription factor Bcl11b/Ctip2 in the maintenance of mossy fibre synapses in the adult murine hippocampus.

Feb 2017 – Sep 2017

Graduate Research Assistant in the Research Group for Neural Circuits Dynamics, Deutsches Zentrum für Neurodegenerative Erkrankungen, Bonn (Germany)



Advisor

Prof. Dr. Gaia Tavosanis



Master Thesis Project

Unravelling the molecular mechanisms of the assembly of a nonstereotyped neural circuit in *Drosophila Melanogaster*

Nov 2016 – Feb 2017

Graduate Research Assistant in the Research Group for Ophthalmic Research, Werner Reichardt Centre for Integrative Neuroscience, Tübingen (Germany)



Advisor

Prof. Dr. Thomas Euler



Lab Rotation Project

Comparative Study of the Cellular Organization of the Retina Between the PWD/PhJ and C57BL/6J Mouse Strains

Sep 2016 – Nov 2016

Graduate Research Assistant in the Research Group for Experimental Embryology, Institute of Anatomy, Eberhard Karls University of Tübingen (Germany)



Advisor

PD Dr. Andrea Wizenmann



Lab Rotation Project

The effect of Islet-1 knockdown on axonal growth of the mesencephalic trigeminal neurons in the PNS of the chick embryo

Sep 2014 – Jul 2015

Undergraduate Research Assistant
in the Research Group for Structural and
Computational Biology,
Department of Molecular Biology and
Genetics, Democritus University of Thrace,
Alexandroupolis (Greece)



Advisor

Prof. Dr. Nicholas M. Glykos



Bachelor Thesis Project

Folding molecular dynamics simulations
of a FMRF-amide-like peptide from *C.elegans*

Feb 2013 – Sep 2014

Undergraduate Research Assistant
in the joined Research Groups for Molecular
Regulation and Developmental Biology &
Molecular Neurobiology,
Department of Molecular Biology and
Genetics, Democritus University of Thrace,
Alexandroupolis (Greece)



Advisors

Prof. Dr. George E. Skavdis

Prof. Dr. Maria E. Grigoriou



Project

Production of antibodies against *elfn1* and *elfn2*
leucine-rich proteins for the study of their
expression in mice with the use of
immunohistochemistry

Publications

Koumoundourou A, Rannap M, De Bruyckere E, Nestel S, Reißner C, Egorov AV, Liu P, Missler M, Heimrich B, Draguhn A, Britsch S. (2023). Regulation of hippocampal mossy fiber-CA3 synapse function by a *Bcl11b/C1ql2/Nrxn3(25b+)* pathway. *eLife*. 12:RP89854. doi:10.7554/eLife.89854.1

Okuyama K, Yamashita M, **Koumoundourou A**, Wiegrefe C, Ohno-Oishi M, Murphy SJH, Zhao X, Yoshida H, Ebihara T, Satoh-Takayama N, Kojo S, Ohno H, Morio T, Wu Y, Puck J, Xue HH, Britsch S, Taniuchi I. (2023). A mutant *Bcl11bN440K* protein interferes with *Bcl11a* function during T lymphocyte and neuronal development. Manuscript submitted for publication.

Baden T, Maina MB, Maia Chagas A, Mohammed YG, Auer TO, Silbering A, von Tobel L, Pertin M, Hartig R, Aleksic J, Akinrinade I, Awadelkareem MA, **Koumoundourou A**, Jones A, Arieti F, Beale A, Münch D, Salek SC, Yusuf S, Prieto-Godino LL. (2020). TREN in Africa: Toward a Truly Global (Neuro)science Community. *Neuron*. Aug 5;107(3):412-416. doi: 10.1016/j.neuron.2020.06.026.

Conferences

2023 | 117th Annual Meeting of the Anatomische Gesellschaft | Talk | Title: "Regulation of hippocampal mossy fiber-CA3 synapse function by *Bcl11b/C1ql2/Nrxn3(25b+)*"

2023 GRC | Excitatory Synapses and Brain Function | Poster presentation | Title: "Regulation of hippocampal mossy fiber-CA3 synapse function by *Bcl11b/C1ql2/Nrxn3(25b+)*"

2022 FENS Forum | Invited speaker | Special interest event: "Colours of the Brainbow: From ethnic diversity to global inclusion in European Neuroscience"

2021 EMBO Workshop | Molecular neurobiology | Poster presentation | Title: "*Bcl11b/Ctip2* controls functional properties of mossy fiber synapse through *C1ql2*"

Scholarships & Awards

DAAD-Prize 2022 for outstanding achievement of a foreign student by Ulm University

Scholarship for the studies in the Graduate Training Center of Neuroscience, Eberhard Karls University of Tübingen for the time period April 2016-December 2016, by the Hertie-Institute for Clinical Brain Research, Tübingen

Volunteering

February 2022 –

Mentor at Open Hardware Makers (<https://openhardware.space/>)

September 2019 –

Alumni Coordinator/Course organiser at TReND in Africa (<https://trendinafrica.org/>)